SYNTHETIC JET APPLICATION ON A FLAPPING AIRFOIL

A THESIS SUBMITTED TO
THE GRADUATE SCHOOL OF NATURAL AND APPLIED SCIENCES
OF
MIDDLE EAST TECHNICAL UNIVERSITY

BY

MELTEM ÇİFTCİ

IN PARTIAL FULFILLMENT OF THE REQUIREMENTS
FOR
THE DEGREE OF MASTER OF SCIENCE
IN
AEROSPACE ENGINEERING

JULY 2014

Approval of the thesis:

SYNTHETIC JET APPLICATION ON A FLAPPING AIRFOIL

submitted by **MELTEM ÇİFTCİ** in partial fulfillment of the requirements for the degree of **Master of Science in Aerospace Engineering Department, Middle East Technical University** by,

Prof. Dr. Canan ÖZGEN   _____
Dean, Graduate School of **Natural and Applied Sciences**

Prof. Dr. Ozan TEKİNALP   _____
Head of Department, **Aerospace Engineering**

Assoc. Prof. Dr. Dilek Funda KURTULUŞ BOZDEMİR   _____
Supervisor, **Aerospace Engineering Dept., METU**

Examining Committee Members:

Prof. Dr. Cahit ÇIRAY   _____
Aerospace Engineering Dept., METU

Assoc. Prof. Dr. Dilek Funda KURTULUŞ BOZDEMİR   _____
Aerospace Engineering Dept., METU

Assoc. Prof. Dr. Oğuz UZOL   _____
Aerospace Engineering Dept., METU

Asst. Prof. Dr. Ali Türker KUTAY   _____
Aerospace Engineering Dept., METU

Asst. Prof. Dr. Mustafa KAYA   _____
Flight Training Dept., UTAA

                                         Date: 14.07.2014

I hereby declare that all information in this document has been obtained and presented in accordance with academic rules and ethical conduct. I also declare that, as required by these rules and conduct, I have fully cited and referenced all material and results that are not original to this work.

Name, Last Name   : Meltem ÇİFTCİ

Signature   :

ABSTRACT

SYNTHETIC JET APPLICATION ON A FLAPPING AIRFOIL

Meltem, ÇİFTCİ

M.S., Department of Aerospace Engineering

Supervisor: Assoc. Prof. Dr. Dilek Funda Kurtuluş Bozdemir

July 2014, 93 pages

In this study, an active flow control method is studied numerically by the application of synthetic jet over SD7003 airfoil. Steady and unsteady flows over the airfoil are computed by using a Navier-Stokes solver. k-ω SST turbulence model is employed for the investigation of the jet parameters at various angles of attacks and Reynolds numbers. The effect of the jet velocity and the jet angle are investigated to increase the lift to drag ratio. The jet slot size and the jet location are kept constant during the parametric study of the jet application. The parametric study has shown that the jet velocity is the dominant variable. Moreover, it is observed that the application of jet delays the flow separation on the suction side of the airfoil and increases the lift to drag ratio significantly at stall angles of attack. However, for attached flows, application of the jet is observed to be less effective. Unsteady flow conditions are employed in hover mode. The effect of zero-net-mass-flux, vertical translation, Reynolds number and the synthetic jet frequency are studied in figure-of-eight motion. In spite of steady state flow conditions, it is observed that the application of synthetic jet causes a slight decrease on mean lift to drag ratio. Increase of the vertical translation amplitude increases the picks and deeps on instantaneous aerodynamic forces. In addition, it is observed that the synthetic jet frequency do not

alter significantly the instantaneous aerodynamic forces for the given figure-of-eight motion.

ÖZ

ÇIRPAN KANAT KESİTİ ÜZERİNDE YAPAY JET UYGULAMASI

Meltem, ÇİFTCİ

Yüksek Lisans, Havacılık ve Uzay Mühendisliği Bölümü

Tez Yöneticisi: Doç. Dr. Dilek Funda Kurtuluş Bozdemir

Temmuz 2014, 93 sayfa

Bu çalışmada, SD7003 kanat kesiti üzerine yerleştirilen yapay jet uygulaması ile aktif akış kontrolü sayısal olarak incelenmiştir. Kanat kesiti üzerinde oluşan zamanla değişmeyen ve zamanla değişen akış Navier-Stokes akış çözücü kullanılarak hesaplanmıştır. Yapay jete ait parametrelerin farklı hücum açıları ve farklı Reynolds sayıları için incelenmesinde k-ω SST türbülans modeli kullanılmıştır. Jet hızı ve jet uygulama açısı incelemeleri sırasında, kaldırma ve sürükleme katsayıları oranının iyileştirilmesi hedeflenmiştir. Jete ait parametrelerin incelenmesi sırasında jet çıkışı genişliği ve jetin konumu sabit tutulmuştur. Parametre çalışmaları sonucunda jetin hızının baskın bir parametre olduğu anlaşılmıştır. Akış ayrılmasının olduğu durumlarda jet uygulamasının perdövites açısına yakın durumlarda akış ayrılmasını geciktirdiği ve kaldırma ve sürükleme katsayıları oranında artış sağladığı gözlemlenmiştir. Kanat üzerindeki akışın yüzeye yapışık olduğu durumlarda ise jetin etkisi azalmaktadır. Zamana bağlı akış hesaplamaları havada asılı durma konumu için incelenmiştir. Sıfır-net-kütle-akışı (zero-net-mass-flux), düşey öteleme genliği, Reynolds sayısı ve yapay jet frekansı etkileri havada asılı durma hareketi için incelenmiştir. Yapay jet uygulamasının kaldırma ve sürükleme katsayıları oranında azalmaya sebep olduğu gözlemlenmiştir. Düşey öteleme genliğindeki değişimin,

havada asılı durma hareketi yapan kanat kesitinin anlık kuvvetlerinin tepe ve çukur noktalarında değişime sebep olduğu anlaşılmıştır. Sekiz şeklinde hareket eden kanat kesitinin anlık aerodinamik kuvvetlerinin yapay jet frekans değişimi ile önemli ölçüde değişmemektedir.

Anahtar Kelimeler: Çırpan Kanat, Zamana Bağlı Aerodinamik, Mikro Hava Aracı, Yapay Jet Uygulaması.

to my parents and brother...

ACKNOWLEDGMENTS

TABLE OF CONTENTS

LIST OF TABLES

TABLES

LIST OF FIGURES

FIGURES

NOMENCLATURE

Latin Symbol	Description	Units
c	Chord length	m
c_μ	Jet momentum coefficient	-
d_o	Jet orifice	m
f_{jet}	Frequency of the synthetic jet	Hz
F^+	Actuation frequency of the synthetic jet	-
k	Reduced frequency	-
Re	Reynolds number	-
Re_{jet}	Jet Reynolds number	-
t	Time variable	s
T	Period of the motion	s
t/T	Non-dimensional time variable	-
U_{ref}	Reference velocity	m/s
$U\infty$	Upstream flow velocity	m/s
V_{jet}	Jet velocity	m/s
$V_{jet\,max}$	Maximum jet velocity	m/s
Y	Vertical translation	-
x_{te}	Distance from trailing edge	m/s

Greek Symbol	Description	Units
α	Angle of attack	deg
μ	Dynamic viscosity of the fluid	kg/m·s
υ	Kinematic viscosity of the fluid	m^2/s
ω	Angular frequency	rad/s

Abbreviations

2-D	Two-Dimensional
LEV	Leading Edge Vortex
MAV	Micro Air Vehicle
SST	Shear Stress Transformation
TEV	Trailing Edge Vortex
UDF	User Defined Functions

CHAPTER 1

INTRODUCTION

Micro Aerial Vehicles (MAV) and Unmanned Aerial Vehicles (UAV) are becoming popular research areas in last decades because of their wide use such as in the military, surveillance, and public safety applications or for personal usage like amateur interests. They can be used on the missions which can pose danger for human beings, like risk of explosion or natural disaster. For all type of applications, whether for military or civilian, it is important to have good control on UAV, and this can be achieved by manipulating the air flow on wing. Flow control can be explained as changing the flow field around airfoils using additional tools on the airfoil, in order to improve or enhance lift or maneuverability. Different types of applications can be used according to the studies done by Gad-El-Hak et al. [1], such as changing the turbulence structure, or preventing the flow separation on wings [2].

Flow controllers can be classified in two broad categories: passive and active controllers. If the system does not need any external energy, then these types of systems are called passive flow control systems. On the other hand, for active flow control, additional energy supply should be provided to the system. Without supplying energy to the system, passive flow control can be achieved by changing the geometry of the airfoil. For example, Large-eddy breakup devices (LEBU) [3], riblets [4] and wavy walls can be classified as passive flow controllers. According to the studies done in Ref. [2], active flow controllers can also be divided into two groups as predetermined (open-loop) and reactive. In predetermined type of active flow controllers, flow actuators are independently operated from the state of the

flow. As a result, these kind of active controllers do not require sensors. An example of this type of controller can be found in References [5], [6], and [7]. In these studies it is demonstrated that during circulation control of wings, lift enhancement is created by blowing a jet over a rounded trailing edge. This flow can create a coanda effect. In reactive/passive flow control, the actuators are controlled using sensors. The control loop in a reactive technique can be open-loop or closed-loop. Open-loop controller, which is also known as non-feedback controller, is a type of controller which uses only the current state information to compute the input of the system. However, closed-loop controller computes the output depending on the feedback and current input of the system. It is understood in the research done by Mejia [8] that most flow control applications are the closed-loop applications.

In the last ten years, especially for Micro Aerial Vehicle (MAV) and Unmanned Aerial Vehicle (UAV) applications, synthetic jet applications are used as a way of flow control. Most of the experimental studies have shown that synthetic jet applications can offer good solutions to the flow separations or they can be used as ways of enhancing the lift by changing the vortex structures. These applications can be found in detail in References [9], [10], and [11]. Some devices such as synthetic jets or control devices, involving zero-net-mass-flux oscillatory jets have been introduced in Ref. [12]. The purpose behind the synthetic jet applications is to stabilize the boundary layer. This can be done by changing the momentum of the boundary layer, such as air blowing or suction on the airfoil profile. In their study, You and Moin [13] state that amplitude, frequency and the location of the synthetic jets are the basic parameters to have an improved lift or more detached flow on the airfoil. With the increased synthetic jet applications, unsteady computations become important in time, since they can provide detailed simulations, and lower the need for more experimental studies with wide range of parameters. In addition, when compared with the experimental studies, simulations can be solved in more than one case and results can be compared with each other in order to identify different solution methods and different flow cases. Because experimental studies need careful and sensitive orientations, by the help of numerical simulation programs, experimental setup cases can be modeled beforehand and setups can be improved

according to the results. This can be another way of saving time and providing a forehand understanding of the experimental studies. As a result, simulation programs may be used not just during the experiments but before and after the experiments.

1.1 Motivation and Purpose of the Study

For unsteady simulations, hover case for controlled flow fields may pose a new challenge in the sense of zero-net-mass-flux oscillatory synthetic jet applications. Figure-of-eight motion is studied for the current thesis. Computational Fluid Dynamics (CFD) simulations are assumed to give an indication of how the synthetic jet application affects the airflow around an airfoil on hovering mode. Synthetic jet application is investigated for both steady and unsteady flow conditions. The initial studies in this research are performed for steady cases to compare controlled and uncontrolled flow fields. Under steady state studies, effect of the jet velocity according to the free stream flow field velocity is examined. In addition, effect of jet angle is checked. The studies are continued by investigating the effect of angle of attack, and Reynolds number on lift to drag ratio. For unsteady flow conditions, effect of the zero-net-mass-flux synthetic jet is analyzed, while applying figure-of-eight motion to the airfoil. In order to examine the characteristic of hover motion, effect of vertical translation and Reynolds number are studied with synthetic jet applied airfoil, and lastly, effect of the synthetic jet frequency is investigated in hover mode.

1.2 Scope of the Work

This thesis has six chapters. Chapter one gives an introduction to this study. In chapter two, literature survey is done with the main focus on active flow control in steady and unsteady flow conditions with synthetic jet applications. In chapter three, numerical methods are explained and equations for the hovering case and synthetic jet are stated. Chapter four explains steady state studies done over synthetic jet applied profile, and the effects of jet velocity, jet angle, angle of attack, and

Reynolds number are investigated on the SD 7003 airfoil. Results of figure-of-eight motion of SD 7003 airfoil in hover mode with synthetic jet applications are presented in chapter five. In chapter six, concluding remarks are made and future work is mentioned.

CHAPTER 2

LITERATURE SURVEY

Passive and active flow control systems are mentioned in the current chapter. Studies related to synthetic jet applications are listed for flapping airfoil studies including pitching and plunging airfoils.

2.1 Flow Control

Flow control is an area which focuses on reducing the undesired effects in the flow field. It can be defined by the definition which is supplied by Fiedler [1]: "Flow control is a process or operation by which certain characteristics of a given flow are manipulated in such a way as to achieve improvements or a specific technical performance". In other words, using low power actuators, flow control can be done by triggering the natural unsteadiness of the flow so that the flow develops naturally in the desired form [15]. That is why flow control techniques are applied generally when a system does not operate under the design conditions. By using the underlying physical mechanisms, flow separation or flow transition areas can be measured experimentally and this knowledge can be used to control the flow. Some of the most common reasons to use flow control are improving the lift, reducing the drag or reducing the pressure fluctuations around an airfoil.

Flow separation and possible techniques are classified by Fiedler et al. [1] as shown Figure 2.1.
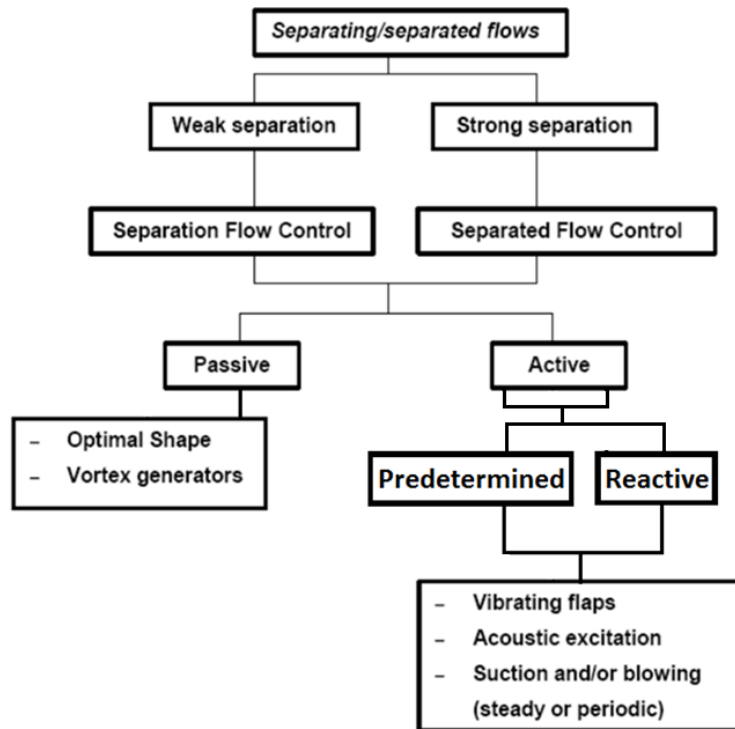
Figure 2.1 Flow management techniques and classification of flow field separation [1, 16].

As seen in Figure 2.1, active flow control can be classified in two groups; predetermined and reactive control loops. Predetermined control loops do not need any sensor to operate because they operate without depending on the particular state of the flow, and they supply steady or unsteady energy into the system. On the other hand, reactive control loops have a sensor to continuously adjust the controller. Feed forward or feedback control can be done by reactive control loops. These two subgroups, active and passive flow control, are classified by Rullan [16].

As mentioned in Chapter 1, flow control can be applied in two ways: passive and active flow controls. Under passive flow control, airfoil design is changed by adding some structures on airfoils; like boundary layer control devices and vortex generators. The general purpose of these passive flow control devices is to achieve higher angle of attack values (α) than normal stalling α. Both C_{Lmax} and α_{CLmax} can be increased by Boundary Layer Control (BLC) devices.
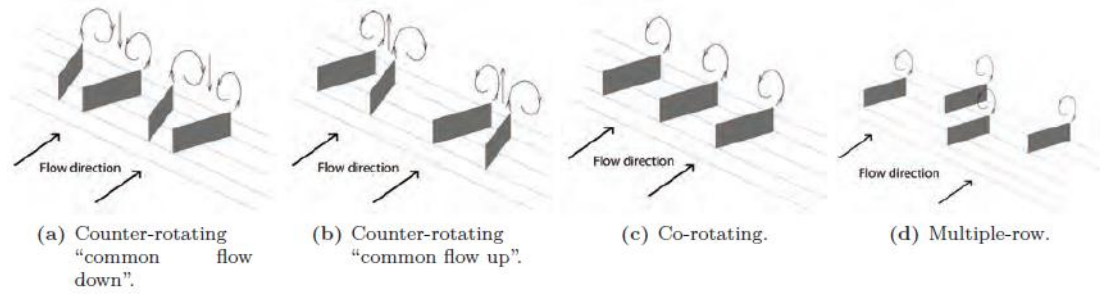
Figure 2.2 Different vortex generator examples [17].

The most commonly known passive flow control devices are Vortex Generators (VG's). VG's can be applied in various shapes and sizes on airfoils, but in general they are in the shape of small vertical plate. They can be employed on an airfoil at an angle with respect to the local free stream flow. Flow control on the suction side of an airfoil can be obtained by appropriate dimensioning and positioning of VG's. In Figure 2.2 *co-rotating* and *counter-rotating* types are presented. In general better results are obtained with *counter-rotating* type VG's [16, 17].

Under the active flow control part, detailed literature survey is presented according to the improvements on the synthetic jet applications.

2.2   Active Flow Control

After Lundwing Prandtl did his pioneering research on boundary layer manipulation in 1904, wide range of techniques have been developed in more than a century of flow control fields. Synthetic jets represent one line of boundary layer flow control. These are used to delay the boundary layer separation on the suction side of an airfoil by either injecting pulses of high-momentum fluid into boundary layer or zero-net-mass-momentum effect. At this point, some attention should be paid to the control of flow separation because the flow-control for boundary layer separation and for separated flow are different cases. The former description represents the flow field control which experiences boundary layer separation from a wall. On the other hand, the latter control type tries to prevent or delay separation and/or reattach the flow [16].

Synthetic jet application, also known as zero-net-mass-flux actuator, can produce a succession of vortex rings without net addition of mass to the flow. Synthetic jets are quite simple when compared with their counterparts due to their abilities such as reducing the drag in turbulent boundary layer, thrust vectoring application of jets, increasing the flow mixing in shear layer, reducing the flow separation, and heat transfer augmentations. Synthetic jets have the ability to create unsteady forcing. It is known that this forcing is more effective when compared with steady forcing. By the help of unsteady forcing effect, flow separation can be reduced on the upper side of the airfoil at high angle of attack cases. Moreover, zero-net-mass-flux jet applications are important because they can eliminate the need for piping system or additional energy supply system on an airfoil. These types of jets introduce linear momentum to the system without net mass injections. Therefore, they can eliminate the systems which are supplying constant suction or blowing to the system. In other words, the need for the piping system on an airfoil can be eliminated [17].

Siegert et al [18] used a pulsed micro flap on the leading edge of a wing to control separated flow. The study focused on the position, amplitude, and frequency of the flap motion for high angle of attack values. It was found that periodic perturbations can organize and improve the average strength of the shedding vortices and may increase the lift in a time average sense by as much as 50%. A following study was done by Hsiao et al. [19]. By making some modifications on their design, they found that larger amplitudes of excitation motion produced a larger lift coefficient.

Miranda et al. [15] showed that a small oscillating flap which was placed on the leading edge of a circular arc sharp edged can be used to create the necessary flow disturbance. In order to affect the flow in a desired way, unsteady excitations were created at the leading edge by the pulsing flap. This study demonstrated that the maximum effect on separated flow can be achieved when the excitation frequency is near the vortex shedding frequency. However, in order to affect the formation of vortices, the flap must penetrate the separated flow region. This explains why the effect reduced when the angle of attack was increased. As a result of this study, it is also found that oscillating flaps are not limited in their frequency domain. On the

other hand, an oscillating flap can generate a wide range of effective frequencies for the control of separated flow over a sharp edged airfoil.

On a NACA 0015 airfoil, oscillatory blowing was applied to the trailing edge by Seifert et al. [6]. In the scope of that study, synthetic jets which are mounted on a two dimensional slot located on the upper surface above the hinge of flap were activated. The airfoil positioned at 20° of angle of attack. It is concluded that steady blowing had no effect on lift or drag. On the other hand, modulated or pulsed blowing can generate an increase in lift and cut the drag half.

A two dimensional piezoelectric diaphragm with the characteristics of 0.5 mm wide and 76.2 mm long orifice was investigated by Allen and Glezer [20] Working frequency was 1000 Hz and the maximum velocity at the orifice was 20 m/s. For the studied orifice size and the peak value of the measured velocity, Reynolds number was determined as 6000 for this study.

Different multi-element airfoils with the application of an oscillatory blowing synthetic jet were studied by Seifert et al. [21]. In order to understand the parameters affecting the performance of an airfoil, flow separations were observed on the suction side of an airfoil. It is understood that if the separation was caused by the flap side but not by the main body, then applying a jet blowing near the leading edge instead of at the leading edge could decrease the separation ratio.

An experimental study on zero-net-mass-flux type synthetic jets was done on a round shaped orifice by James et al. [22]. Turbulent water jet was used and actuated by a resonantly driven diaphragm. By the application of zero-net-mass-flux synthetic jet, the flow is formed by axisymmetrically entrained fluid. It is understood after the study done by Smith et al. [23] that a synthetic turbulent jet could be achieved by a train of vortex rings, which were formed at the edge of a circular orifice with a vibrating membrane.

With the purpose of thrust vectoring and small scale motion manipulations in conventional air jets, synthetic jets were used in Ref. [24]. The actuators were positioned along the long sides of the primary rectangular jets and operated at one and two orders lower magnitudes. The turbulent dissipation was improved and directly exited small scale motions were achieved by the millimeter scale high aspect ratio actuators.

Synthetic jet actuators can be chosen to achieve dynamic blowing and suction. The synthetic jet actuators whose working principles are based on piezoelectric devices are the most efficient ones at the resonance frequency of the device and limited by the natural frequency of the cavity. A small positive displacement machine with six reciprocating compressors was placed by Rao et al. [25] on a NACA 0015 airfoil. This device was driven by two DC motors. These piston/compressors generated zero-net-mass-flux synthetic jets. It is found that flow separation control can be done as high as 25° angle of attack values, and 45 m/s free stream velocities [25].

Actuator types also can have two broad subgroups, piezoelectric and electro hydrodynamic. The former group has wider application areas when compared with electro hydrodynamic actuators. A piezoelectric actuator which had a piezoelectrically driven cantilever mounted flush with a flow wall was designed in Ref. [26]. This design could be applied in large arrays to control the transitional and turbulent boundary layers actively. The resulting flow disturbance over the actuator is a quasi-steady pair of counter rotating streamwise vortices which has strengths controlled by the amplitude of actuator drive signal. The electro hydrodynamic group was introduced in Ref. [27]. Flush mounted electrodes were used in a flat plate which is driven by a DC power supply. This type of actuator was used to create a plasma sheet. This plasma sheet induced acceleration in the flow close to the surface, which increases the momentum and introduce a faster reattachment.

Multiple synthetic jet application was performed experimentally in Ref. [28]. According to this study, in order to produce a single coherent synthetic jet from a multiple jet configuration which is positioned in an array, a minimum spacing

between actuators was needed. The amount of coherent vorticity occurring in the fluid could be decreased or increased by the combined effect of yaw angle and orifice spacing of the multiple jets.

The application of synthetic jet on the upper side of an airfoil and smoke visualization was performed on NACA0036 airfoil by Martin et al. [29]. The results of this study are represented in Figure 2.3. As a result of this study, it can be seen that even at zero angle of attack values, flow separation could be observed and becomes more severe at 10^0 angle of attack. The flow separation could be decreased by application of synthetic jet near the leading edge and flow reattachment could be seen clearly for the zero angle of attack position.
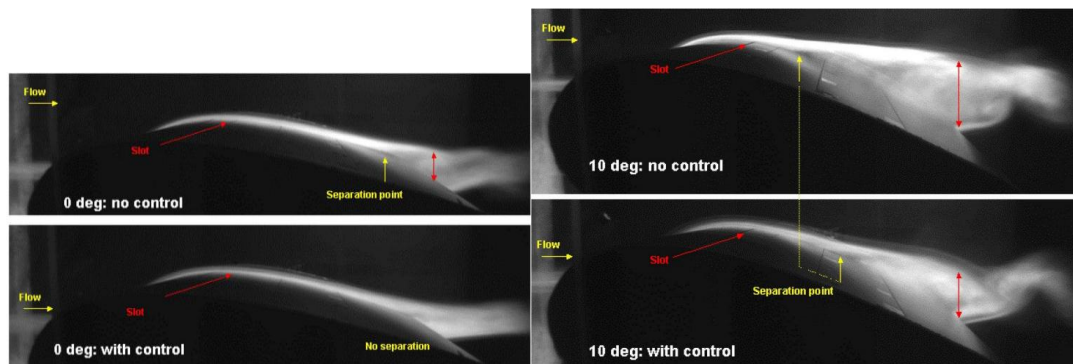
Figure 2.3 Smoke visualization with and without active flow control at $\alpha = 8^o$ and $\alpha = 10^o$ [29].

Many researchers have investigated the characteristics of synthetic jets as a function of location of the orifice, size of the orifice, type of the blowing/suction waves, frequency of the blowing/suction, and velocity of the jet. Most of these studies are done both experimentally and numerically, but the models are designed assuming that there is a cross flow over an airfoil. That is why the effect of the Reynolds number is also searched by many researchers for the linear flow regimes which correspond to the low Reynolds numbers of order 10^5.

Some studies in the literature focused on the behavior of synthetic jet applications as in Ref. [30] and Direct Numerical Simulation (DNS) solutions were used to model synthetic jets. In order to validate the results, they used the result of experiments conducted by Smith and Glezer [23]. Except the corners, the velocity profile of the synthetic jet can be well predicted with the applied solution method. The comparison of the experimental and numerical results is shown in Figure 2.4. With the application of DNS method, the velocity profile could be well predicted except at the corners of the orifice as shown in Figure 2.4.
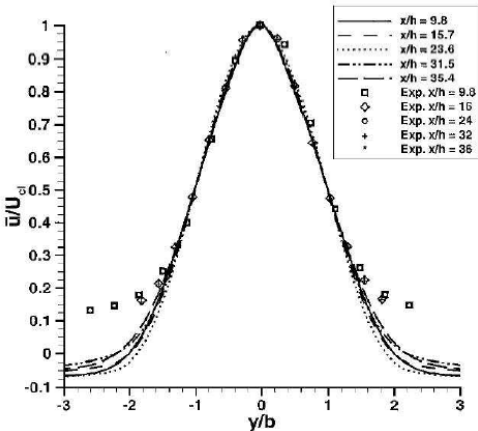
Figure 2.4 Comparison of numerical and experimental studies of mean velocities in terms of the distances from the orifice [30].

Mossi et al. [31] searched experimentally three different types of piezoelectric actuators which are enclosed on a cavity with a slot in order to produce a synthetic jet. Bimorphs and pre-stressed curved unimorphs (thunder) are the actuator types studied in this research, and a new type of actuator, which is called Radial Field Diaphragms (RFD) with inter-digitated electrodes, was designed. These studied piezoelectric actuators have zero-net-mass-flow rates, and were tested in a constant size equipped cavity with a slot. In this study, the actuators were tested for different types of wave forms - a sine wave, a square wave and a saw wave, and different frequencies along with 2 mm fixed slot exit being used for all type of actuators. It is understood from this study that all of the actuators showed maximum speed at 5 Hz

12

with a saw tooth waveform being related not only to the actuator displacement performance but also to the cavity size and geometry.

An experimental study of flow separation over a synthetic jet applied to NACA 0015 airfoil is performed in Ref. [32]. Flow separation on a controlled, and uncontrolled airfoil was performed, and the results are reported. During the experimental studies, the NACA 0015 airfoil profile with 375 mm chord length was used. The slot of actuator had a 2 mm width across the entire length of span and was placed at 12% of the chord measured from the leading edge, on the suction side of the airfoil. The location was determined to leave enough space for the synthetic jet actuator inside the airfoil [33]. With synthetic jet application, the trailing edge stall is effectively controlled and produces further enhanced lift coefficient up to the angle of attack approximately 18°. However for angle of attack values greater than 18°, the controlled airfoil has a sharp drop of the lift coefficient due to the leading edge stall. This is caused by the formation of a separation bubble near the leading edge. Although the massive stall is reached, the synthetic jet application increases the maximum lift coefficient when compared with the uncontrolled case, but the lift augmentation amount is relatively small. In accordance with these positive effects of the synthetic jet application, the mechanisms for separation control and boundary layer modification by flow control have not been identified clearly.

Because the control performance of the synthetic jets rely on parameters such as location of the actuation, frequency and amplitude, an extensive parametric study is necessary for optimization of the control parameters. You et al. [33] performed the parametric study and compared its results with the experimental research data of the Gilarranz et al. [32] for both controlled and uncontrolled situations of a NACA 0015 airfoil. Effect of flow control on boundary layer properties, flow separation, and lift improvement were discussed within that comparison.

Synthetic jet application and optimization study was performed on NACA 0015 airfoil by Akcagoz [34]. Optimization was done by the method of Response Surface Methodology (RSM). Over a C-grid application, unsteady, turbulent, Navier-Stokes

equations were solved. The parameters affecting characteristics of synthetic jet were studied such as jet velocity, frequency, location, and angle. Flow fields around airfoil for angle of attack values of 18° and 25° were compared with experimental results and numerical calculations (Figure 2.5). It was understood that synthetic jet applications for active flow control could be a good solution to the suction side flow separations [34].
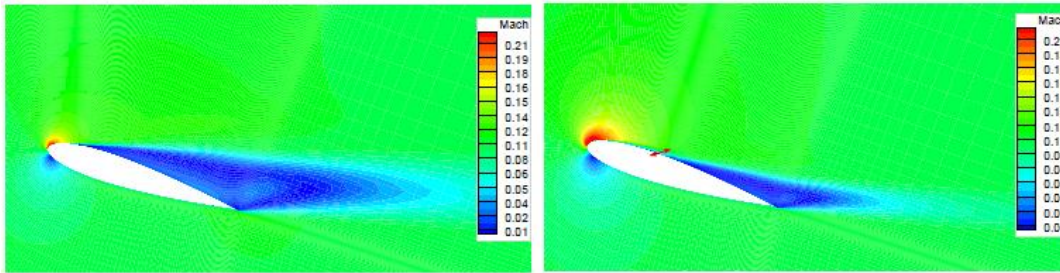
Figure 2.5 Comparison of average Mach number contours at $\alpha = 18^o$ value without (a) and with (b) synthetic jet application [34].

Kang et al.[35] compared experimental and numerical results for pitching and plunging SD7003 airfoil profile at $1x10^4$, $3x10^4$ and $6x10^4$ Reynolds numbers in a water tunnel. In their study, computational results for modified shear stress transport (SST) and Original SST methods were compared with experimental results. The experimental part of that study was carried out by University of Michigan (UM) and Air Force Research Laboratory (AFRL) using the phase-averaged Particle Image Velocimetry (PIV). According to the pure plunging case results, the comparison of original SST turbulence model and modified SST turbulence model showed that modified version could provide better prediction for the vertical structure with reattachment areas of the flow separation. The numerical results for that study are represented in Figure 2.6.
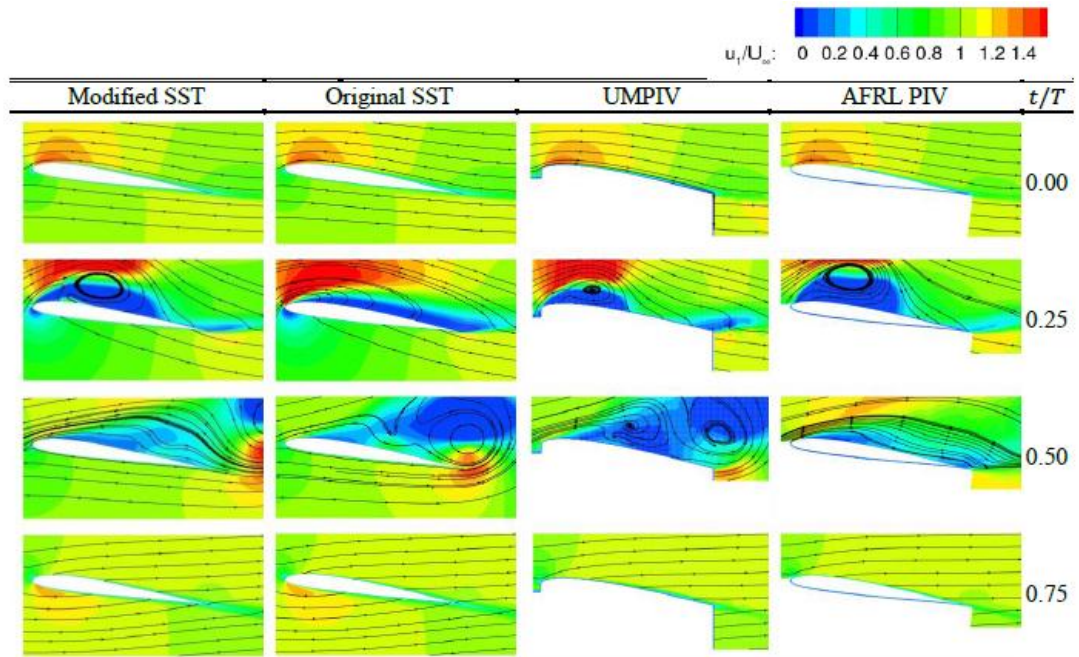
Figure 2.6 Normalized mean streamwise velocity contours and streamlines over pure plunging SD7003 airfoil at k = 0.25, λ = 0.0, and Re = 6x10^4 from numerical models, modified SST and original SST, and experimental results, conducted at UM and AFRL [35].

In this figure, reduced frequency of pitch or plunge movements are represented with k, k=πfc/(U$_\infty$), λ represents the ratio of pitch-amplitude to plunge-induced angle of attack. According to this study, the agreements between the computational and experimental results were favorable when the flow was largely attached to the upper surface. When the flow started to experience massive separations, noticeable differences could be seen in phase and also in the size of the flow separation. In the same study, the pitching and plunging case results were also examined for k = 0 and 0.25 and λ=0.6. The results are presented in the Figure 2.7 at Re = 6x10^4.
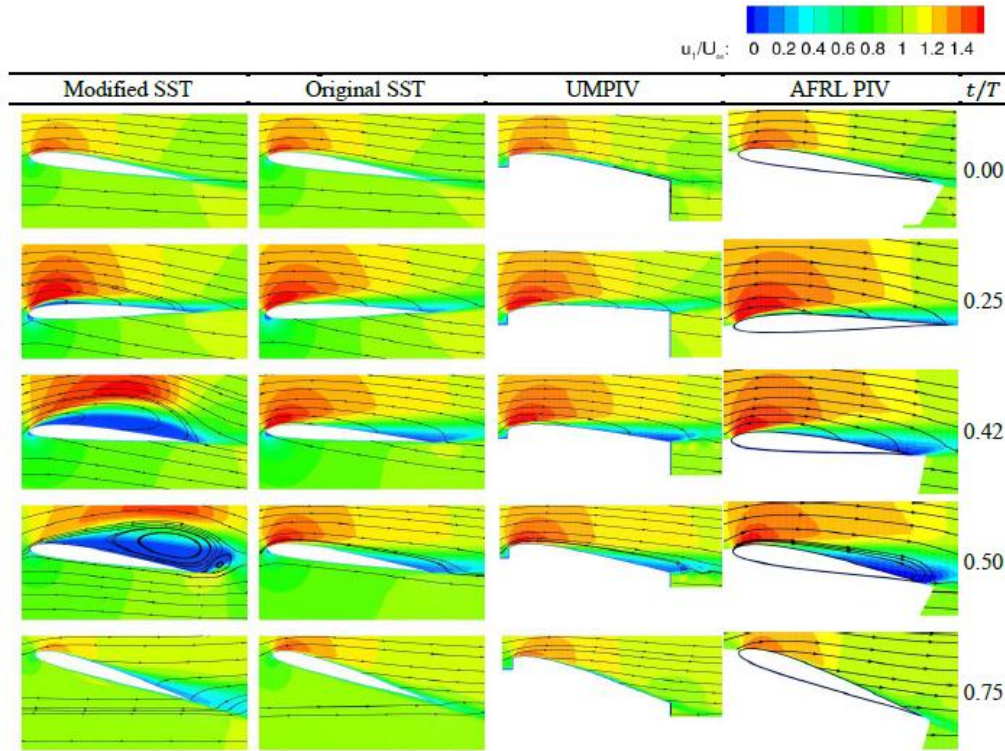
Figure 2.7 Normalized mean streamwise velocity contours and instantaneous streamlines over pitching and plunging SD7003 airfoil at k=0.25, λ=0.6, and Re=6x10^4 from numerical models, modified SST and original SST, and experiments from UM and AFRL [35].

It can be concluded from this study that flow tends to separate substantially under modified SST model because of different predicted eddy viscosity levels. Moreover, Re = 3x10^4 and Re = 6x10^4 results indicated that original SST model has more attached flow simulation. On the other hand, experimental and modified SST model results show that the flow was more separated than the result of original SST model. This could be because original SST model limits the production of turbulence kinetic energy, which reduces the eddy viscosity [35].

Another computational study was done Riazi [36] on SD7003 airfoil for low-Reynolds number application. Reynolds number was taken as 1x10^4, and steady uniform synthetic jet application was performed on the low-pressure side of airfoil. For different angle of attack values ranging between 0 to 12 degrees, effect of jet application was examined numerically. Applied jet orifice to chord ratio was kept at

0.5. It was understood that synthetic jet application could improve the lift coefficient value [36].

CHAPTER 3

NUMERICAL METHOD

In this chapter, governing fluid equations, computational grid, boundary conditions, and methods used are explained. After explaining the equation for incompressible, two dimensional, constant properties Navier – Stokes equation, User defined functions (UDFs) and boundary conditions are defined. Structured O-type grid generation of hovering flight is performed on commercially available CFD Fluent 13.0. Hovering flight is applied to the airfoil by User Defined Functions (UDFs).

3.1   Governing Equations

During figure of eight motion Unsteady Reynolds Averaged Navier Stokes (URANS) equations are solved. Incompressible, two-dimensional, constant property Navier –Stokes equations are given as [37].

$$\frac{\partial}{\partial x_i}(u_i) = 0 \tag{3.1}$$

$$\frac{\partial}{\partial t}(u_i) + \frac{\partial}{\partial x_j}\left(u_j u_i\right) = -\frac{1}{\rho}\frac{\partial p}{\partial x_i} + \nu \frac{\partial^2}{\partial x_j^2}\{u_i\} \tag{3.2}$$

Where t is time, ρ is density, p is pressure, ν is kinematic viscosity. x_i is the ith component of position vector, and u_i is the velocity component in i^{th} direction.

During parametric study of jet application Unsteady Reynolds Averaged Navier Stokes (URANS) equations are coupled with Menster's Shear Stress Transport (SST)

turbulence model. For incompressible, two dimensional flow, the URANS equations with continuity equation are as follows [14, 37]:

$$\frac{\partial}{\partial x_i}(u_i) = 0 \tag{3.1}$$

$$\frac{\partial}{\partial t}(u_i) + \frac{\partial}{\partial x_j}(u_j u_i) = -\frac{1}{\rho}\frac{\partial p}{\partial x_i} + \frac{\partial}{\partial x_j}\left\{(v + v_t)\frac{\partial u_i}{\partial u_j}\right\} \tag{3.2}$$

$$\frac{\partial k}{\partial t} + \frac{\partial}{\partial x_j}(u_j k) = \frac{\tau_{ij}}{\rho}\frac{\partial u_i}{\partial x_j} - \beta^* \omega k + \frac{\partial}{\partial x_j}\left\{(v + \sigma_k v_t)\frac{\partial k}{\partial x_j}\right\} \tag{3.3}$$

$$\frac{\partial \omega}{\partial t} + \frac{\partial}{\partial x_j}(u_j \omega) = \frac{\gamma}{v_t}\frac{\tau_{ij}}{\rho}\frac{\partial u_i}{\partial x_j} - \beta \omega^2 + \frac{\partial}{\partial x_j}\left\{(v + \sigma_\omega v_t)\frac{\partial \omega}{\partial x_j}\right\}$$

$$+2(1 - F_1)\sigma_{\omega 2}\frac{1}{\omega}\frac{\partial k}{\partial x_j}\frac{\partial \omega}{\partial x_j} \tag{3.4}$$

$$v_t = \frac{a_1 k}{max(a_1 \omega; \Omega F_2)} \tag{3.5}$$

$$\tau_{ij} = \rho v_t \left(\frac{\partial u_i}{\partial x_j} + \frac{\partial u_j}{\partial x_i}\right) - \frac{2}{3}\rho k \delta_{ij} \tag{3.6}$$

Where v_t is eddy viscosity, Ω is the absolute value of vorticity, k is the turbulent kinetic energy, ω is the specific dissipation rate, δ_{ij} is the kronecker delta, and τ_{ij} is the stress tensor. a_1, $\sigma_\omega, \sigma_k, \beta,$ and β^* are the modeling constants in Menter's SST formulation [14, 42]. F_1 and F_2 are the blending functions which allows switching between $k - \varepsilon$ model out of the boundary layer. In the prediction of adverse pressure gradient flows, Menter's SST formulation stands as the most advanced two-equation turbulence model [14, 43]. The mass of the airfoil was ignored throughout the equations. In addition, the working fluid was chosen as air. The body force term was dropped from the governing equations. On moving two-dimensional grid, the sets of equations were solved with the pressure based finite volume solver. Convective and

diffusive terms were treated using second order accurate schemes. The pressure and velocity coupling were handled by SIMPLE algorithm [14, 44].

3.2 Computational Grid and Boundary Conditions

The main geometry in this thesis was chosen as SD7003 airfoil. The profile has the Reynolds number application range between $0.5x10^5$ and $2x10^5$. The steady state results were validated with experimental studies in literature [38, 39]

The applied grid domain for both steady state jet parametric study and hovering cases was O-type grid. For steady state cases, mesh structure was stationary and there was no motion prescribed for the mesh domain. On the other hand, for hover motion cases, User Defined Functions (UDFs) were applied to move the airfoil and grid domain in the hover mode around a pivot point with a figure-of-eight motion. The surface of airfoil was chosen as no-slip wall boundary condition. For steady state cases, half of the free stream boundary was set as velocity inlet, and the rest of the free stream boundary was set as pressure-outlet as shown in Figure 3.1. However, for hover cases, the all free stream grid domain was set as pressure-outlet boundary condition. On both cases, jet application was placed on aerodynamic center of the airfoil, 0.25 chords down from the leading edge of airfoil, and the boundary condition was set as velocity inlet.

In Figure 3.1, hybrid grid structure, which consists of triangle and rectangular elements, is shown around SD7003 airfoil. For both steady state and hover cases, the grid had a diameter 30 times bigger than the chord of the airfoil. In order to handle boundary layer effect, on the mesh structure, dense structural mesh was applied near the airfoil profile. The first cell on the airfoil has y^+ value equal to 1, and 30 grid points which are normal to flow direction are applied for the boundary layer effect.
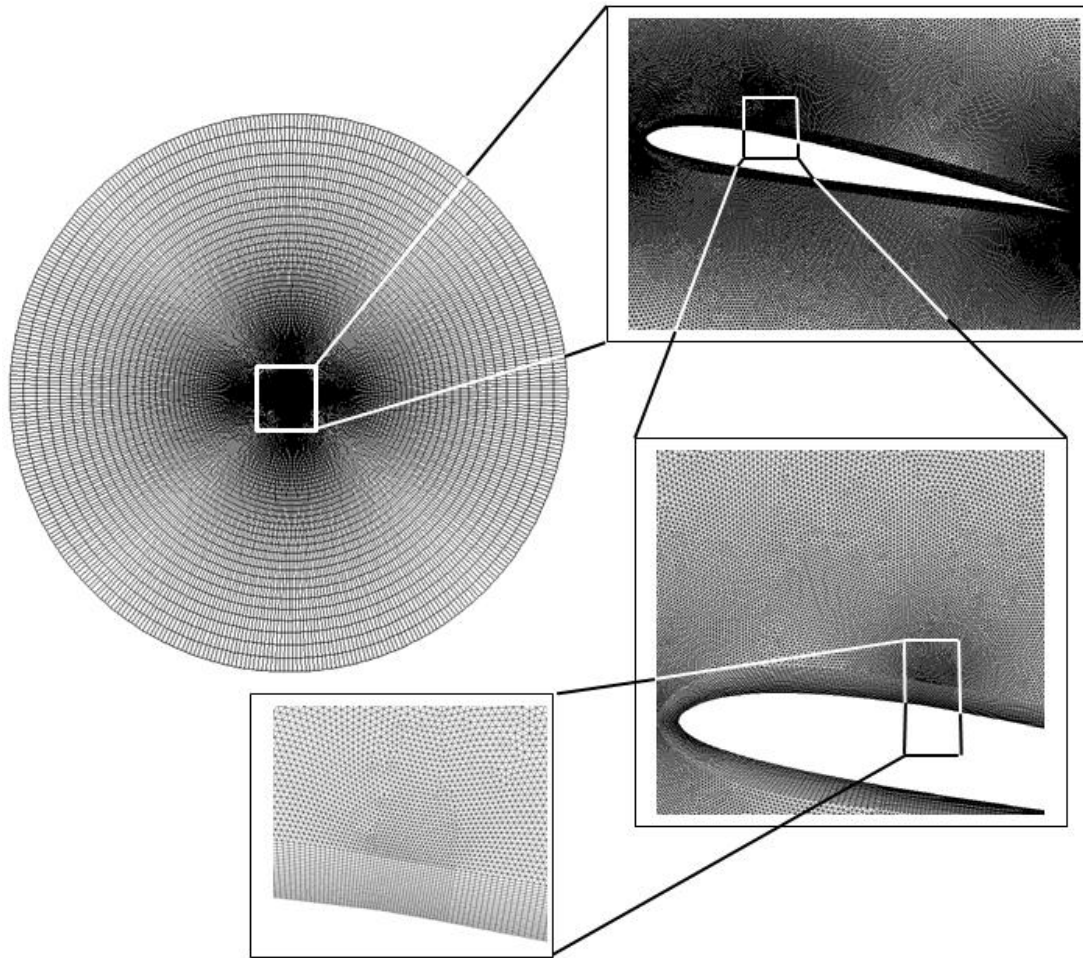
Figure 3.1 Hybrid grid around SD7003, for farfield, and its distribution close to the airfoil and jet location.

In addition to leading and trailing edge dense mesh applications, on the synthetic jet area, dense mesh was performed to solve velocity and pressure changes more adequately. Ratio of the orifice size (d_o) to chord (c) was kept as 0.03. For hover cases, overall outlet boundary condition was taken to be pressure outlet. Whole grid domain was moved with the motion specified in User Defined Functions (UDFs). Jet orifice was always defined as velocity inlet boundary conditions for both steady and unsteady flow cases. Airfoil surface except the orifice was defined as no-slip wall boundary condition.

3.3 Grid Refinement Studies for Steady Cases

Refinement studies were carried out before assessing all the case studies. In order to examine grid independency, three different meshes have been applied. Details regarding the number of cells, and synthetic jet area mesh refinements applied in three different meshes are listed in Table 3.1. A medium grid distribution with 175 282 cells was refined and coarsened with ratio of 2 (Table3.1). The jet slot is defined by 15, 20 and 30 point for the coarse, medium and fine grids, respectively. O-type hybrid grid was applied for all cases. Schematic view of the synthetic jet on the airfoil is shown in Figure 3.2.

Table 3.1 Details of applied different meshes for grid refinement study.

	Number of cells in flow domain	Number of cells on synthetic jet area
Coarse mesh	90 124	15
Medium mesh	175 282	20
Fine mesh	302 492	30
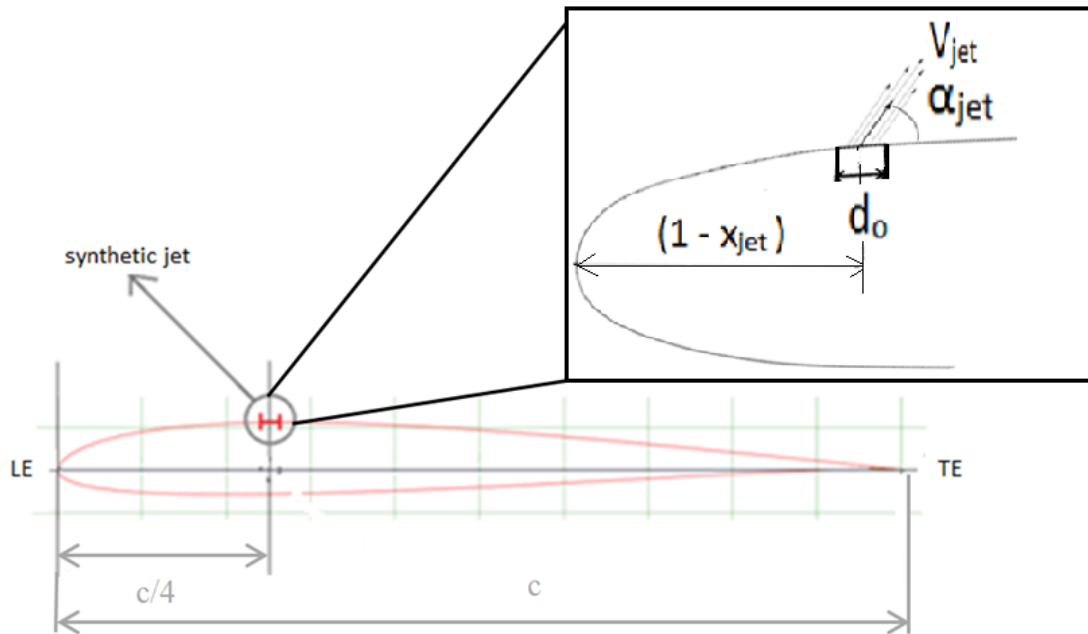
Figure 3.2 Schematic presentations of leading and trailing edges, aerodynamic center, and position of applied synthetic jet (c/4) location.

For grid refinement study, $Re = 6 \times 10^4$ case was solved with coarse, medium and fine meshes, and resultant lift and drag coefficients were compared to each other under different angle of attack values. Lift coefficient to drag coefficient graph was obtained. The numerical results obtained in the present were compared with the wind tunnel test results done by Ol et al. [38] and Selig et al. [39]. Related results are listed in Figure 3.3 and 3.4. The lift and drag coefficient versus angle of attack results revealed that the results obtained from medium and fine grids are similar. Thus, medium grid with 175,282 cells found adequate for the rest of this study.
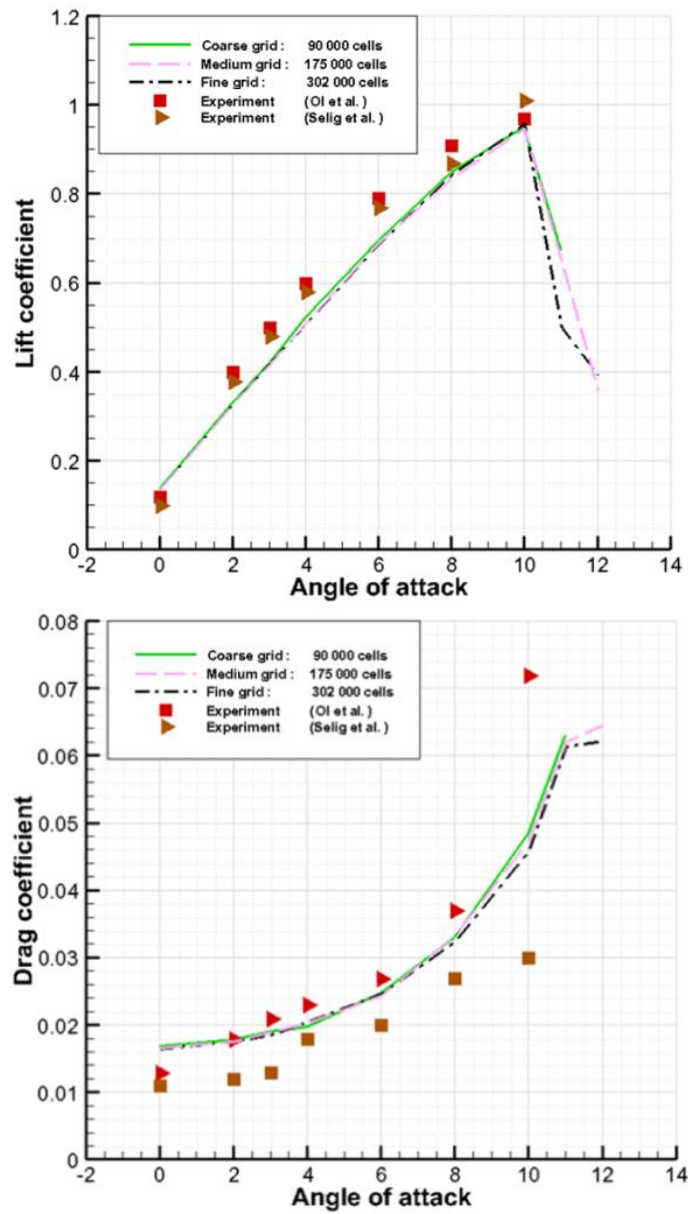
Figure 3.3 Lift coefficient to angle of attack and drag coefficient to angle of attack comparison of grid sensitivity at Re = $6x10^4$, no jet.
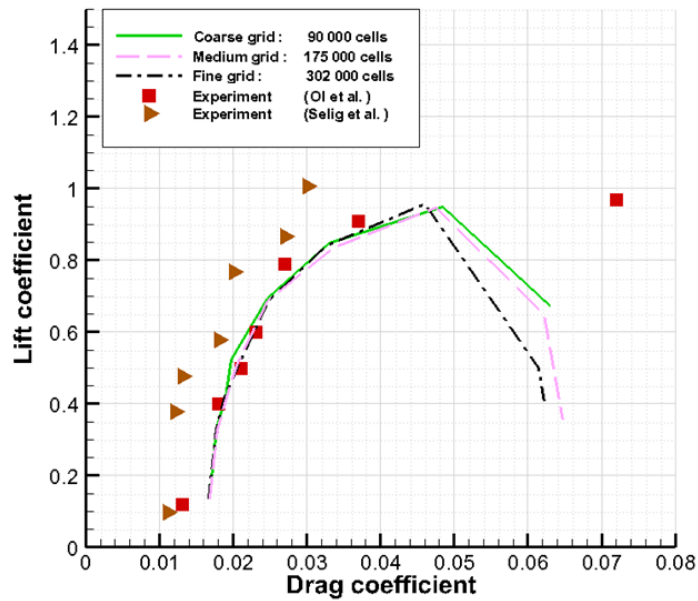
Figure 3.4 Lift coefficient to drag coefficient comparison of grid sensitivity at Re = 6x10^4, no jet.

Equations of lift and drag coefficients are given in the Equation 3.7 and 3.8 where (c) is chord length, (V) is velocity, (q) is dynamic pressure and (L) is lift force. Similarly, (D) is drag force, (ρ) is density. Total force and force direction equations are given in Equations 3.10 and 3.11.
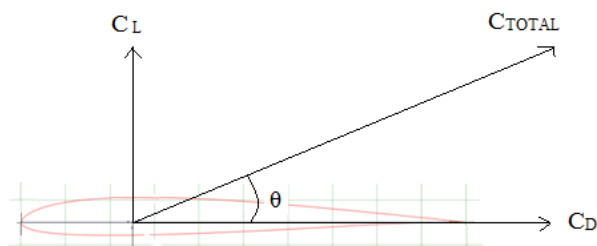
Figure 3.5 Schematic presentations of lift, drag and total force directions on airfoil.

$$C_L = \frac{L}{\frac{1}{2}\rho V^2 c} \qquad (3.7)$$

$$C_D = \frac{D}{\frac{1}{2}\rho V^2 c} \qquad (3.8)$$

26

3.4 Hovering Kinematics

For hovering motion, "figure-of-eight" movement was implemented. This movement has three degrees of freedom. Details of hovering motion are given in Chapter 5. Figure of eight motion can be defined by [14],

$$x(t) = 2\,c\,\sin(\omega t + \pi/2) \tag{3.9}$$

$$y(t) = Y\,c\,\sin(\omega\,t) \tag{3.10}$$

$$\alpha(t) = \pi/2 + \pi/2\,\sin(\omega t) \tag{3.11}$$

where $x(t)$ and $y(t)$ are instantaneous horizontal and vertical coordinates of the pivot point in inertial frame of reference. c is chord length of airfoil profile. ω is circular frequency which can be defined as $\omega = 2\pi f$, where f is frequency of the hovering motion. Y is the amplitude of vertical translation of the airfoil. In these set of equations, $\alpha(t)$ defines the flapping motion of the airfoil, and these motions are defined as Lissajous curve. General shape of Lissajous curves is defined by the coefficients of ωt terms in the set of equations above. The amplitude and the vertical and horizontal translation of airfoil can be controlled by the coefficients of $\sin(\omega t)$ term. However, these coefficients do not change the general shape of hover motion, but change only the amplitude and translation in two dimensions.

Reynolds number (Re) and reduced frequency (k) are the two significant non-dimensional parameters in the flapping wing aerodynamics. Reynolds number is the ratio of inertial force to viscous forces. However, in hovering cases, free stream flow velocity is determined by the maximum velocity of the hovering motion of the airfoil, and can be calculated as using reference free stream flow velocity U_{ref}, given in Equation 3.14. Reynolds number calculation for hovering cases is given in Equation 3.12. Reynolds number related to Jet velocity is given in Equation 3.13. The reduced frequency is the ratio of vertical velocity to the axial velocity and the equation of reduced frequency for hovering cases is given in Equation 3.14 [14].

$$Re = U_{ref}c/\nu \tag{3.12}$$

$$Re_{jet} = V_{jet\,max}d_o/\nu \tag{3.13}$$

$$U_{ref} = 2\,wc\,\sqrt{1 + Y^2} \tag{3.14}$$

$$k = \frac{1}{2}\frac{max(\dot{y})}{max(\dot{x})} = \frac{2wcY}{4wc} = \frac{Y}{2} \tag{3.15}$$

3.5 Time-Step Refinement Studies for Hover Cases

The time step refinement was performed for unsteady hover cases. Grid domain outer surface was applied as pressure outlet. Solver type was applied as laminar. The effect of time-step size resolution was examined. Time-step studies were done for three different time steps over one period of hover motion (T). 200, 400 and 800 time-steps (Δt) over one period hover motion were applied. The comparison of the coefficients of lift and drag predictions over one period of hover movement by using different step sizes are shown in Figure 3.6. During time-step refinement study, Reynolds number was kept constant at 1×10^3. The amplitude of vertical translation (Y) of hover motion was kept equal to 1, and frequency of the hover motion was taken as 0.1 Hz. Synthetic jet was kept as steady blowing over the all time-step of refinement studies and the velocity of the synthetic jet was kept equal to 0.1 times of the reference velocity of the motion of the airfoil (Eq. 3.14). Since the lift and drag forces in hover mode are the vertical and horizontal components of the net force applied on the airfoil, extreme values of drag force when compared with conventional fixed-wing aerodynamics can be explained by that sign convention. As shown in Figure 3.4, 400 and 800 time-steps were applied over nine period of the hover motion to examine the changes of lift and drag coefficients. Based on the time averaged lift and drag coefficient values over 1 and 9 cycles of hover motion, it can be deduced that the resolution of the 400 time-steps per cycle resolution is refined enough and predicts an averaged lift and drag coefficients within 4.8% of that using

800 time-steps per cycle. As it can be seen in Figure 3.6, over one period of motion, 400 time-steps can be used to demonstrate the behavior of the coefficients of lift and drag, and can be applied for further studies.
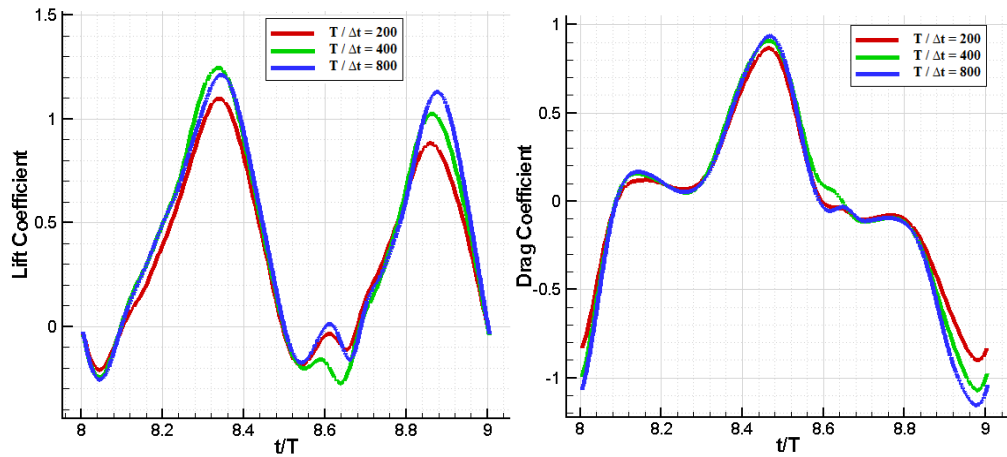
Figure 3.6 Time histories of lift (left) and drag (right) coefficients with different time-steps in hover motion over one period.

3.6 User Defined Functions

User Defined Functions (UDFs) are subroutines that can program the solver dynamically in order to improve the abilities of the standard features of commercial code Ansys FLUENT [37]. They can be used to define specific boundary conditions, initial conditions, material properties, mesh domain movement, or source terms for flow domains [40]. One UDFs file can contain more than one source file. They can be either compiled or interpreted to the solver to apply or insert the solver type. In this thesis, UDFs have been used to specify jet wave types. In Chapter 5, UDFs are applied both to specify synthetic jet on the orifice and to move mesh domain dynamically to supply hover mode in figure-of-eight motion.

CHAPTER 4

STEADY STATE CASE STUDIES

In this chapter, results of jet application on an airfoil are introduced. Different solutions as laminar, k-ω, and k-ω shear stress transformation (SST) are implemented and results are compared with experimental studies [38, 39]. Constant blow and constant suction jet application parameters are examined under steady state conditions. Effect of jet velocity with respect to free stream velocity, synthetic jet angle, angle of attack, and Reynolds numbers are introduced.

4.1 Validation Cases

Validation cases are conducted under steady state and unsteady flow conditions. Numerical results of steady state case are compared with experimental results obtained by Ol et al. [38] and Selig et al [39]. Synthetic jet application is performed under unsteady flow conditions, and results are compared with the study done by Nakhla et al. [41]

4.1.1 Steady State Case

Steady state simulation of SD7003 airfoil has been performed. For $6x10^4$, laminar and turbulence models (k-ω and k-ω SST) are compared. For this study no jet is applied on the airfoil. In Figure 4.1 comparison of lift coefficients versus to angle of attack can be seen. According to this case study, it is understood that k-ω SST model can produce closer results to the experimental results. "At the design Re of $6x10^4$,

convergence is difficult, and depends to some extent on user choice of paneling and execution parameters" [38, 39]. Experimental results are obtained from figures by Ol et al. [38], and Selig et al. [39].
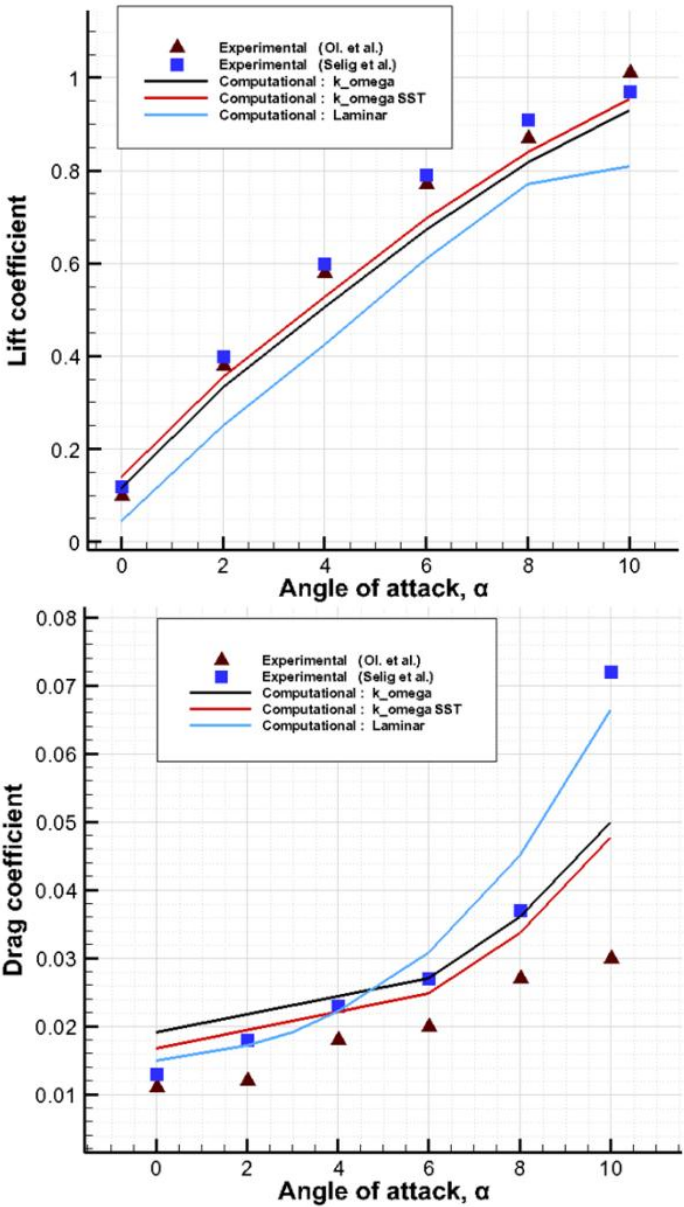
Figure 4.1 Comparison of lift and drag coefficients versus angle of attack values for different model types.

4.1.2 Flowfield around airfoil at α = 8° with synthetic jet application

The unsteady flowfield over SD7003 airfoil with jet flow was computed using the optimum grid size determined in grid refinement study. Flowfields after the application of synthetic jet were compared with the numerical data of Nakhla H. et al [41] at α = 8° and at Re = 5.4x10⁴. SD7003 airfoil with a chord length of 0.025m was used. The ratio of jet orifice width d_o to the airfoil chord length c was fixed, d_o/c = 0.005. The jet orifice was embedded 0.3 chord length downstream from the leading edge on the airfoil suction side, where a laminar separation zone forms [41]. The non-dimensional actuation frequency F^+ (Eq. 4.1) and the jet momentum coefficient C_μ (Eq. 4.2) are defined as

$$F^+ = \frac{f_{jet}\, x_{te}}{U_\infty} \tag{4.1}$$

$$C_\mu = \frac{(\rho d_o V^2)_{jet}}{(\rho c U^2)_\infty} \tag{4.2}$$

where f_{jet} is actuation frequency, x_{te} is the distance from actuator to the trailing edge of the airfoil, U_∞ is upstream flow velocity and V_{jet} is jet velocity. It is stated by Mc Cormick [43] that the jet momentum coefficient should generally exceed the value of 0.002 for any substantial effects on the flow to be observed. F^+ was taken equal to 1 and C_μ kept equal to 0.002. The expression in Eq. 4.3 was employed at the orifice of the jet to obtain the fluctuation velocity.

$$V_{jet} = 0.5cos(\omega_{jet}t) \tag{4.3}$$

where $\omega_{jet} = 2\pi f_{jet}$ was kept equal to 9. The actuator oscillation period was $T = 0.7$ and oscillation frequency was $f_{jet} = 1.43$.

(a)

(b)
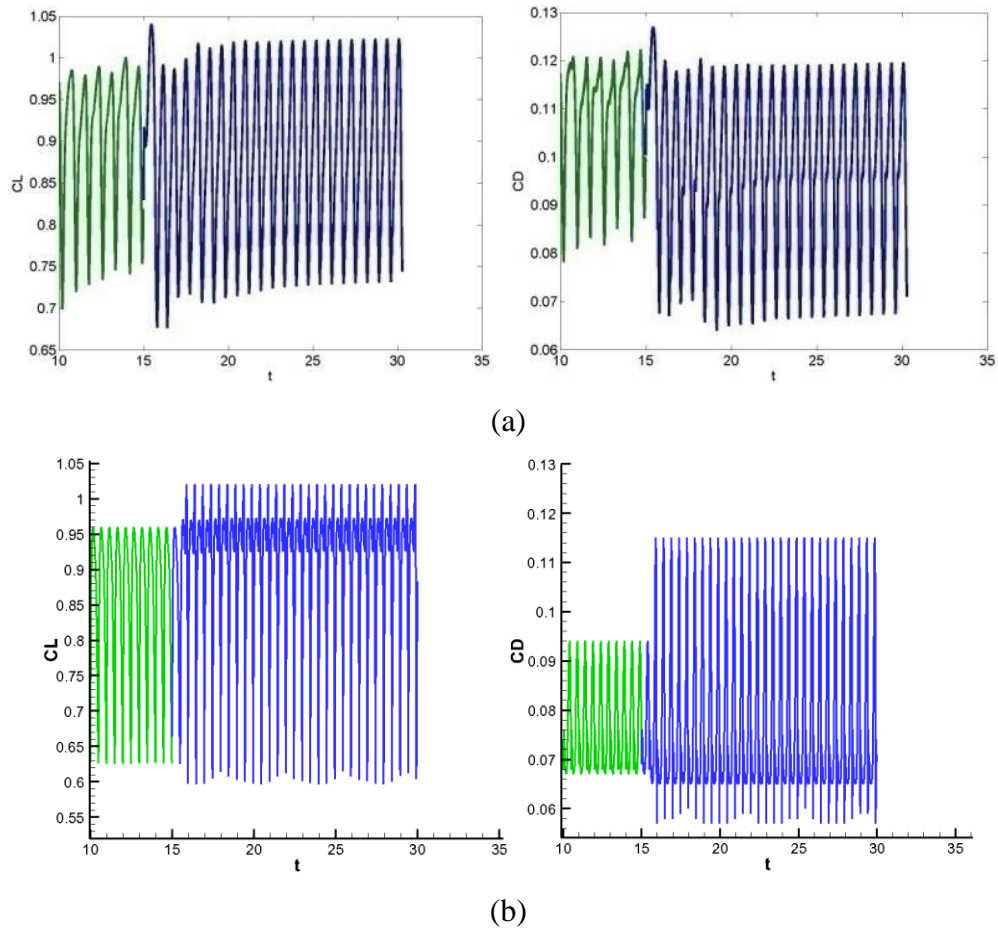
Figure 4.2 Airfoil aerodynamic response with Active Flow Control (AFC) on at t = 15, $\omega_{jet} = 9$. (a) from Nakhla et al.[41], (b) this study.

Results of aerodynamic coefficients obtained by Nakhla et al [41] and results of this study are compared in Figure 4.2. Synthetic jet is activated at t = 15. By the jet application, an increase on the lift coefficient and a decrease on the drag coefficient are obtained. The aerodynamic coefficient results show similarities to the results obtained in Ref. [41]. Vorticity contours and streamlines are also compared in Figure 4.3. The size of the upper surface vortex and trailing edge vortex structures are slightly bigger than the validation study. However, it should be noted that the vorticity contours in Ref. [41] are not given, and the slight differences can be explained by that.
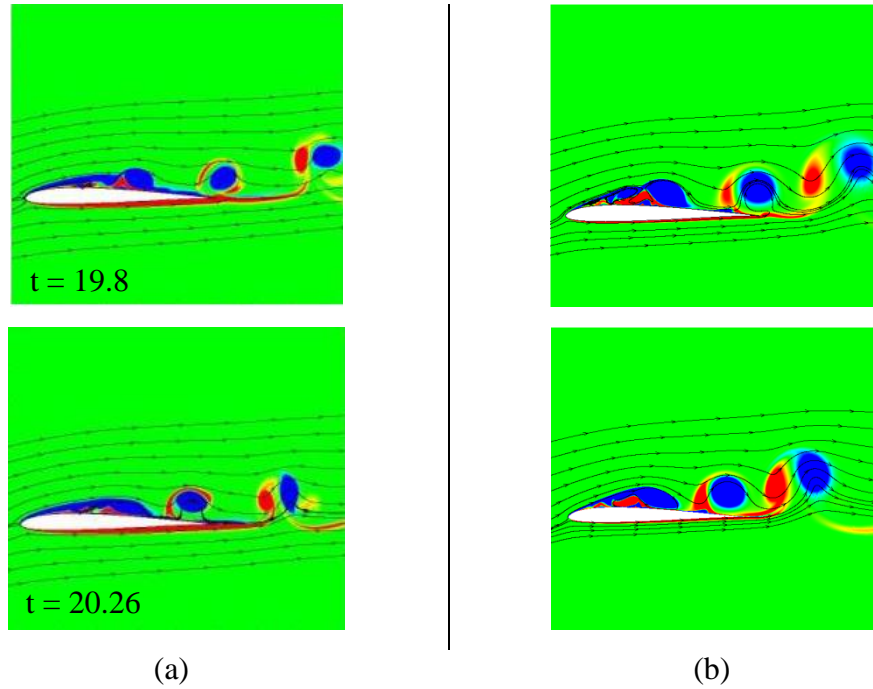
Figure 4.3 Time snapshots of instantaneous vorticity contours and streamlines over the actuation period for $\omega_{jet} = 9$[41]. (a) from Nakhla et al. [41], (b) current study.

4.2 Parametric Study for the Synthetic Jet Variables

A parametric study was carried out by varying the jet velocity, the jet angle, the angle of attack and Reynolds number to investigate the sensitivity of the jet parameters on lift to drag ratio, L/D. The jet slot size and the jet location were kept constant. The jet slot size was chosen to be 3% of the chord length. In each parametric study, the value of a single parameter was changed while keeping values of the other parameters constant. The jet velocity was changed between 0.1 U_∞ and 0.5 U_∞ velocities, where U_∞ corresponds to the upstream flow velocity. Constant suction and constant blow jet types were compared with the no jet case. The jet angle was changed between 0° and 90° while jet velocity was kept at 0.1 U_∞. Angle of attack values was changed between 0° and 11°. Reynolds number effect was investigated between Re = $1x10^4$ and Re = $6x10^4$.

4.2.1 Effect of Jet Velocity

A parametric study was carried out at $\alpha = 10^o$ for varying jet velocities. Different jet velocities were applied according to the free stream flow velocity (U_∞). Steady, uniform, constant blow and constant suction type jets were applied on the orifice which was located at aerodynamic center of the airfoil. Jet velocity was changed to the following values, $0.1U_\infty$, $0.3U_\infty$ and $0.5U_\infty$. Resulting lift and drag coefficient values were compared with the condition of no jet application case.

Reynolds number was kept constant for all cases at $6x10^4$. Applied angle of attack was 10°. Uniform, steady flow was applied on jet orifice and jet orifice was defined as velocity inlet with different velocities for every different case. Airfoil was assumed as no-slip wall. Model type was chosen as k-omega SST. Pressure based Navier-Stokes equations were solved in two dimensional conditions. Half of the outer surface of the grid domain was defined as velocity inlet and the remaining half of that was defined as pressure-outlet boundary condition. Resulting L/D for different jet velocities are listed in Table 4.1. The parametric study shows that L/D ratio of the jet application increases as the suction jet velocity increase. However, L/D ratio of the jet velocity decreases for increased constant blow jet velocities.

Table 4.1 L/D ratio for different jet velocities at Re = $6x10^4$ and $\alpha = 10^o$.

Re = $6x10^4$	Constant blow			No jet	Constant suction		
	$V_{jet} = 0.5\ U_\infty$	$V_{jet} = 0.3\ U_\infty$	$V_{jet} = 0.1\ U_\infty$	No jet	$V_{jet} = 0.1\ U_\infty$	$V_{jet} = 0.3\ U_\infty$	$V_{jet} = 0.5\ U_\infty$
L/D	10.9	12.6	14.9	20	24.6	31.3	36.9

According to the results of jet velocity analysis, under constant blow jet application, increase in the jet velocity can cause increase in the vorticity structures on the areas close to trailing edge. Therefore, increase in drag coefficient and decrease in lift coefficient can be observed. In addition, when the jet velocity increases trailing edge vorticity (TEV) grows.
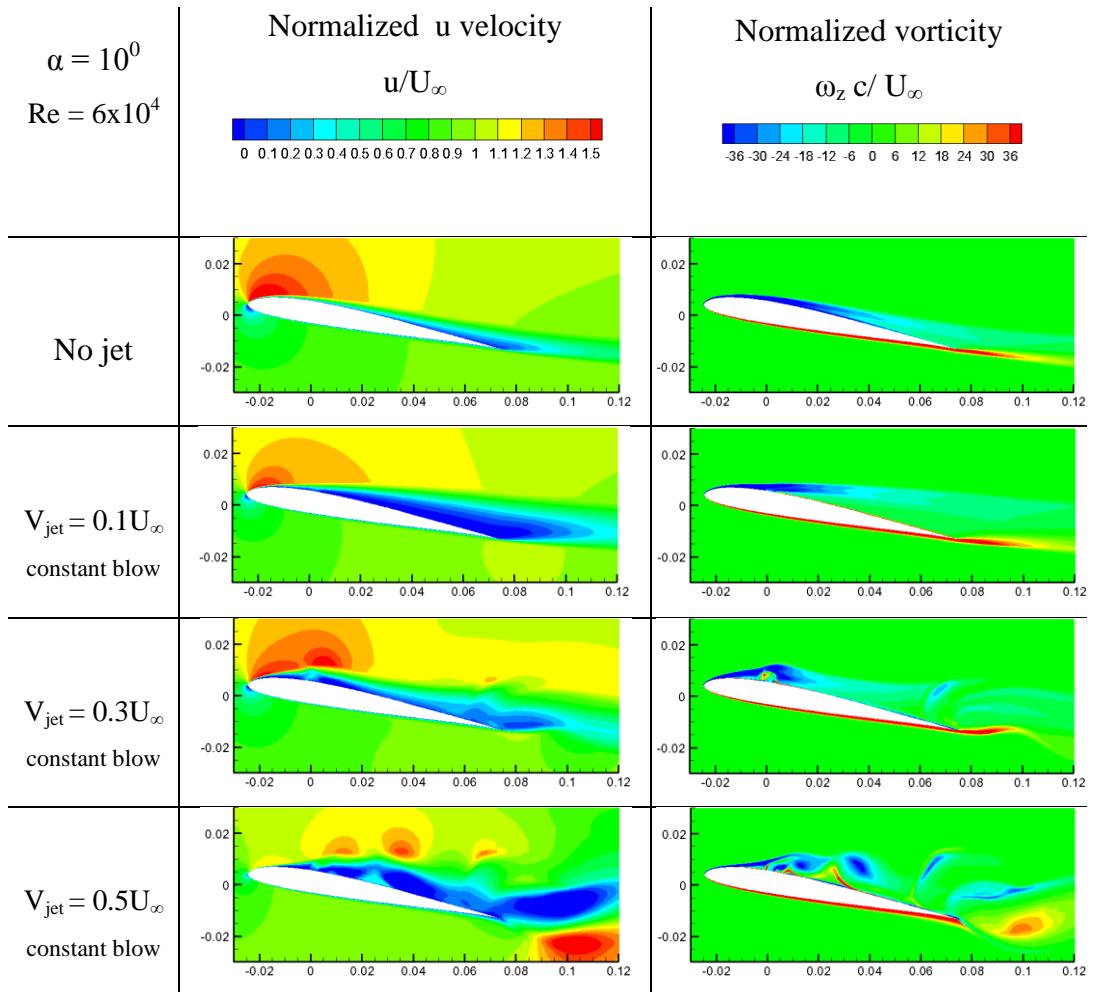
Figure 4.4 Normalized u velocity (left), and normalized vorticity (right) contours of different jet velocity applications at constant blow jet application. Re = 6x10^4, α = 10^0.

In the left column of Figure 4.4, left column streamwise velocity component is presented. This component was normalized with free stream flow velocity. When the blowing jet was applied, vorticity structures started to be seen on the upper side of the airfoil, and become dominant as the constant blow jet velocity increased. In the right column of the figure, the out-of-plane component of vorticity is represented. The vorticity was normalized with chord length and free stream flow velocity. Normalized u-component velocity and normalized vortices are given for 10° angle of attack value for constant blow jet application. When the constant blow jet is applied,

separation point goes towards to leading edge at $V_{jet} = 0.1 \ U_\infty$. For increasing jet velocities, upper surface vortex structures are observed. For $V_{jet} = 0.3 \ U_\infty$ counter rotating vortex structure is generated on the upper surface of the airfoil close to the leading edge. Flow separates from the upper surface. In addition, more abundant vortex structures are observed for high jet velocity condition.

In Figure 4.5 both normalized u component velocity and vorticity contours show that there is a slight separation at $\alpha = 10^o$ without jet application. However, by the application of constant suction jet, separated flow attaches to the upper side of the airfoil. With increase of jet velocity for constant suction case, the separation point moves towards the trailing edge. At $V_{jet} = 0.3 \ U_\infty$, flow is fully attached on the airfoil upper surface.
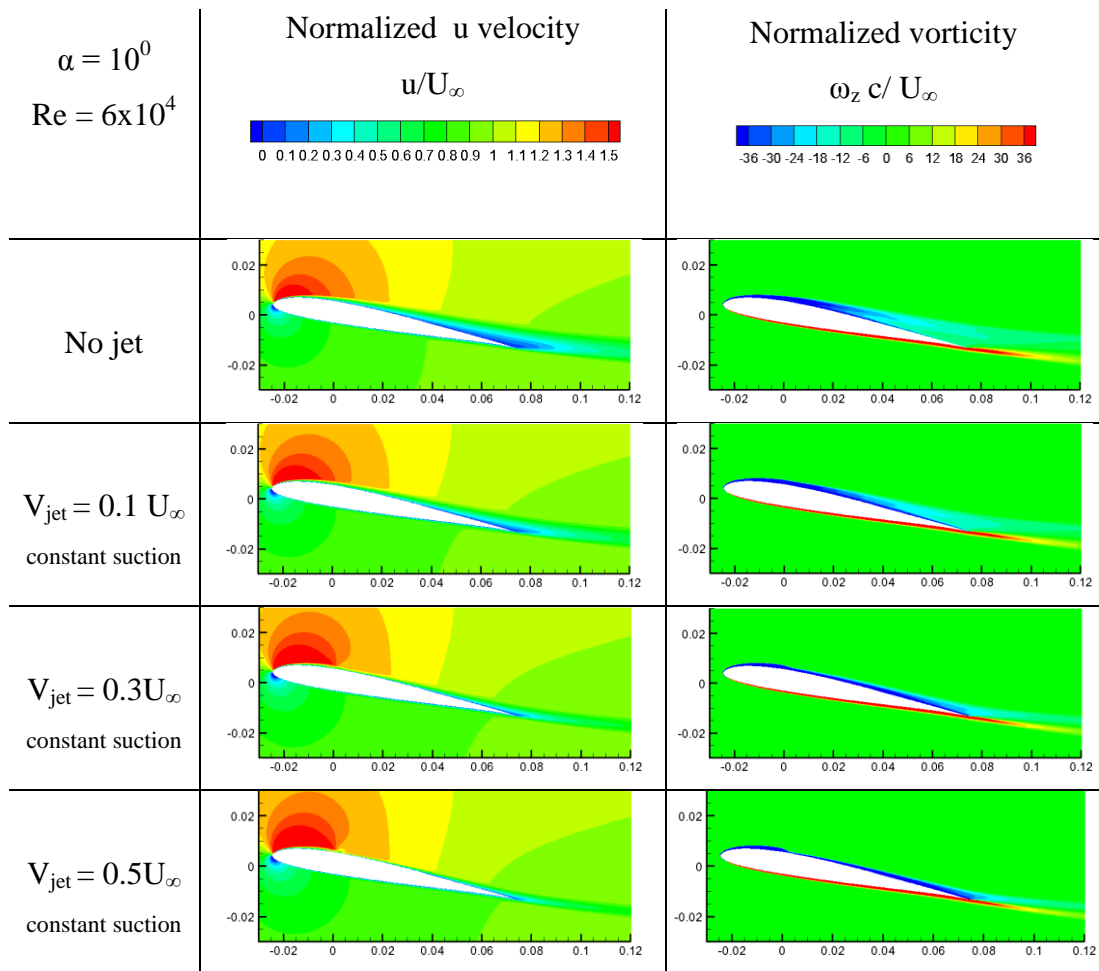
Figure 4.5 Normalized u velocity (left), and normalized vorticity (right) contours of different jet velocity application at constant suction jet application. Re = 6×10^4, α = 10^0.

According to the results of jet velocity analysis, under constant suction jet application, increase in the jet velocity can cause increase in the lift coefficient. On the other hand, increase in the constant blow jet velocity can cause decrease in the lift coefficient. In Figure 4.6 shows the variation of L/D with varying jet velocities for both constant blow and constant suction jet applications. When the suction jet velocity increased, an increase on C_L was obtained, and a decrease was obtained on C_D. Therefore, L/D ratio was increased.
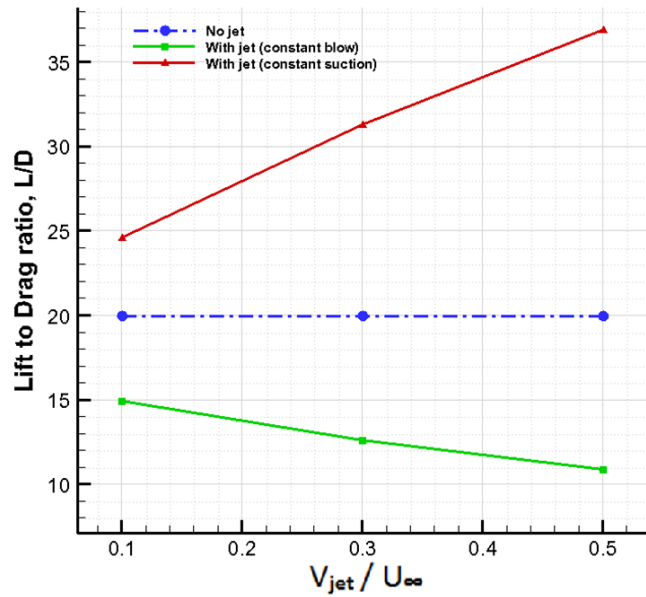
Figure 4.6 L/D variation with the constant suction jet velocity over free stream velocity ratio.

4.2.2 Effect of Jet Angle

The parametric study was performed for the jet angle at Re = 6×10^4, and α = 10°. Jet angle was varied between 0° and 90°. 0° jet angle corresponds to blow or suction jet which is tangential to the upper surface of the airfoil. Similarly, 90° jet angle corresponds to blow or suction jet perpendicular to the upper surface of the airfoil.

Figure 4.7 indicates the variation of L/D with constant blow and suction jet. Comparison of L/D reveals that L/D ratio is maximized as the jet angle is normal to the upper surface of the airfoil under constant suction jet application. However, reverse effect can be seen under constant blow jet application. The L/D ratio of constant blow jet decreases as the jet angle increase
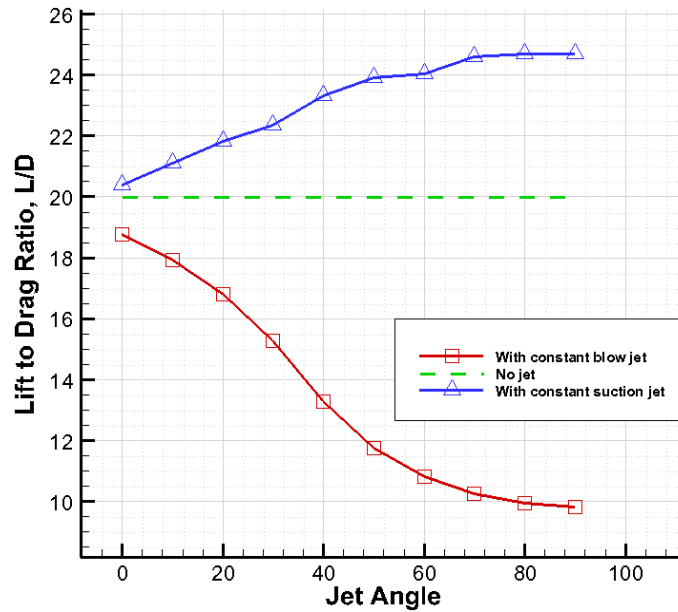
Figure 4.7 L/D variation with the various jet angles.

Figure 4.8 demonstrates normalized vorticity contours around SD7003 and close-up view of streamlines over jet orifice. The results are shown at Re = $6x10^4$, α = 10°, and V_{jet} = 0.1 U_∞ with constant suction jet. By the increase of jet angle, constant suction becomes dominant and separated flow over airfoil attaches to the upper side. This effect can be seen in the close-up view of streamlines. At α = 0°, separation point is observed around jet. When the jet angle increases, separation point on the upper side of the airfoil goes towards the leading edge. In the right column of Figure 4.8, close-up view of the stream lines are presented. The jet angle is represented with and arrow for different jet angles. Velocity vectors are tangential to the streamlines. When the jet angle increases, formation of the streamlines alters.

$\alpha = 10^{\circ}$ $Re = 6\times10^{4}$ $V_{jet} = 0.1\, U_{\infty}$	Normalized vorticity $\omega_z c/\, U_{\infty}$	Close-up view of streamlines
No jet		
$\alpha_{jet} = 0^{\circ}$ constant suction		
$\alpha_{jet} = 30^{\circ}$ constant suction		
$\alpha_{jet} = 50^{\circ}$ constant suction		
$\alpha_{jet} = 70^{\circ}$ constant suction		
$\alpha_{jet} = 90^{\circ}$ constant suction		
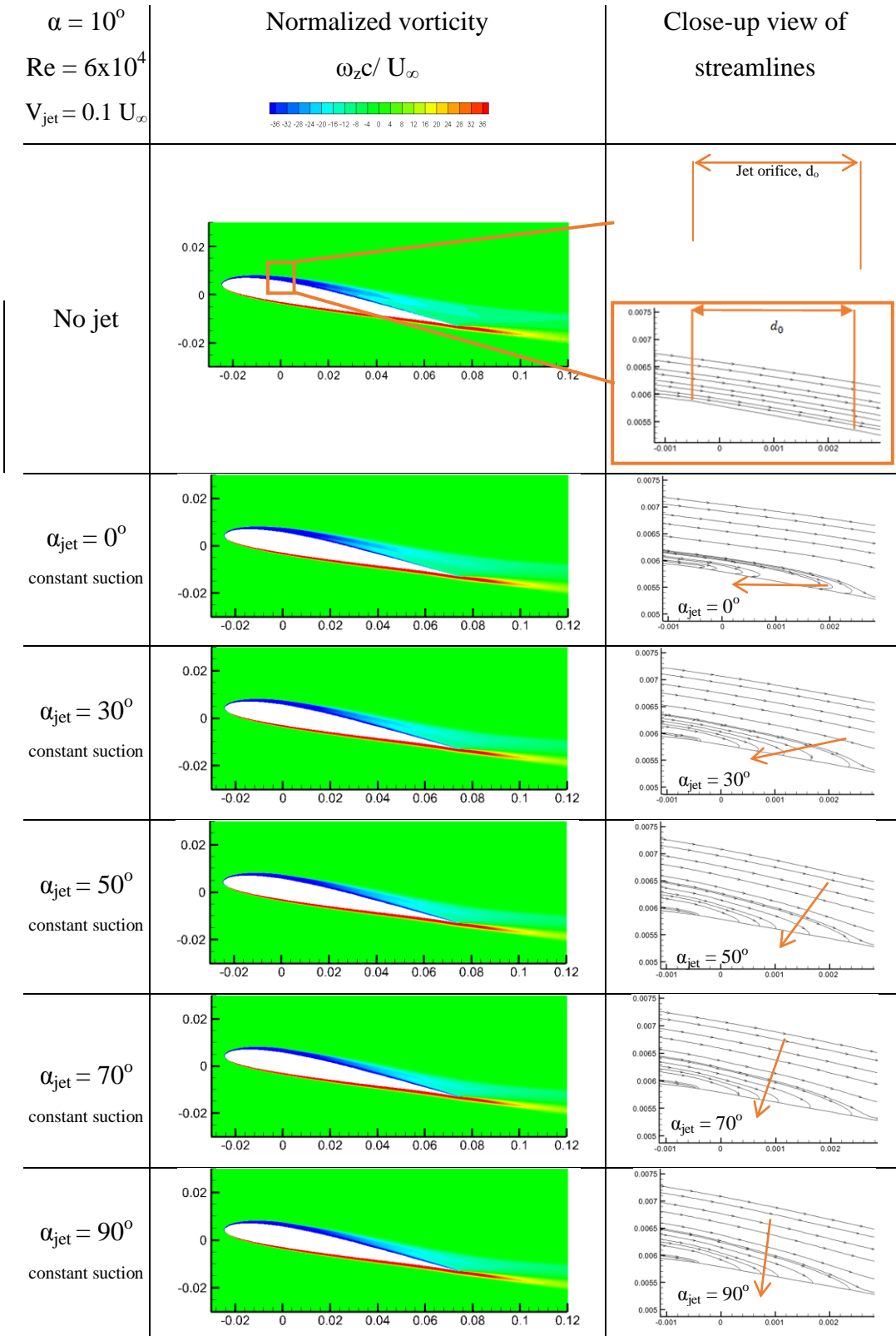
Figure 4.8 Normalized vorticity (left) contours with varying jet angles and close-up view of streamlines around jet orifice over SD7003. Re = 6x10^4, α = 10°.

4.2.3 Effect of Angle of Attack

Angle of attack effect was investigated in addition to the synthetic jet velocity and the jet angle effects. SD7003 airfoil profile goes under stall conditions for angle of attack values around 10°. To understand the effect of angle of attack, position of airfoil was changed, and angles between 0° and 11° were computed. Free stream flow velocity was kept constant at Re = 6x10^4, and constant suction jet applied. Jet velocity was taken 0.1 times of free stream flow velocity. Computed aerodynamic forces and L/D ratio are presented in Figure 4.9 and 4.10 for different angles of attack. By the application of constant suction jet, an increase on the lift coefficient is obtained. Similarly, a decrease on the drag coefficient is observed. Lift to drag ratio is improved. Moreover, it is obtained that the effect of constant suction jet is not dominant for the angles of attack smaller than 4°.However, at α = 6° effect of constant suction jet becomes dominant on L/D ratio.
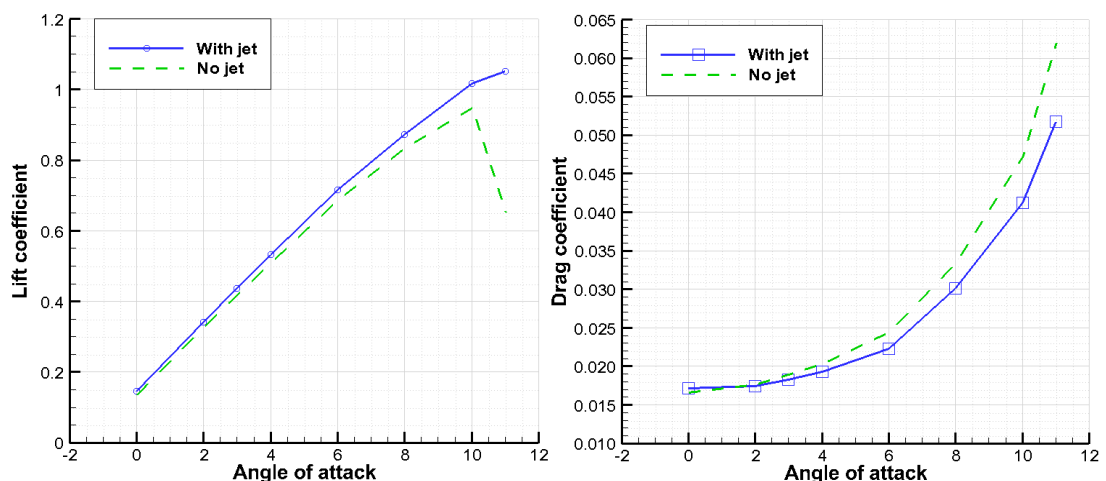
Figure 4.9 Aerodynamic coefficient variations with varying angle of attack values at Re = 6x10^4, V$_{jet}$ = 0.1U$_\infty$, constant suction jet application.
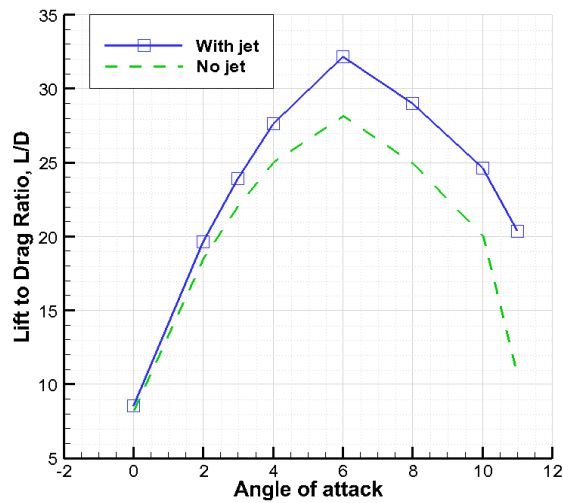
Figure 4.10 L/D variation with varying angle of attack values at Re = 6x10^4, V$_{jet}$ = 0.1U$_\infty$, constant suction jet application.

Normalized vorticity $\omega_z c / U_\infty$
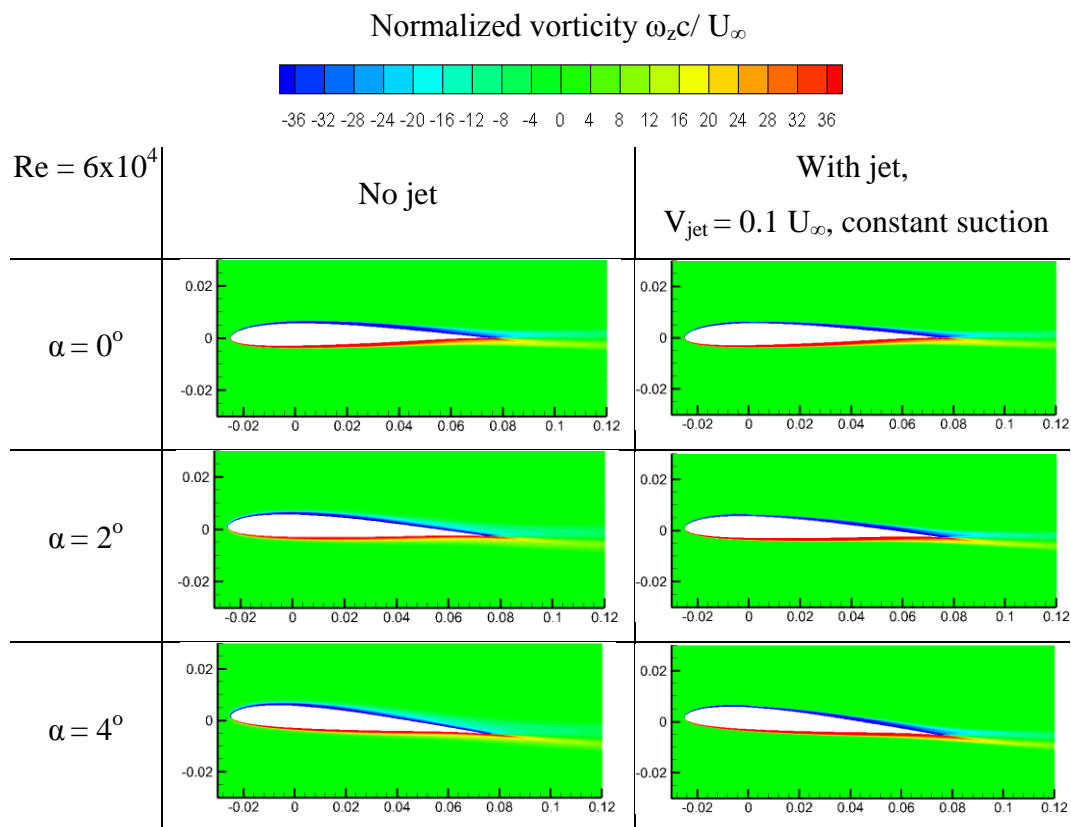
Figure 4.11 Normalized vorticity contours with 0° and 11° angle of attack values for no jet (left) and with constant suction jet (right) applications at Re = 6x10^4, V$_{jet}$ = 0.1U$_\infty$.

44

Normalized vorticity $\omega_z c / U_\infty$
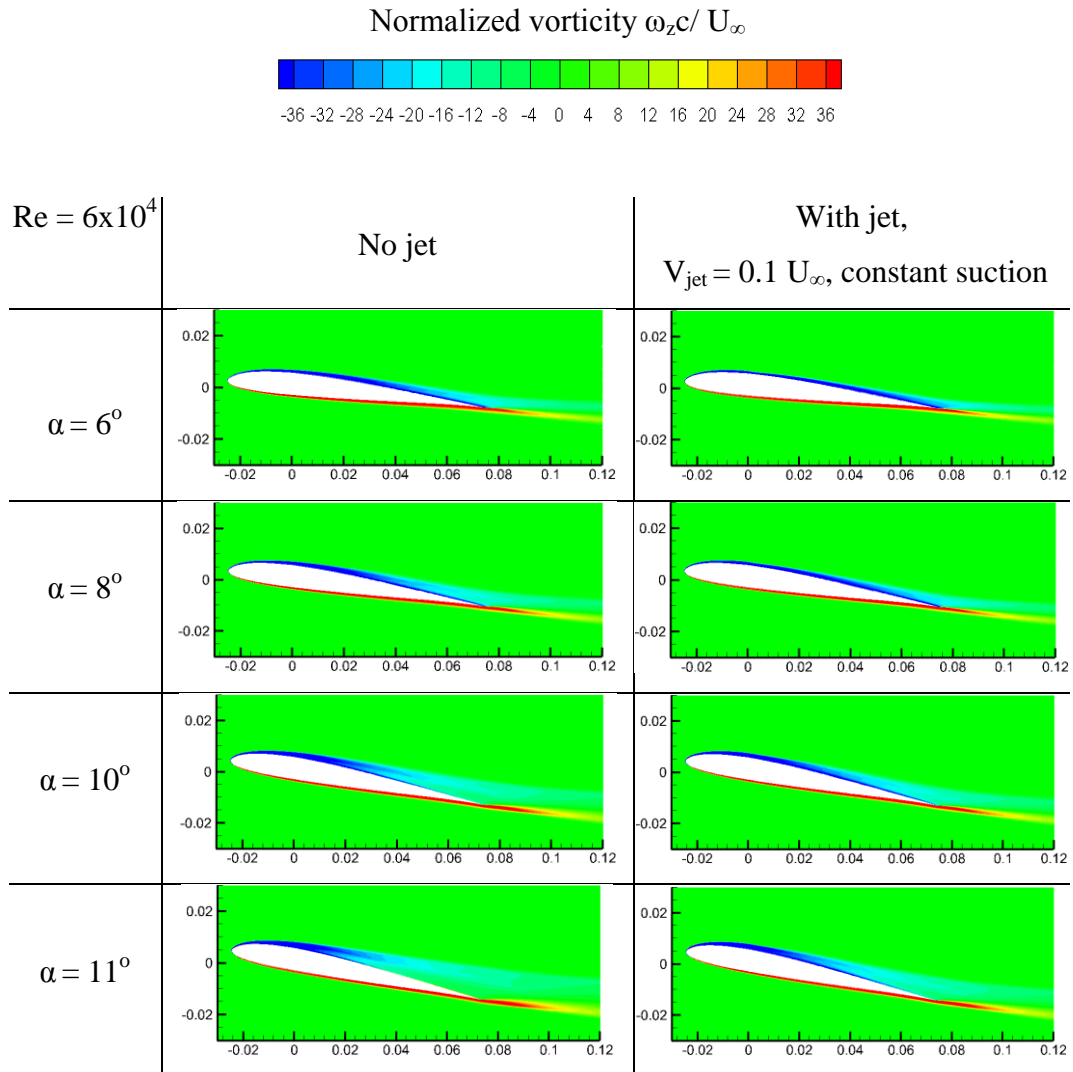
Figure 4.12 (Continued) Normalized vorticity contours with 0° and 11° angle of attack values for no jet (left) and with constant suction jet (right) applications at Re = $6x10^4$, $V_{jet} = 0.1U_\infty$.

In Figure 4.11 and Figure 4.12 normalized u component of velocity counters for different angles of attack with constant suction jet application are presented. In the left column of the figure no jet case is presented. For increasing α, separation point on the upper side of the airfoil gets closer to the leading edge of the airfoil under no jet application conditions. On the other hand, by the application of constant suction jet, separation point moves toward to the trailing edge, and flow attaches to the upper side of the airfoil. Effect of jet application becomes visible at α = 6°. For increasing

angles of attack, separation point goes towards to the trailing edge of the airfoil by the help of jet application.

4.2.4 Effect of Reynolds Number

Reynolds number effect study was performed for varying Reynolds number between 1×10^4, 3×10^4, and 6×10^4. Angle of attack was kept constant at 10°. Constant suction jet was applied, and the jet velocity was taken as $V_{jet} = 0.1U_\infty$. For each examined Reynolds number, results are compared with and without synthetic jet applications. In Table 4.2, relations between three computed Reynolds numbers are compared in terms of lift coefficients and angles of attack for the cases between with and without jet application.

Table 4.2 Aerodynamic coefficients at $\alpha = 10^o$

$\alpha = 10^o$	C_L	C_D	L/D
No jet, Re = 1×10^4	1.0345	0.1350	7.7
With jet, Re = 1×10^4	1.0072	0.1189	8.5
Change (%)	-2.6	-11.9	10.6
No jet, Re = 3×10^4	0.8336	0.0943	8.8
With jet, Re = 3×10^4	0.9420	0.0597	15.8
Change (%)	13.0	-36.7	78.5
No jet, Re = 6×10^4	0.9491	0.0474	20.0
With jet, Re = 6×10^4	1.0161	0.0412	24.6
Change (%)	7.1	-13.1	23.1

It is obtained that the effect of constant suction jet application is dominant at Re = 3×10^4. However, in all examined flow regimes and improvement on L/D ratio is obtained.
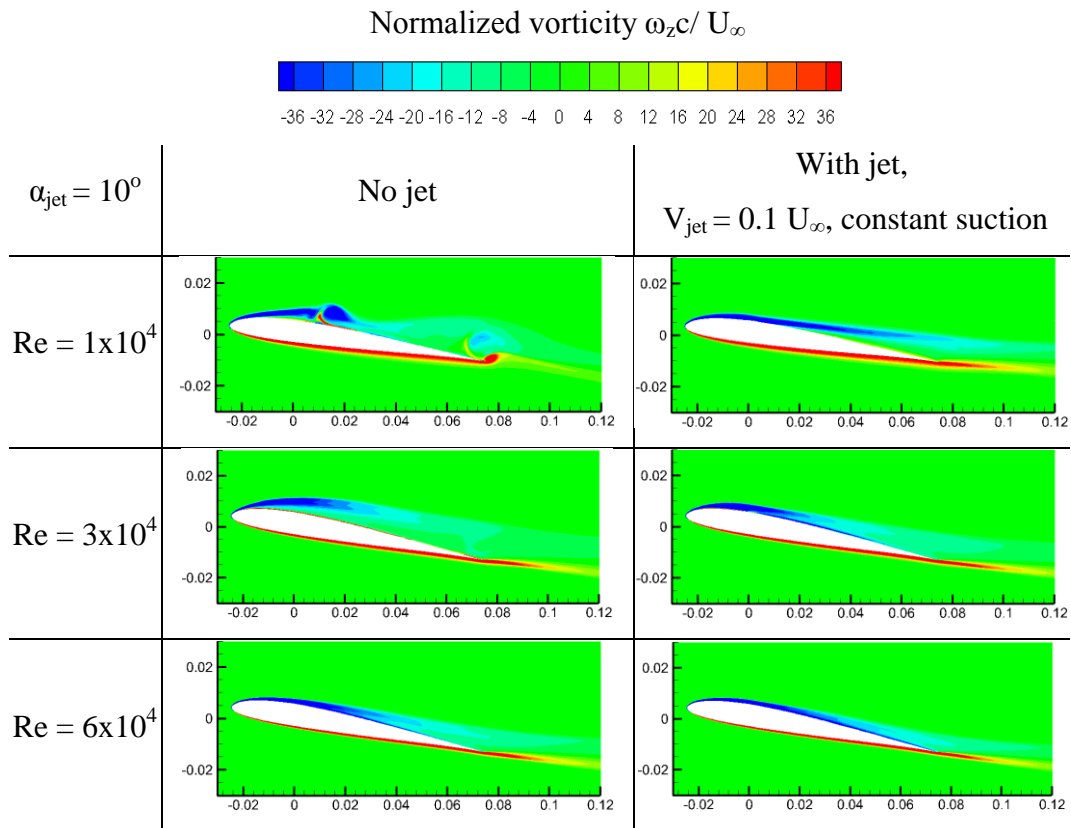
Figure 4.13 Normalized vorticity counters at Re = 1x10^4, Re = 3x10^4, and Re = 6x10^4 of synthetic jet application on SD7003 airfoil for α = 10°, V$_{jet}$ = 0.1U$_\infty$, constant suction jet.

In Figure 4.13, normalized vorticity counters are listed for Reynolds number 1x10^4, 3x10^4, and 6x10^4. In the left column of the figure, no jet cases are presented. At Re = 1x10^4, upper surface vortex can be seen. When Reynolds number decreases, separation point goes toward to the leading edge of the airfoil. In the right column of Figure 4.13 results with constant suction jet is presented. By the application of constant suction jet, vortex structures at Re = 1x10^4 fades away and separation point moves towards to the trailing edge of the airfoil. It is also observed that for increasing Reynolds number, separation point goes towards to the trailing edge of the airfoil.

CHAPTER 5

HOVER CASE STUDIES

This chapter is devoted to the results of hover cases. The hovering motion is applied as horizontal and vertical translation in addition to the pitching motion of the airfoil around the quarter chord point. The hovering mode with figure-of-eight motion is investigated with synthetic jet application on SD7003 airfoil. Zero net mass flux effect is compared with constant blowing, constant suction and without synthetic jet cases. The figure of eight motion is investigated in terms of the effect of vertical translation and Reynolds number. Results of these cases are compared for the situations with and without synthetic jet applications.

5.1   Hovering Kinematics

Effects of constant blowing jet, constant suction jet and zero-net-mass-flux synthetic jet are studied. The hovering motion is defined similarly with the study done by Gunaydinoglu [14]. The equations of motion are given in detail in Chapter 3. Hovering motion is explained in Figure 5.1.
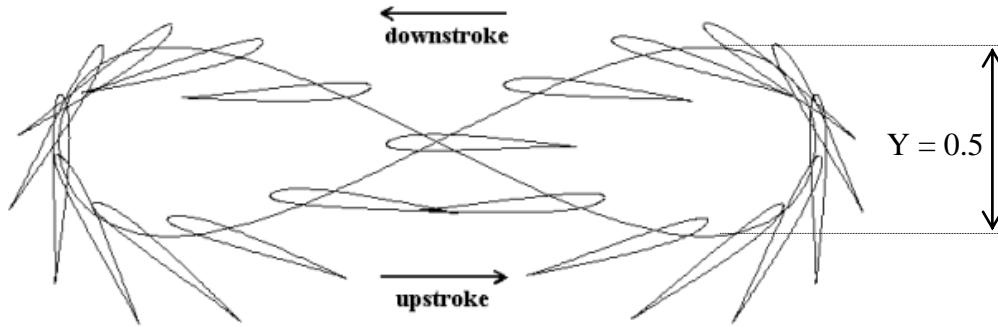
Figure 5.1 Schematic view of hovering mode with figure-of-eight motion, for Y = 0.5 amplitude. Each position is taken with 0.05T time intervals [14].

Cases of application without synthetic jet were compared with different types of jet applications during the studies of hover motion. Different jet applications are presented in Figure 5.2. Effect of constant blowing, constant suction and synthetic jet applications are compared under the study of zero-net-mass-flux effect. In addition to that study, effect of vertical translation was studied. In the vertical translation equation, Equation 3.9, Y denotes the amplitude of vertical translation of airfoil in terms of chord length. These equations are also known as Lissajous curves. The vertical translation effect are studied for the values between Y = 0.0 and Y = 1.5 at $Re = 1x10^3$. Moreover, in order to examine the effect of Reynolds number, different Reynolds numbers were applied between 1000 and 5000 for Y = 0.5 case. Figure 5.3 illustrates hover motion for different vertical translation amplitudes.

(a)

(b)

(c)
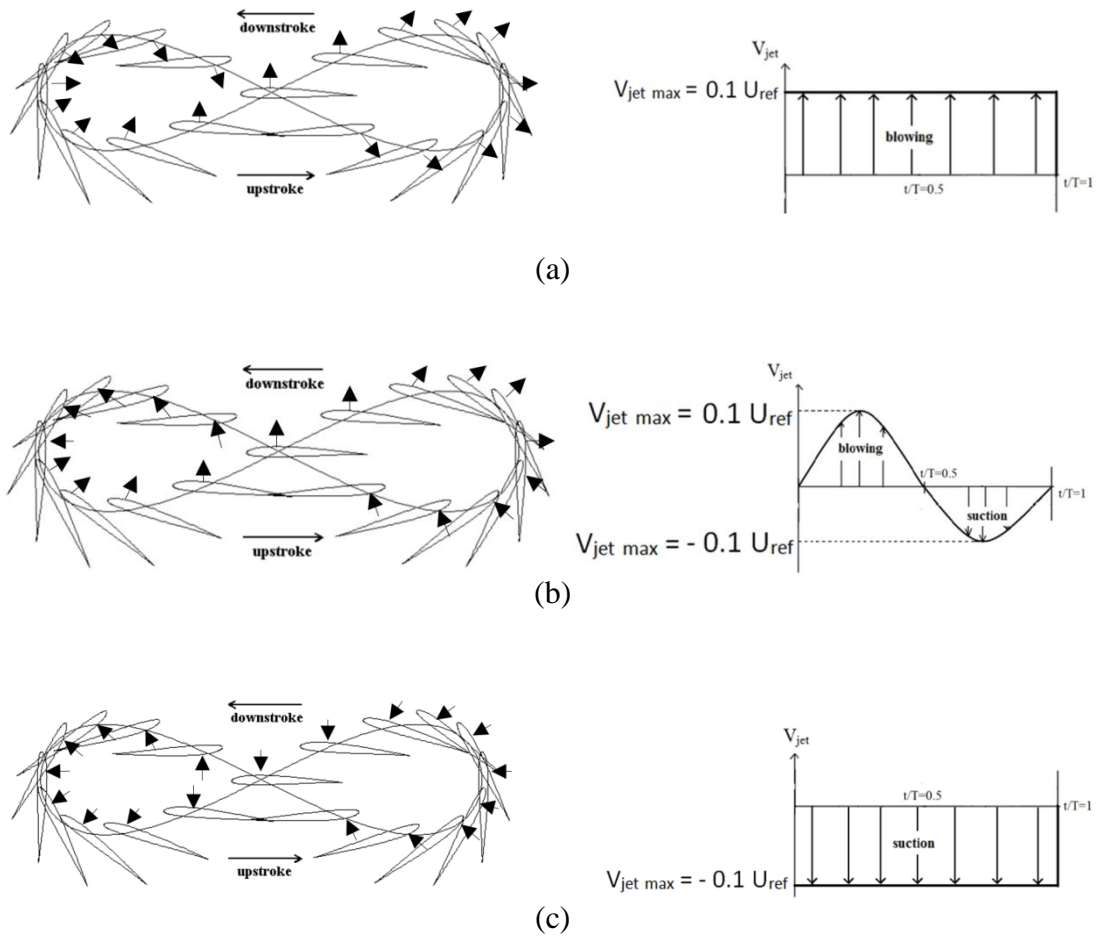
Figure 5.2 Schematic views of applied jets over one period of hover motion. (a) constant blowing jet, (b) synthetic jet, and (c) constant suction.
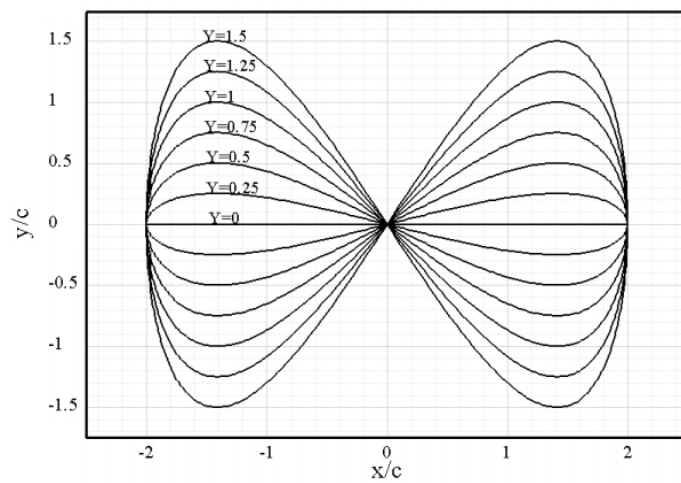
Figure 5.3 Hover motion for varying vertical translation amplitudes [14].

5.2 Effect of Zero-Net-Mass-Flux

Constant blow jet, constant suction jet and zero-net-mass-flux type synthetic jet applications were investigated. Figure 5.2 shows the applied jets. Y was kept constant at 0.5. Synthetic jet was chosen as velocity inlet boundary condition, while the outer grid domain was applied as pressure outlet.

Normalized vorticity contour of hovering motion are given in Figure 5.4 and Figure 5.5 over one period. SD7003 airfoil is not a symmetric airfoil, and during one period of figure-of-eight motion, for the second half of the period lower side of the airfoil turns out to be the upper side. By this side change of airfoil, effect of asymmetry can be observed. During downstroke steps, between $0.0 < t/T < 0.5$, the movement of airfoil squeeze the air around itself and Leading Edge Vortex (LEV) hits to pressure side of airfoil. For without jet application case, LEV detaches from the surface and moves towards trailing edge of the airfoil. At the period $0.4 < t/T < 0.6$, detached LEV on the lower side is squeezed.

During the first half of the hover motion, the synthetic jet is in the blowing regime. At $t/T = 0.1$, small sized upper surface vortex is observed as seen in the left column of Figure 5.4. Effect of the synthetic jet becomes visible at $t/T = 0.2$, and around the jet location, flow separation can be seen. On the lower side of the airfoil, normalized vorticity structures are same for with and without synthetic jet application cases.
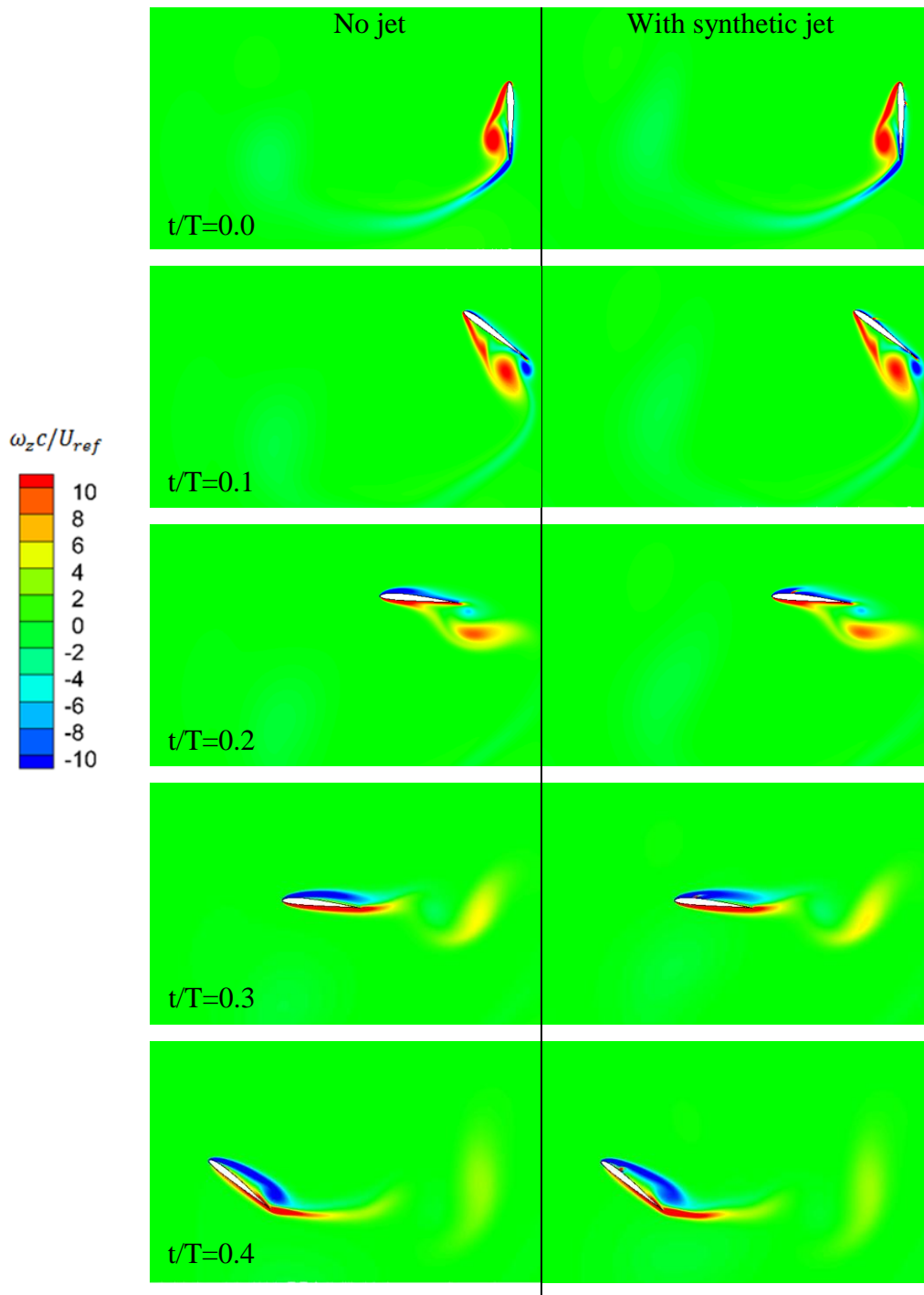
Figure 5.4 Normalized vorticity contours of hovering motion for the first half period of figure-of-eight motion at Re = 1000, Y = 0.5, $V_{jet\ max} = 0.1U_{ref}$ and $0.0 < t/T < 0.4$ with no jet (left) and synthetic jet (right) applications.
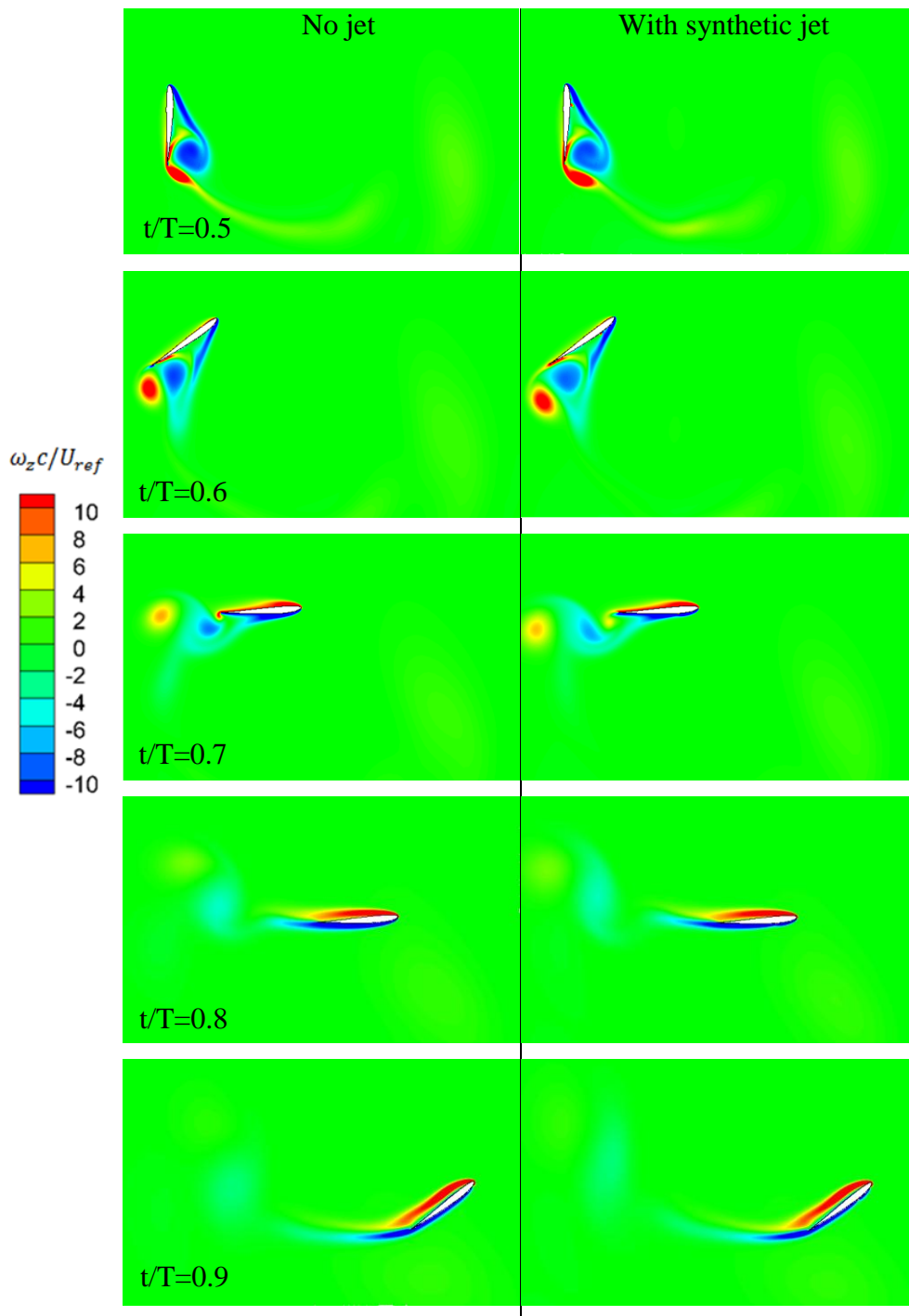
Figure 5.5 Normalized vorticity contours of hovering motion for the second half period of figure-of-eight motion at Re = 1000, Y = 0.5, $V_{jet\ max} = 0.1U_{ref}$ and $0.5 < t/T < 0.9$ with no jet (left) and synthetic jet (right) applications.

Between t/T = 0.5 and t/T = 0.9, the synthetic jet applied surface of the airfoil is located on the lower side in the normalized vorticity contours, in Figure 5.5. In addition, between the same time intervals, the synthetic jet is in the suction mode. Thus, it is observed that flow on the lower side of the airfoil is more attached to the surface. It is obtained that in the left and the right columns of Figure 5.5, vorticity structures are similar.

Close-up views of the different jet applications are presented in Figure 5.6 and Figure 5.7. Between 0.0 < t/T < 0.5, the synthetic jet is in the blowing regime. Hence, normalized vorticity contour structures are similar for the constant blowing and the synthetic jet cases. After t/T = 0.1, effect of the jet application become visible. At t/T = 0.4 it is observed that the location of the separation point on the upper surface of the airfoil does not change significantly. In Figure 5.6, at t/T = 0.6 separation point on the lower side of the airfoil moves towards to the trailing edge. It is obtained that flow on the lower side of the airfoil becomes more attached to the airfoil at t/T =0.7 and t/T = 0.8.
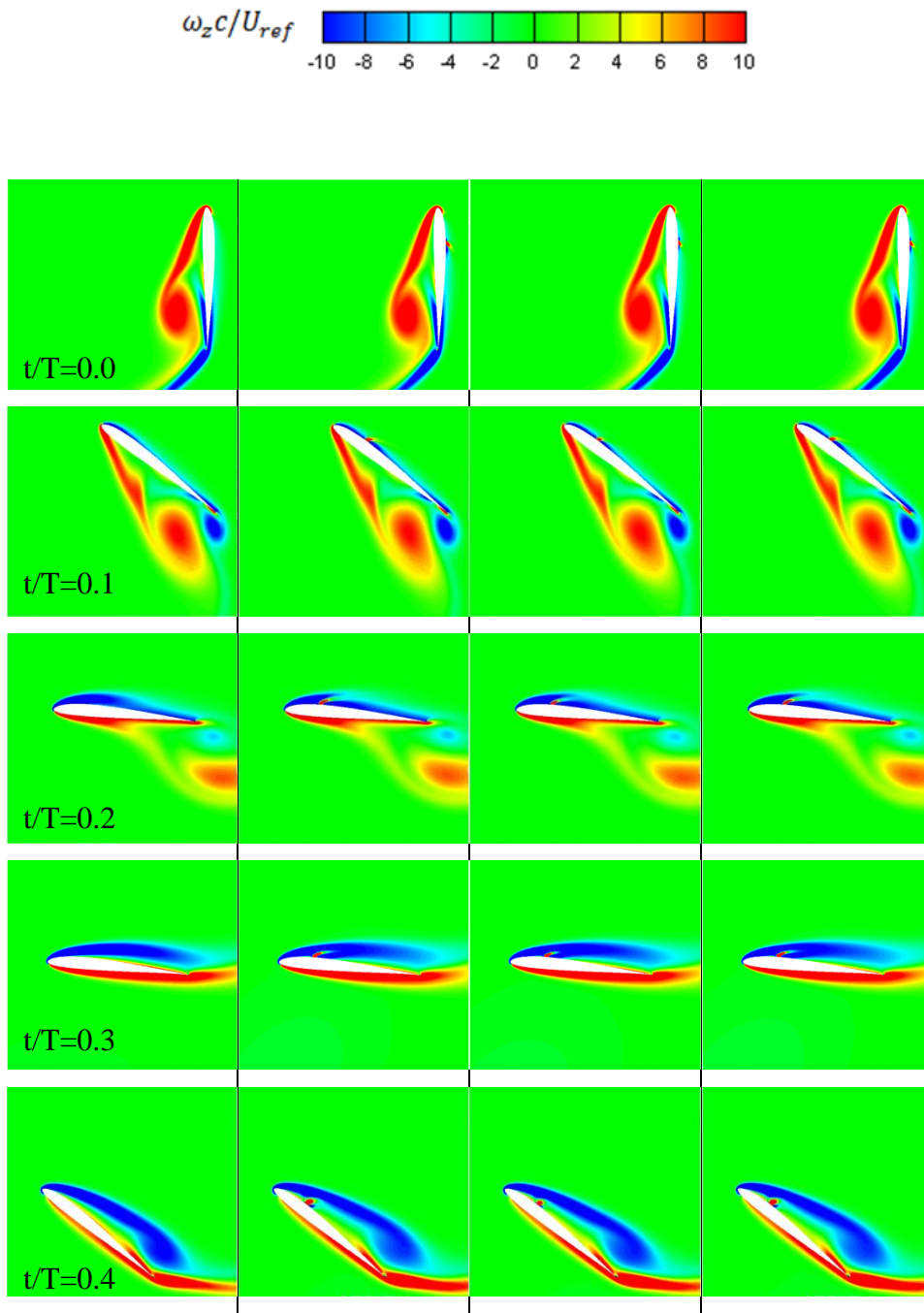
Figure 5.6 Close-up views of normalized vorticity contours of hovering motion for the first half period of figure-of-eight motion at Re = 1000, Y = 0.5, $V_{jet\ max} = 0.1 U_{ref}$ and $0.0 < t/T < 0.4$ with varying jet applications.
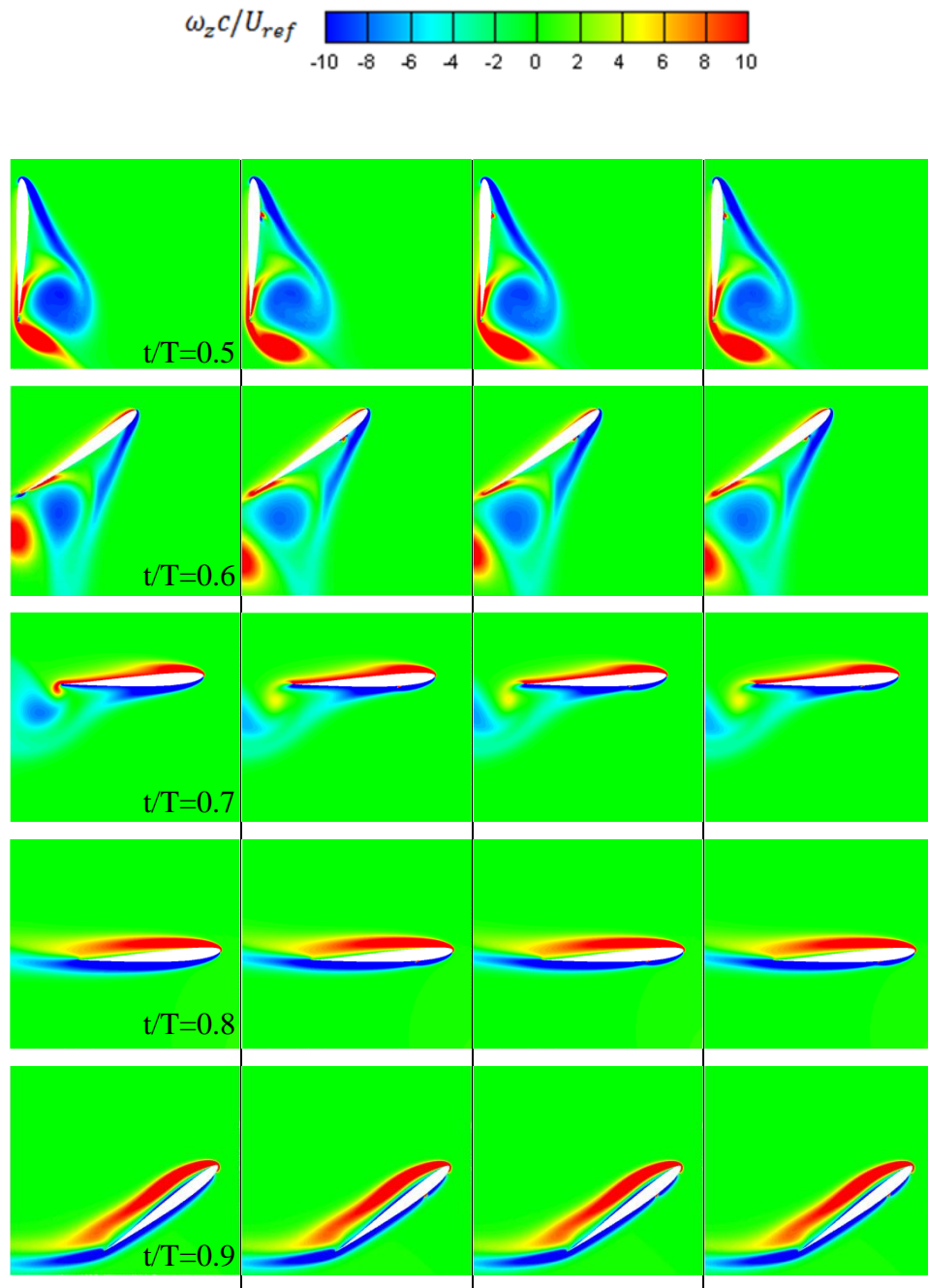
Figure 5.7 Close-up views of normalized vorticity contours of hovering motion for the second half period of figure-of-eight motion at Re = 1000, Y = 0.5, $V_{jet\ max}$ = 0.1U_{ref} and 0.5 < t/T < 0.9 with varying jet applications.
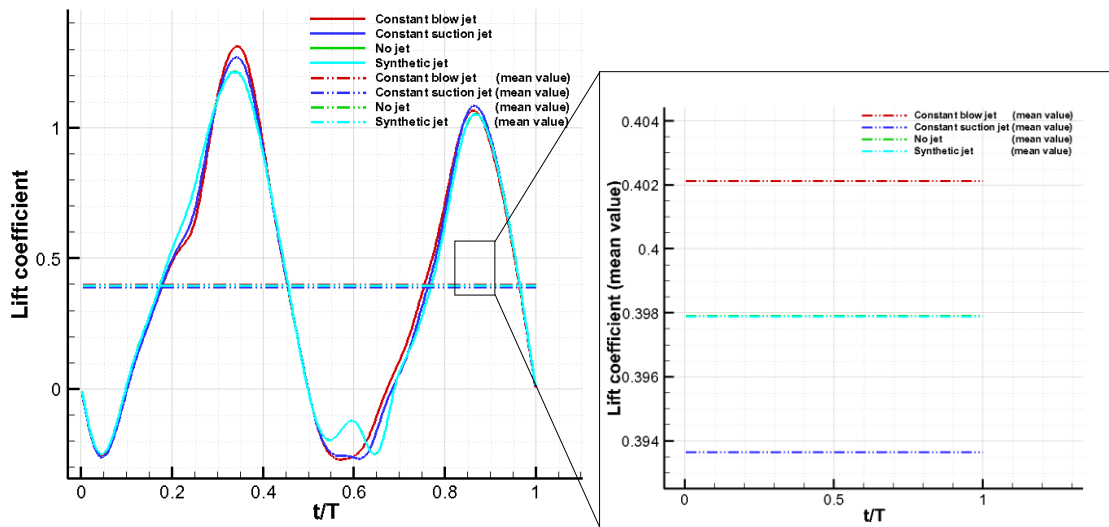
Figure 5.8 Time histories and mean values of lift coefficients over one period of hover motion with different jet applications. $Y = 0.5$, $Re = 1000$ and $V_{jet\ max} = 0.1U_{ref}$.

Figure 5.8 presents the time histories and mean values of lift coefficient over one period of hover motion for different jet applications at $Y = 0.5$, $Re = 1000$, and $V_{jet\ max} = 0.1U_{ref}$. Synthetic jet application shows a similar pattern to the case of no jet application. However, the applications of constant blow and constant suction jets cause slight shifts on the peak values. A slight increase in C_L is observed during the first half of the hover motion period with the application of constant blow jet. Similarly, constant suction jet caused a slight increase on the peak value of the history of lift coefficient at the second half of the hover motion period. In addition, mean values of lift coefficient are compared with each other. Constant blow jet supplied the highest mean lift coefficient value, while the lowest value was obtained by constant suction jet. However, the cases of no jet and synthetic jet application supplied the same value for mean lift coefficient over one period of hover motion.
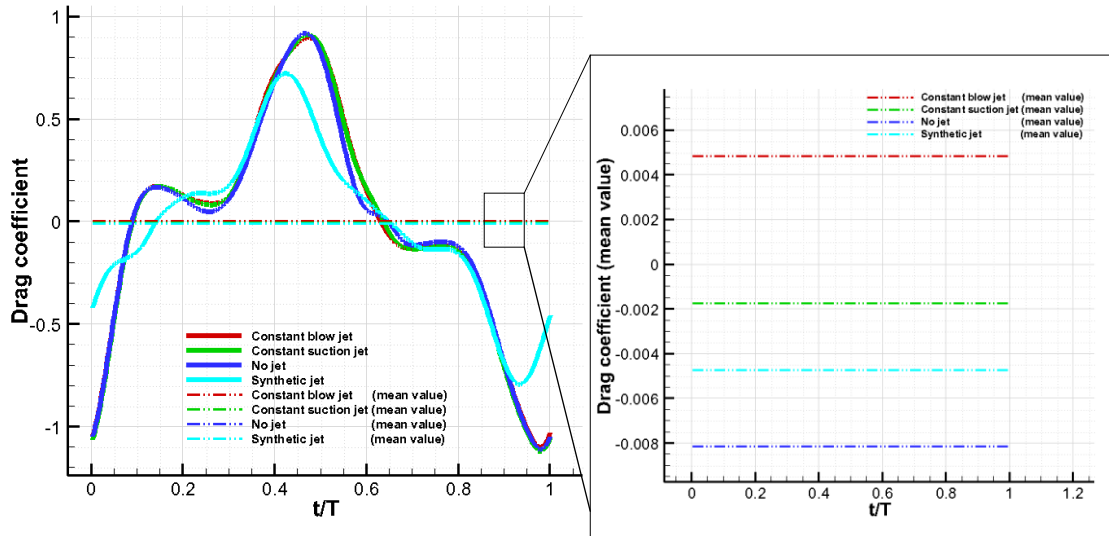
Figure 5.9 Time histories and mean values of drag coefficients over one period of hover motion with different jet applications. Y = 0.5, Re = 1000 and $V_{jet\ max}$ = $0.1U_{ref}$.

As seen in Figure 5.9, except the case of synthetic jet application, all the cases have the similar pattern over one period of motion. Since the synthetic jet does not have a uniform flow over the orifice, the pattern of the history of drag coefficient has different shape, and the peak value is shifted in time. When the mean values of drag coefficient histories were compared, it can be seen that all jet applications caused an increase on the mean value of drag coefficient. However, the least increase was obtained on the synthetic jet application.

Table 5.1 Mean values of aerodynamic coefficient and L/D over one period of hover motion for varying jet applications at Y = 0.5, Re = 1000, and $V_{jet\ max}$ = $0.1U_{ref}$.

	C_D	C_L	L/D
No jet	-0.01075	0.39696	36.92
Constant blow jet	0.00487	0.40215	82.61
Synthetic jet	-0.00238	0.39994	168.01

Calculated aerodynamic coefficients and L/D is presented in Table 5.1. Although all the jet application cases caused an increase on the values of mean drag coefficient, improved L/D is observed with jet applications.

5.3   Effect of Vertical Translation

In order to examine the effect of vertical translation, seven different Y values applied between 0.0 and 1.5 at Re=1000 and $V_{jet\ max} = 0.1U_{ref}$. Normalized vorticity contours were for the cases with and without jet application. Applied jet was kept equal to sinusoidal wave. Figure 5.8 and 5.9 present normalized vorticity contours at Y=0, 1, and 1.5 over one period figure-of-eight motion.   L/D values calculated from corresponding mean lift and drag coefficient values were listed in Table 5.2.

Figure 5.10 and Figure 5.11 present the normalized vorticity contours of hovering motion for varying vertical translation values. It ıs observed that increase in the vertical translation cause flow separation on the upper surface of the airfoil. At t/T = 0.3 upper surface vortex structures are observed for Y = 1 and Y = 1.5. At t/T = 0.4, created vortex structures get bigger and separates from the upper surface of the airfoil.

In Figure 5.12 and Figure 5.13 normalized vorticity contours with the synthetic jet applications over one period of hover motion are presented. At t/T = 0.3 in addition to the counter rotating vortex structures, counter clockwise rotating vortex structures are observed on the upper surface of the airfoil close to the jet location. In Figure 5.13, between 0.5 < t/T < 0.9, the synthetic jet is in the suction mode. At t/T = 0.6 a smaller vortex structure is observed on the lower surface of the airfoil.
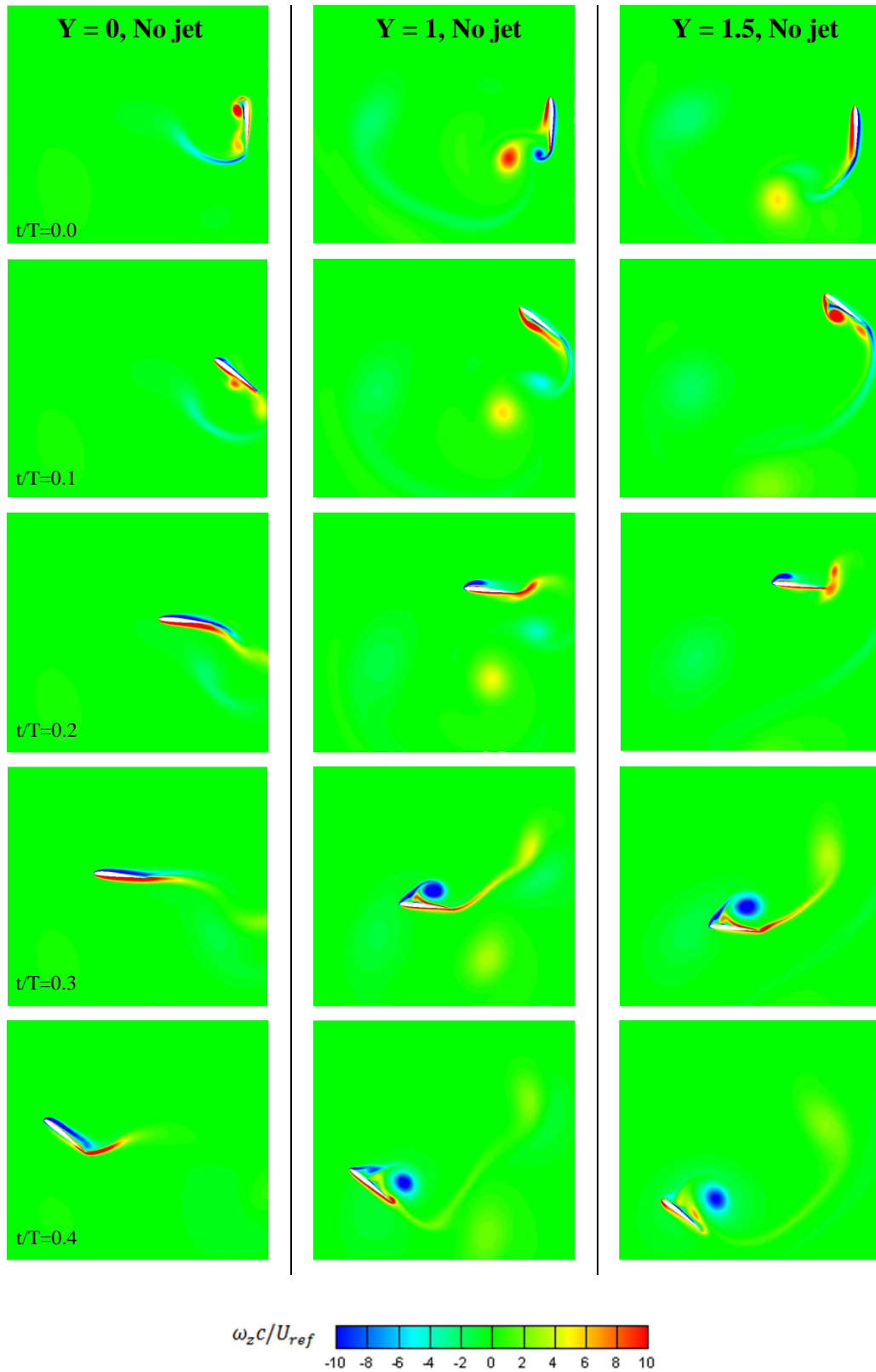
Figure 5.10 Normalized vorticity contours of hovering motion for varying vertical translation (Y), at Re = 1000, 0.0 < t/T < 0.4 and no jet condition.
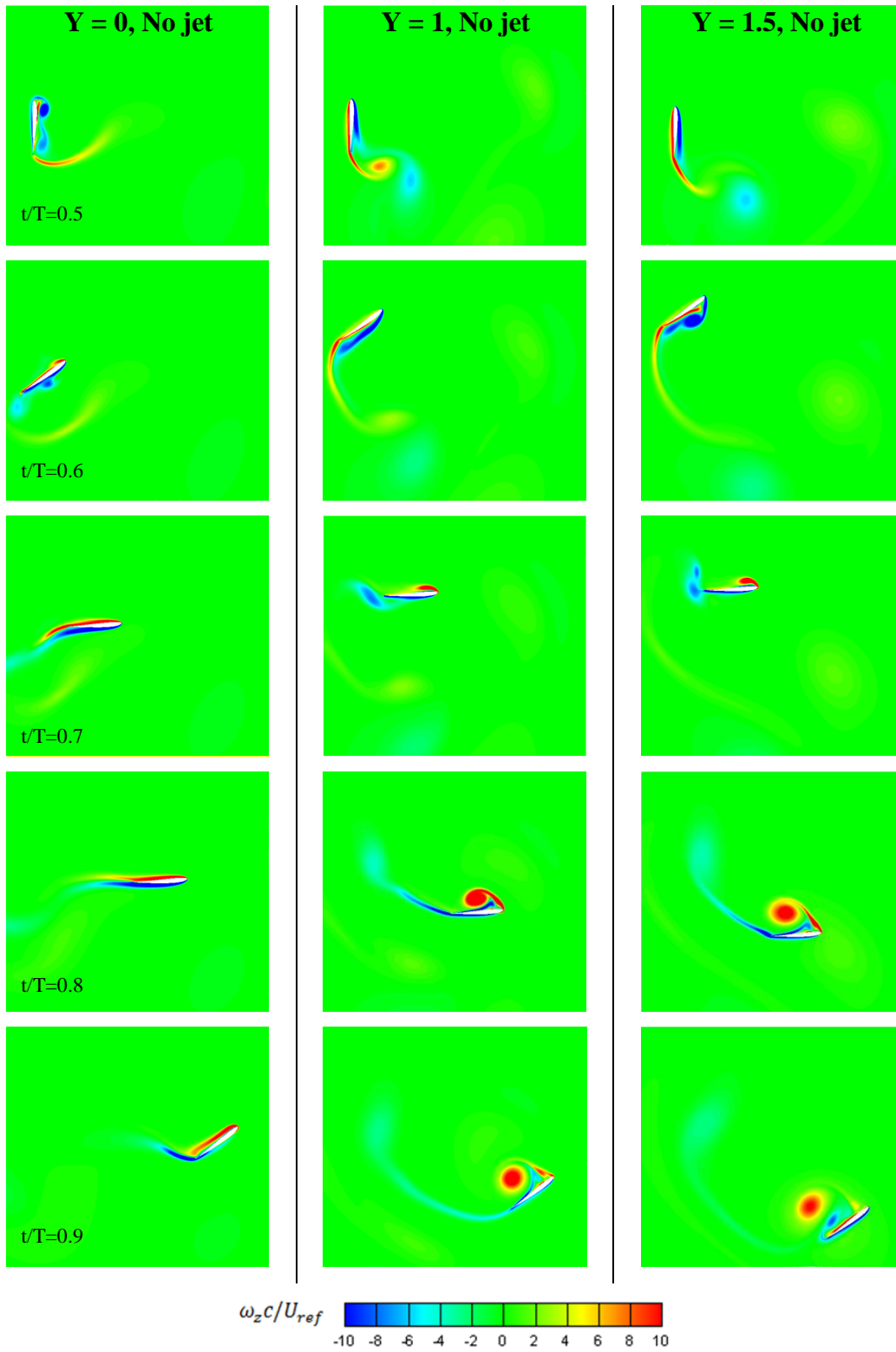
Figure 5.11 Normalized vorticity contours of hovering motion for varying vertical translation (Y), at Re = 1000, 0.5 < t/T < 0.9 and no jet.
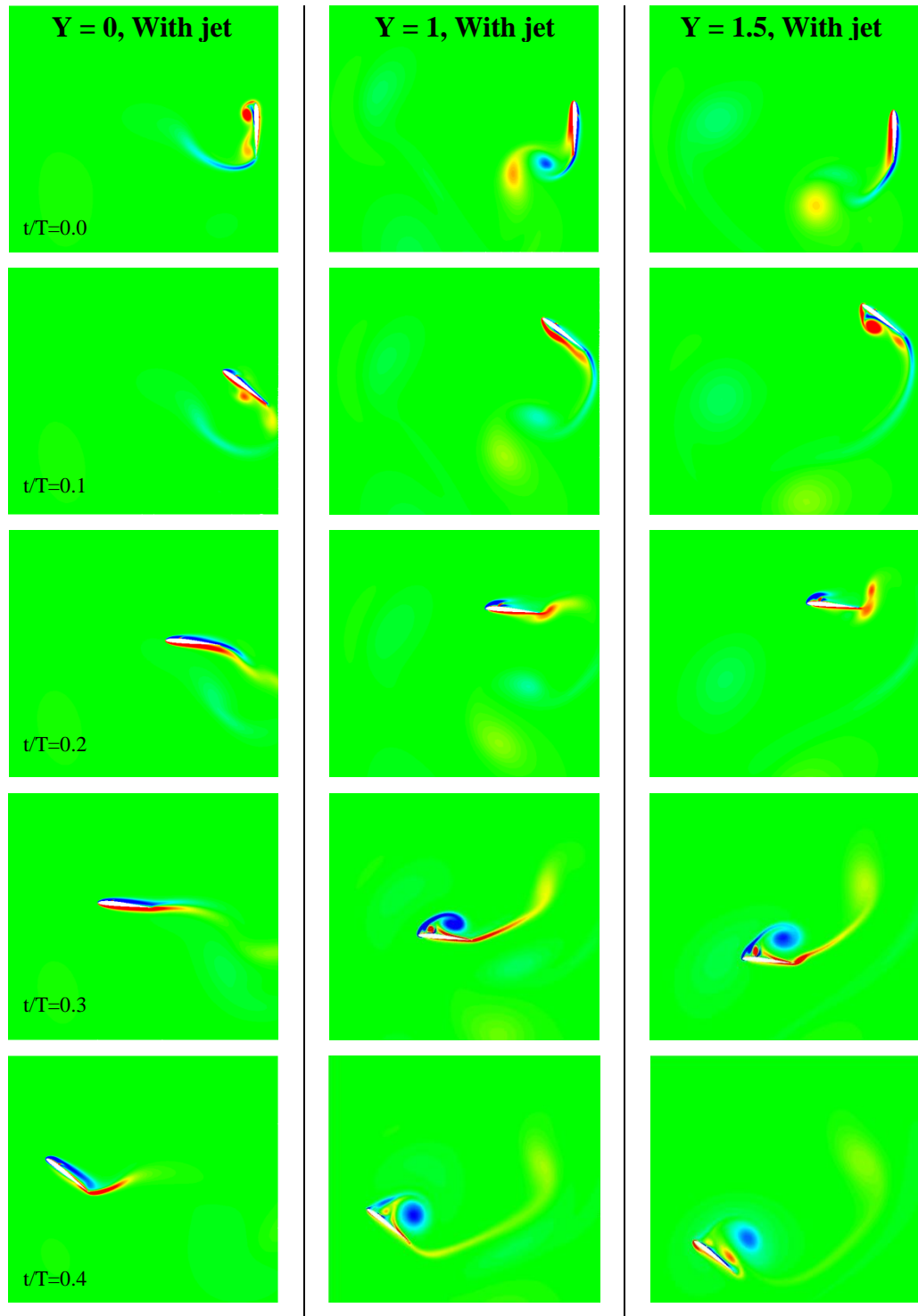
Figure 5.12 Normalized vorticity contours of hovering motion for varying vertical translation (Y), at Re = 1000, 0.0 < t/T < 0.4 and $V_{jet\,max} = 0.1U_{ref}$.
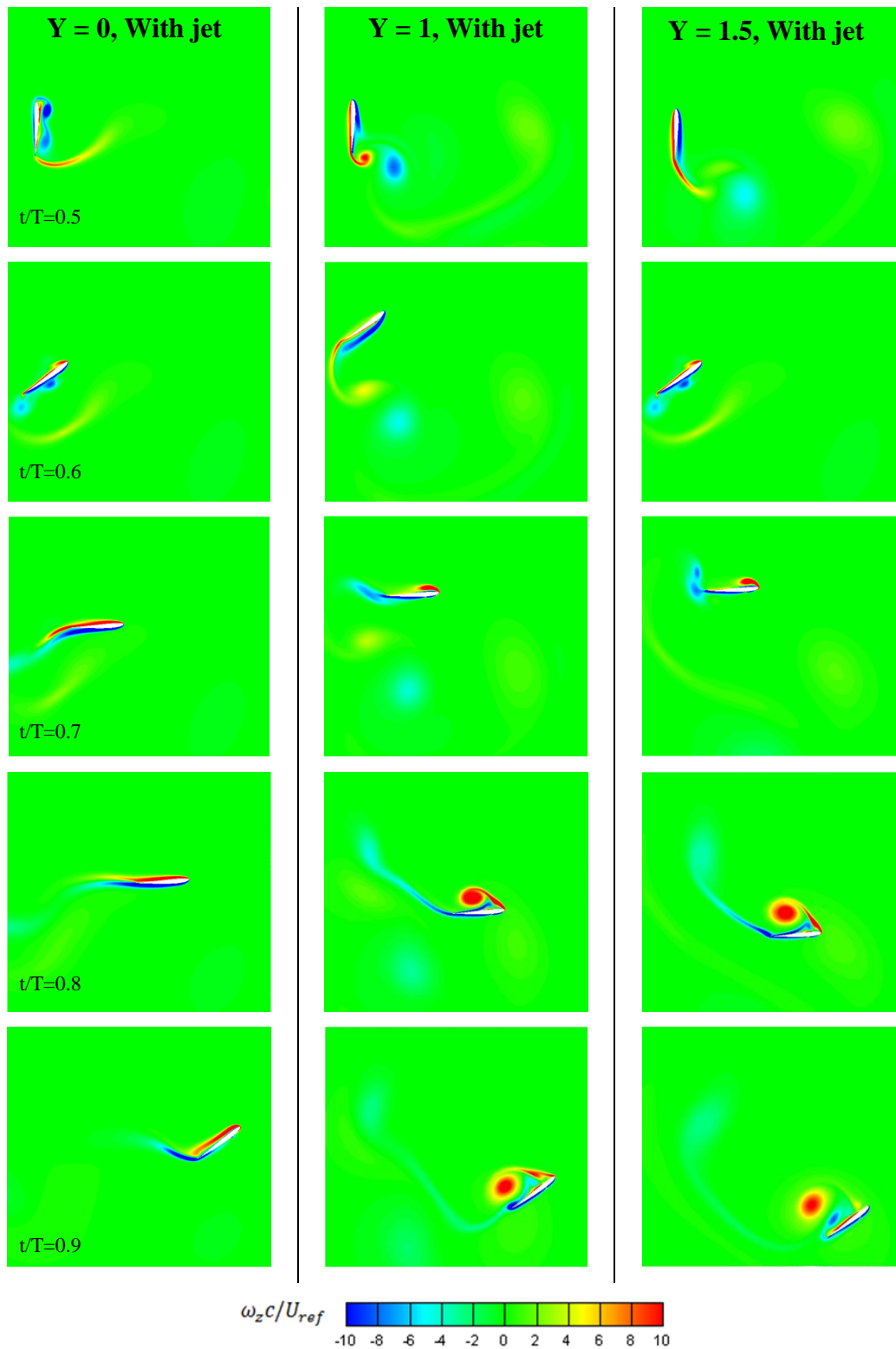
Figure 5.13 Normalized vorticity contours of hovering motion for varying vertical translation (Y), at Re = 1000, 0.5 < t/T < 0.9 and $V_{jet\ max} = 0.1U_{ref}$.

No jet With jet No jet With jet No jet With jet

t/T=0.0, Y=0 | t/T=0.0, Y=0 | t/T=0.0, Y=1 | t/T=0.0, Y=1 | t/T=0.0, Y=1.5 | t/T=0.0, Y=1.5

t/T=0.1, Y=0 | t/T=0.1, Y=0 | t/T=0.1, Y=1 | t/T=0.1, Y=1 | t/T=0.1, Y=1.5 | t/T=0.1, Y=1.5

t/T=0.2, Y=0 | t/T=0.2, Y=1 | t/T=0.2, Y=1 | t/T=0.2, Y=1.5 | t/T=0.2, Y=1.5

$\omega_z c / U_{ref}$

-10 -8 -6 -4 -2 0 2 4 6 8 10
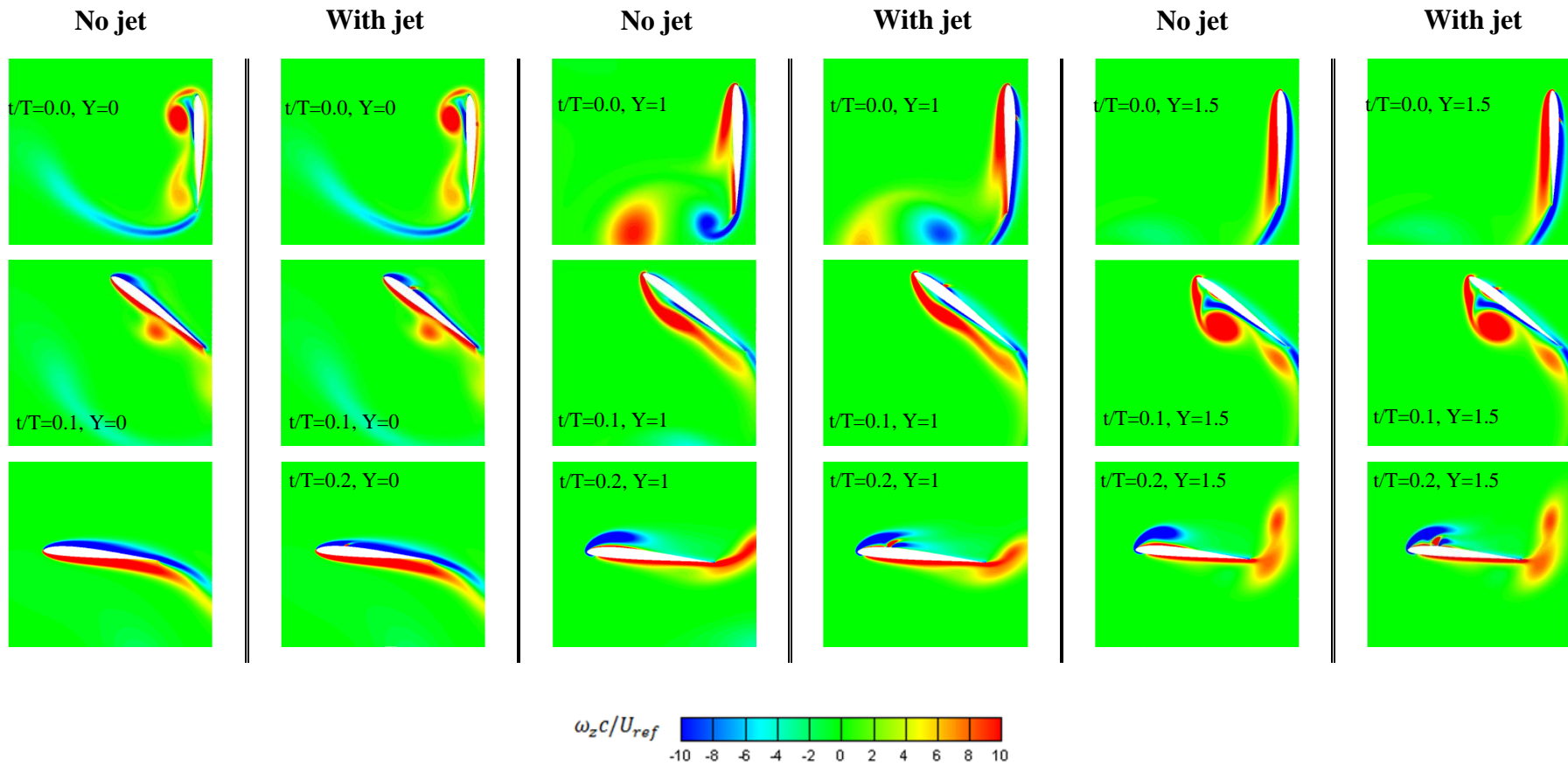
Figure 5.14 Close up views of normalized vorticity contours for different vertical translations, $0.0 < t/T < 0.2$.
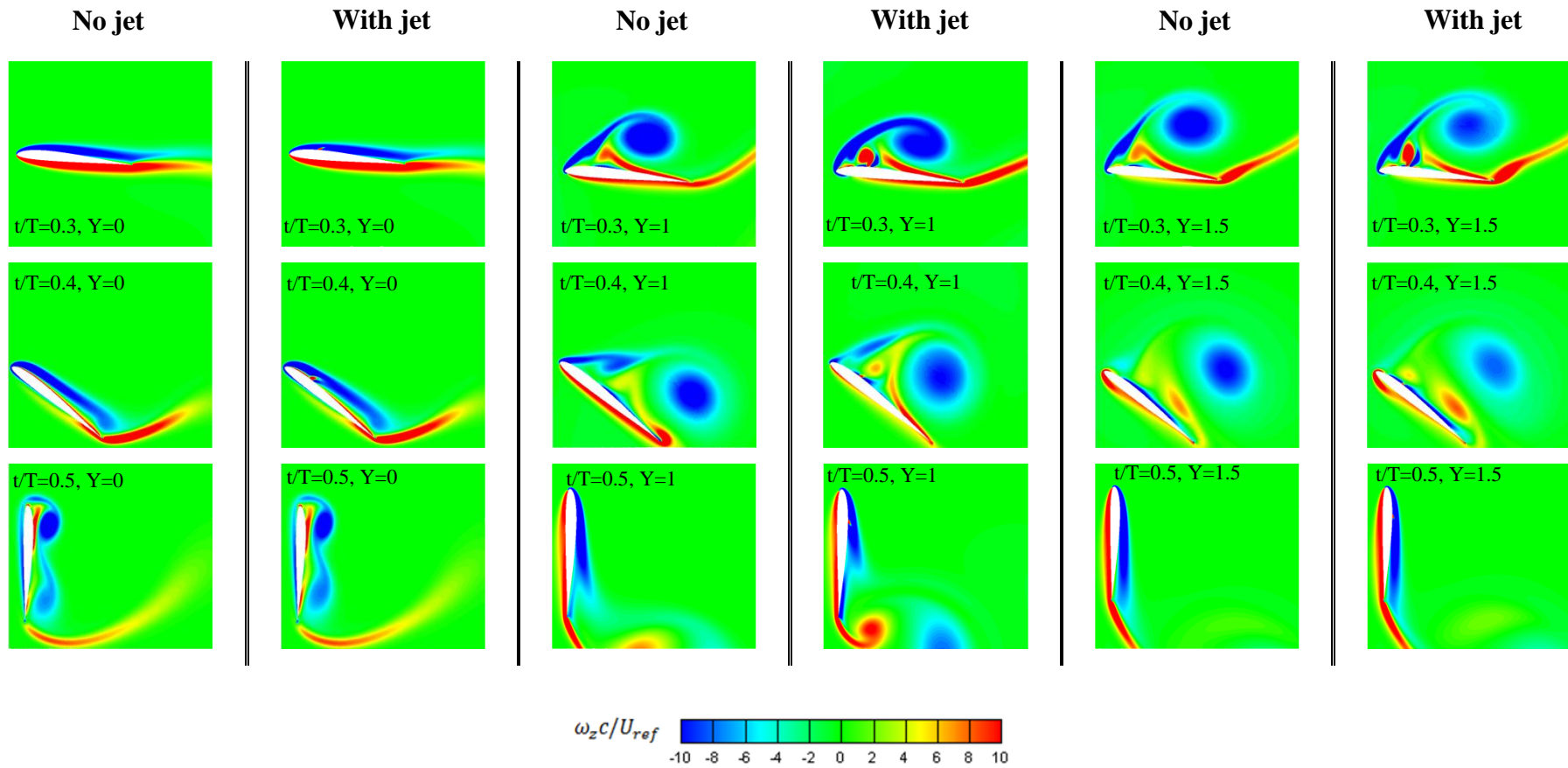
Figure 5.15 Close up views of normalized vorticity contours for different vertical translations, 0.3 < t/T < 0.5.
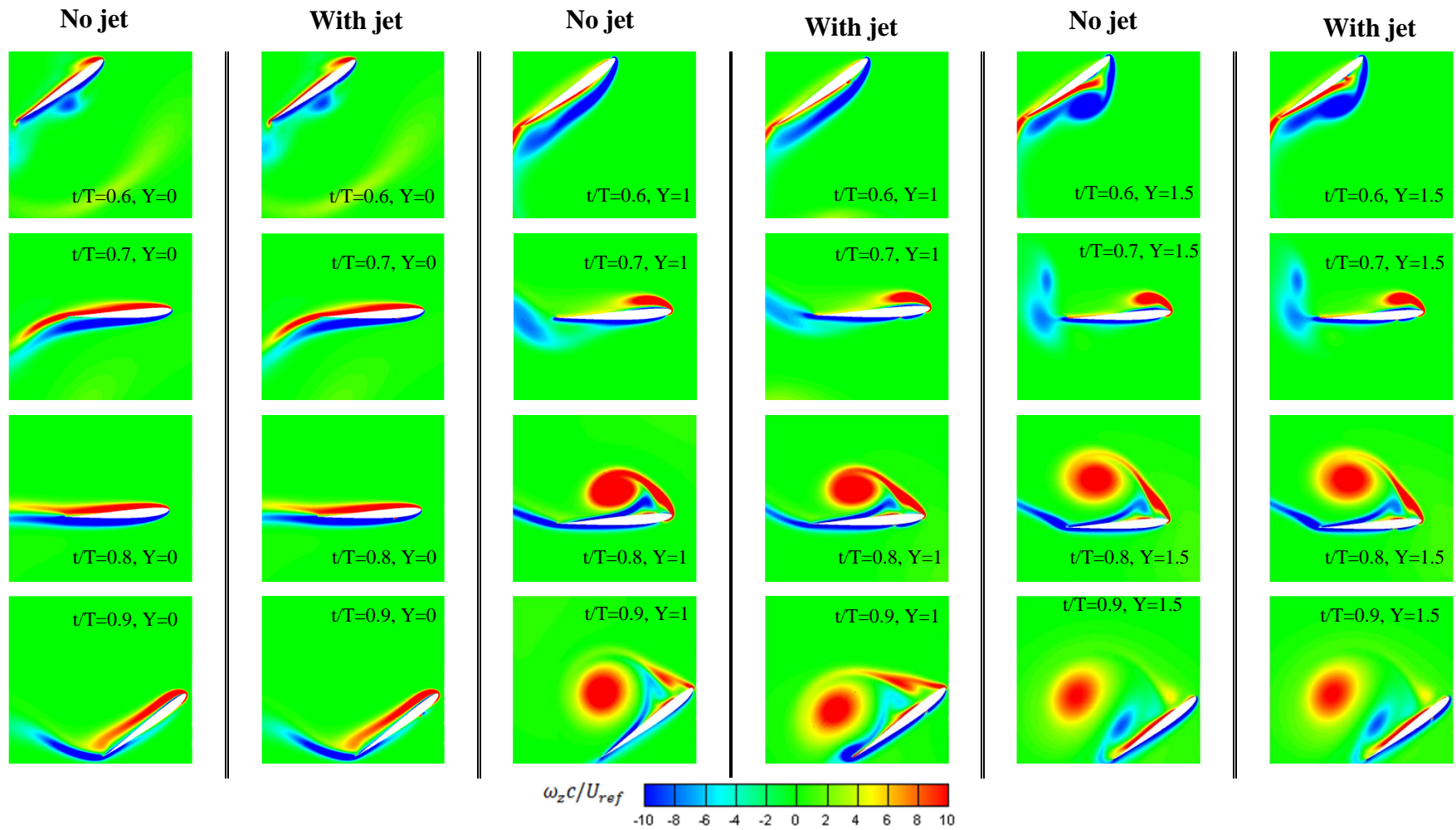
Figure 5.16 Close up views of normalized vorticity contours for different vertical translations, $0.6 < t/T < 0.9$.

Figure 5.14, 5.15 and 5.16 present the close-up views of the normalized vorticity contours over one period of hover motion for different vertical translations.

Table 5.2 L/D for different Y values at Re = 1000, with and without synthetic jet application.

Y	0	0.25	0.5	0.75	1	1.25	1.5
L/D $_{no\ jet}$	42.4	56.6	36.9	28.7	7.1	13.3	19.5
L/D $_{with\ jet}$	37.4	39.6	168.0	46.5	45.1	29.4	36.8

In Table 5.2, L/D over one period of hover motion is represented with and without synthetic jet applications. For Y= 0 and Y = 0.25 cases, application of synthetic jet decreases the L/D ratio, while an increase is obtained for higher Y values. The maximum L/D ratio was obtained on the case where Y=0.5. The decrease on L/D at Y=0 and Y=0.25 can be explained by having only horizontal motion on the hover mode. During the figure-of-eight motion at Y=0, only x component of the motion is changing. Since the application of synthetic jet creates additional drag the airfoil, L/D was decreased with synthetic jet application. Moreover, percentage changes on L/D ratios for the cases with and without jet applications are obtained to be higher than 11% in all different Y values. As the percentage change is higher than 11%, it is obtained that the applied time-step in figure of eight motion is refined enough. In addition, decrease of L/D at Y=0 and 0.25 was corroborated by normalized vorticity contours in Figures 5.8 and 5.9.

In Figure 5.17, Figure 5.18 and 5.19, time histories of aerodynamic coefficients are presented for every analyzed Y values. It is obtained that aerodynamic coefficient histories with and without synthetic jet applications have similar trend. Changing Y values are changing the peaks and deeps in the time histories of aerodynamic coefficients. At Y = 0.5 and Y = 1, trends of the aerodynamic coefficients are slightly different and shifted in time for with and without synthetic jet applications.
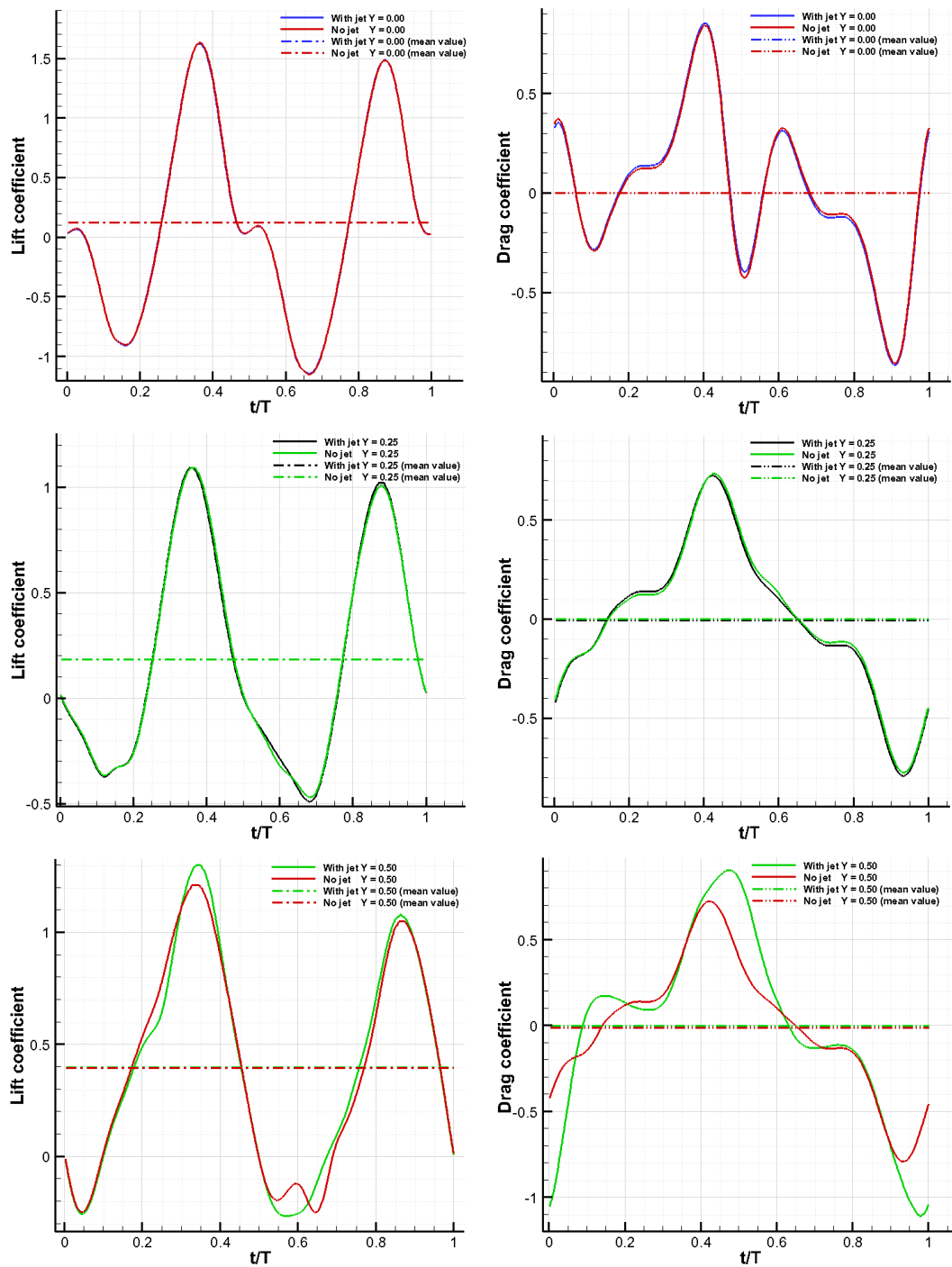
Figure 5.17 Time histories of lift and drag coefficients for varying vertical translations of hover motion at Re = 1000, $V_{jet\ max} = 0.1 U_{ref}$, and $0.0 < Y < 0.5$.
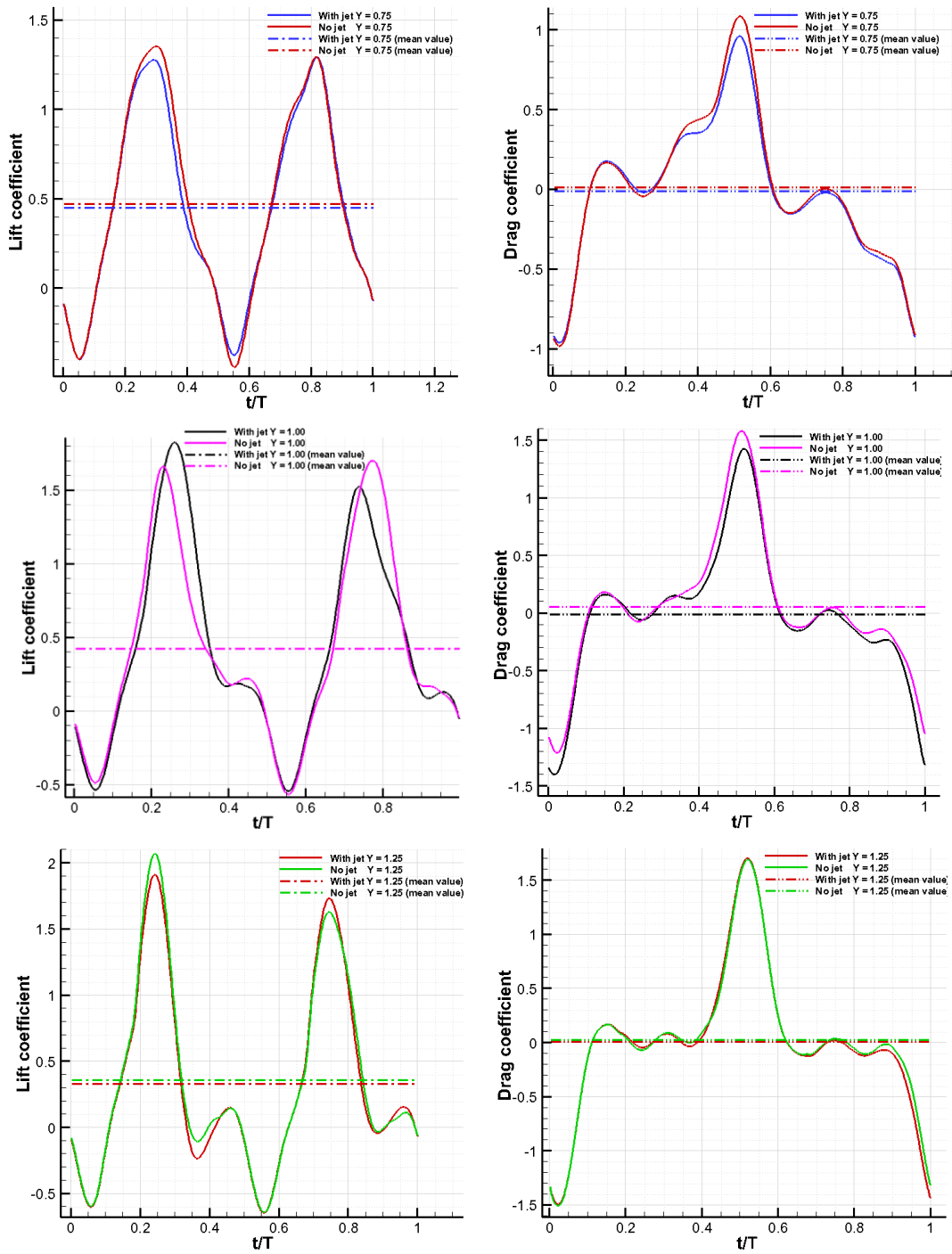
Figure 5.18 Time histories of drag coefficients for varying vertical translations of hover motion at Re = 1000, $V_{jet\ max} = 0.1U_{ref}$, and $0.5 < Y < 1.25$.
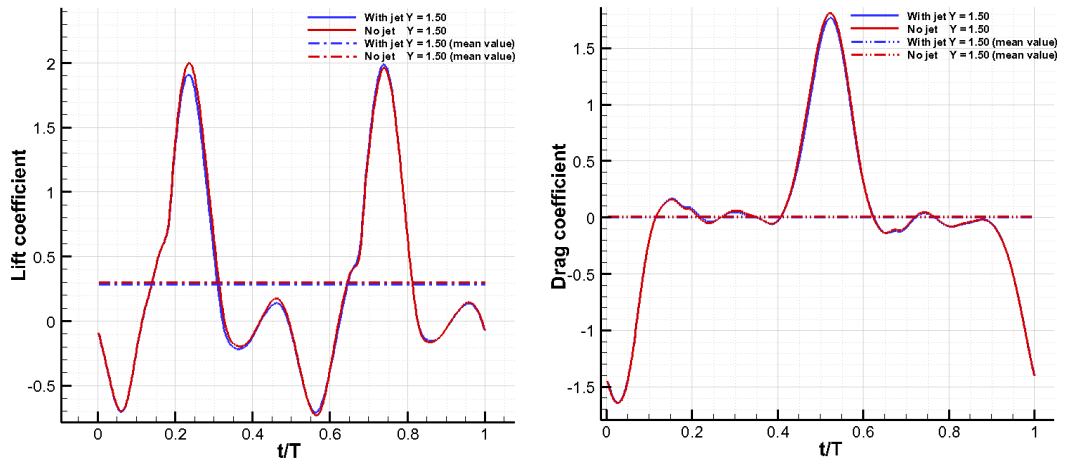
Figure 5.19 Time histories of drag coefficients for Y = 1.5 in hover motion at Re = 1000, and $V_{jet\ max} = 0.1 U_{ref}$.

In Figure 5.20, time histories of lift and drag coefficients are presented for three different Y values. Lift to drag ratios with and without jet application cases has similar trend as lift and drag coefficient values. Moreover, the general trends of the time histories are shifted forward in time for increasing in Y values. However it is observed that the effect of jet application is dominant on the peaks and deeps.

As seen in Figure 5.21, increase in vertical translation causes an increase in the amplitude of time histories of drag coefficient. Moreover, peak values of drag coefficient were shifted in time. On the other hand, increase in vertical translation does not cause a regular pattern on mean values of drag coefficient. While Y = 0.25 condition has increased the mean drag coefficient with jet application, Y = 0.75 case has a decreasing effect. In addition, jet application improved the mean value of drag coefficient at Y = 1.25.
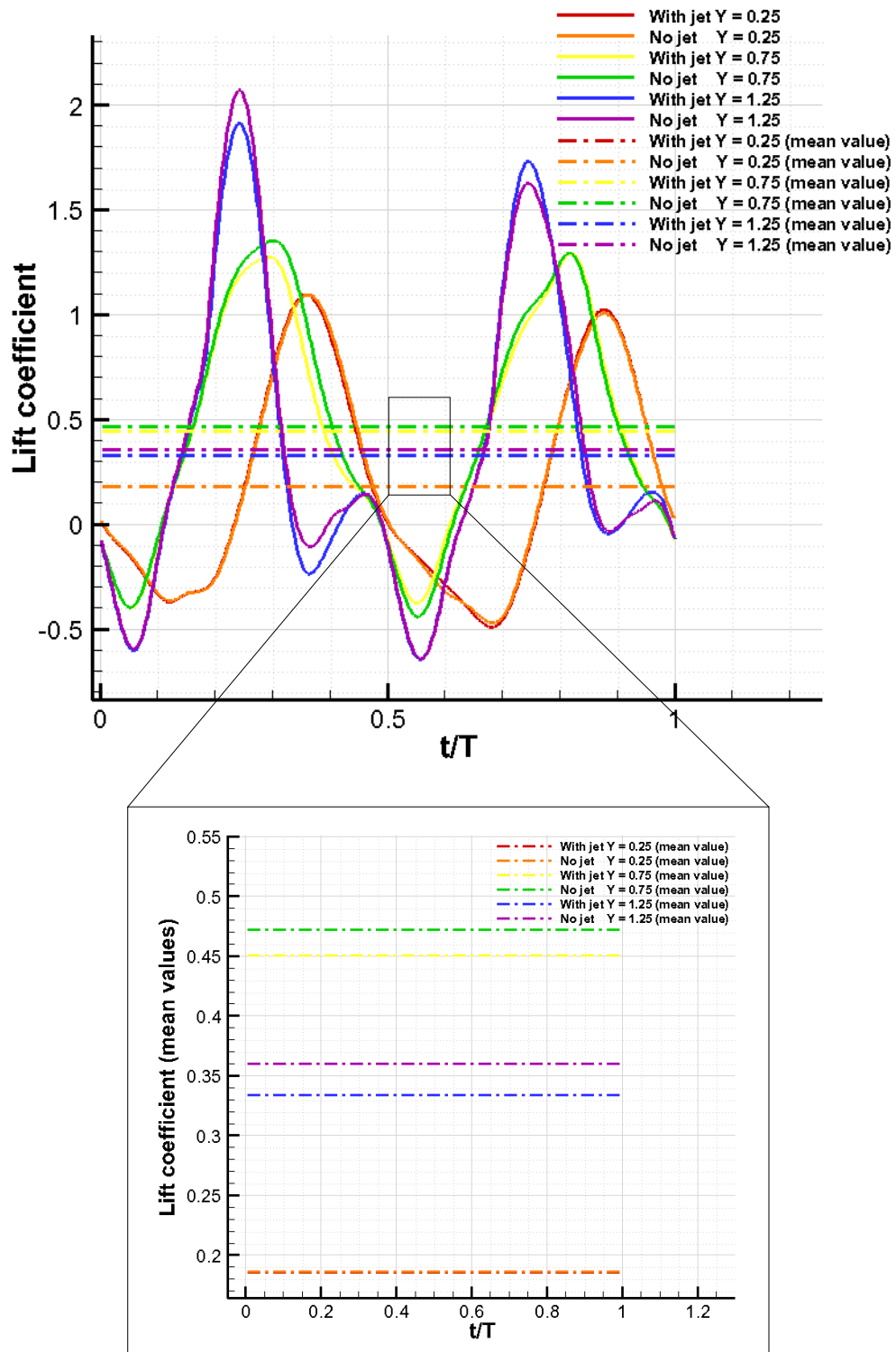
Figure 5.20 Time histories of lift coefficients for varying vertical translations of hover motion at Re = 1000, $V_{jet\,max} = 0.1U_{ref}$.
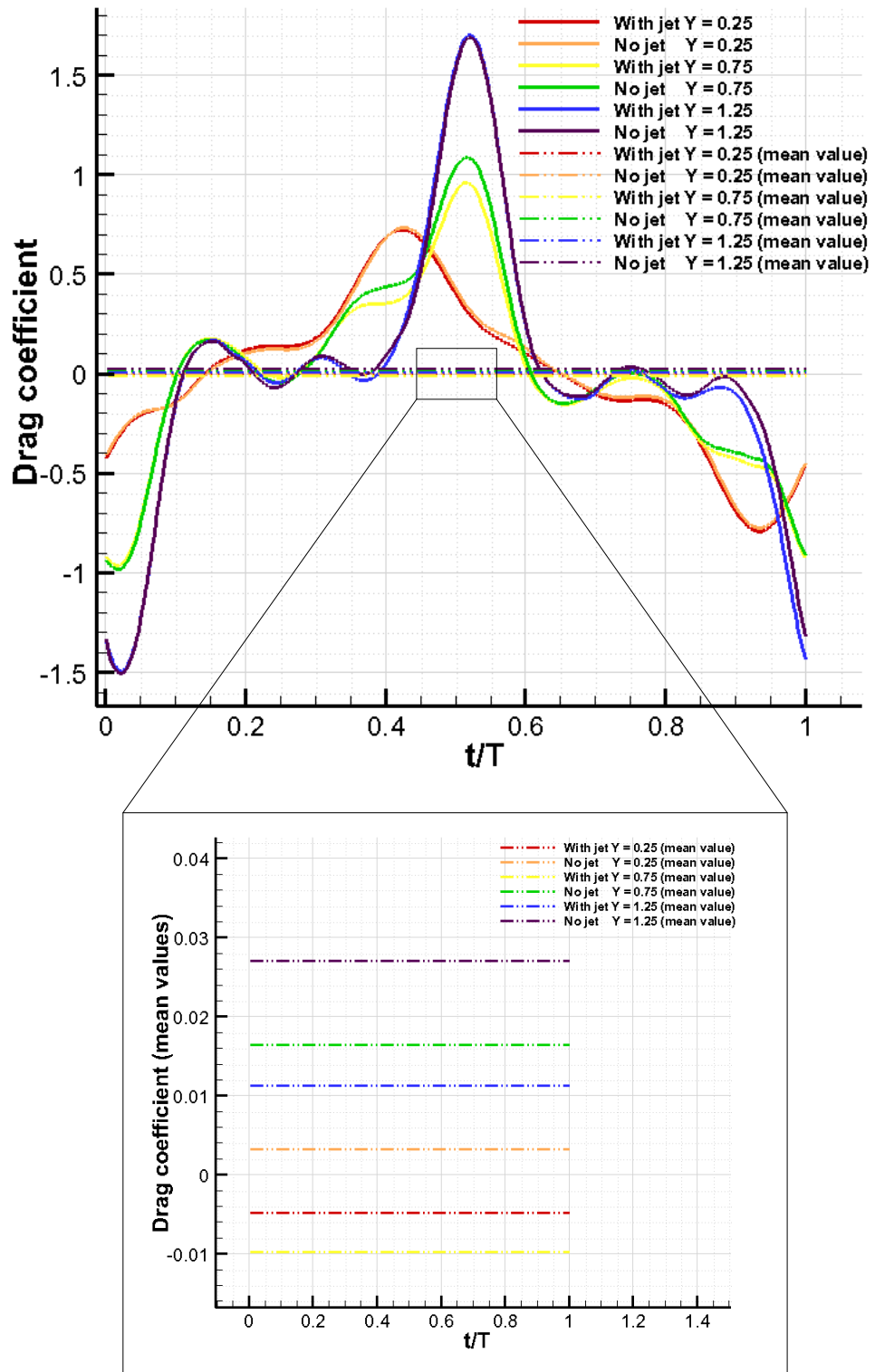
Figure 5.21 Time histories of drag coefficients for varying vertical translations of hover motion at Re = 1000, $V_{jet\,max} = 0.1U_{ref}$.

5.4   Effect of Reynolds Number

Effect of Reynolds number is computed for 5 different values ranging between 1000 and 5000. During these computations, vertical translation of figure-of-eight motion is kept at 0.5. Normalized vorticity contours are given in Figure 5.23 with synthetic jet application. For increasing Reynolds counter rotating and counter clock wise rotating vortex vorticities become smaller on the upper side of the airfoil. From period $t/T = 0$ to $t/T = 0.15$, positive (counter clockwise rotating) vorticities starts to form and extend on the lower side of the airfoil.

Figure 5.22 presents Reynolds number in terms of U_{ref} (see Eq. 3.13) versus jet flow Reynolds number trend curve (see Eq. 3.14) for present study.
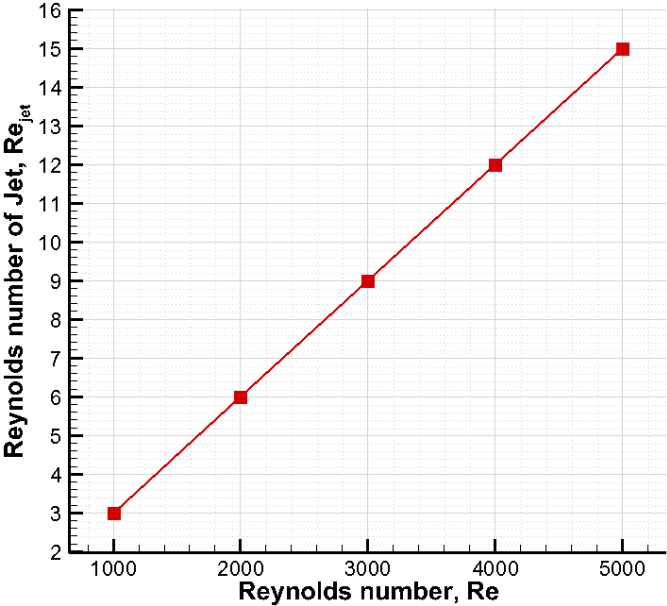
Figure 5.22 Jet Reynolds number versus Reynolds number of the motion at $Y = 0.5$, $V_{jet\,max} = 0.1U_{ref}$.

Time histories of lift and drag coefficients with and without jet application are given in Figure 5.27 over one period of figure-of-eight motion.
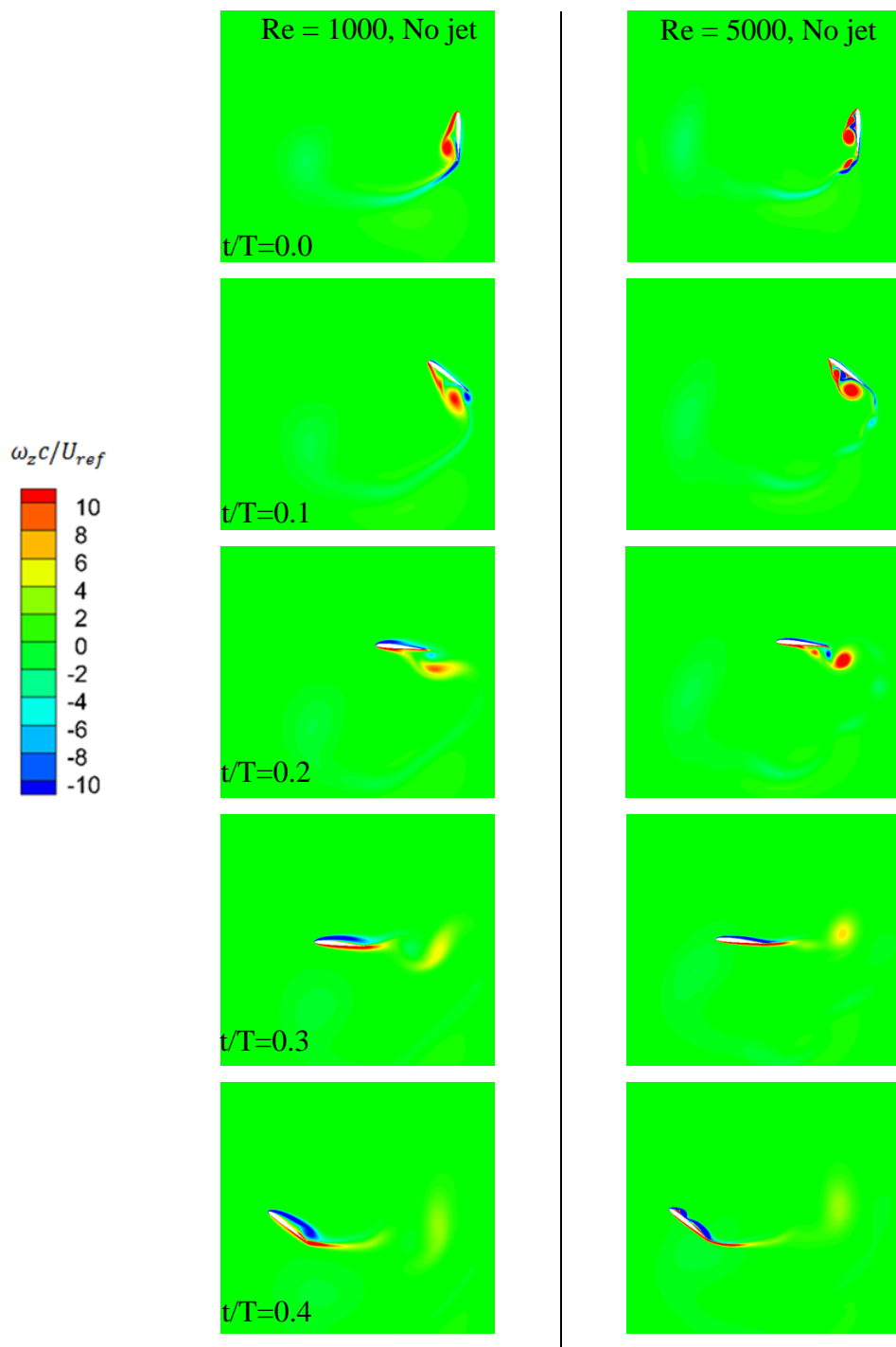
Figure 5.23 Normalized vorticity contours of hovering motion for the first half period of figure-of-eight motion at Re = 1000, Y = 0.5, $V_{jet\ max}$ = 0.1U_{ref} and 0.0 < t/T < 0.4 with no jet (left) and synthetic jet (right) applications.
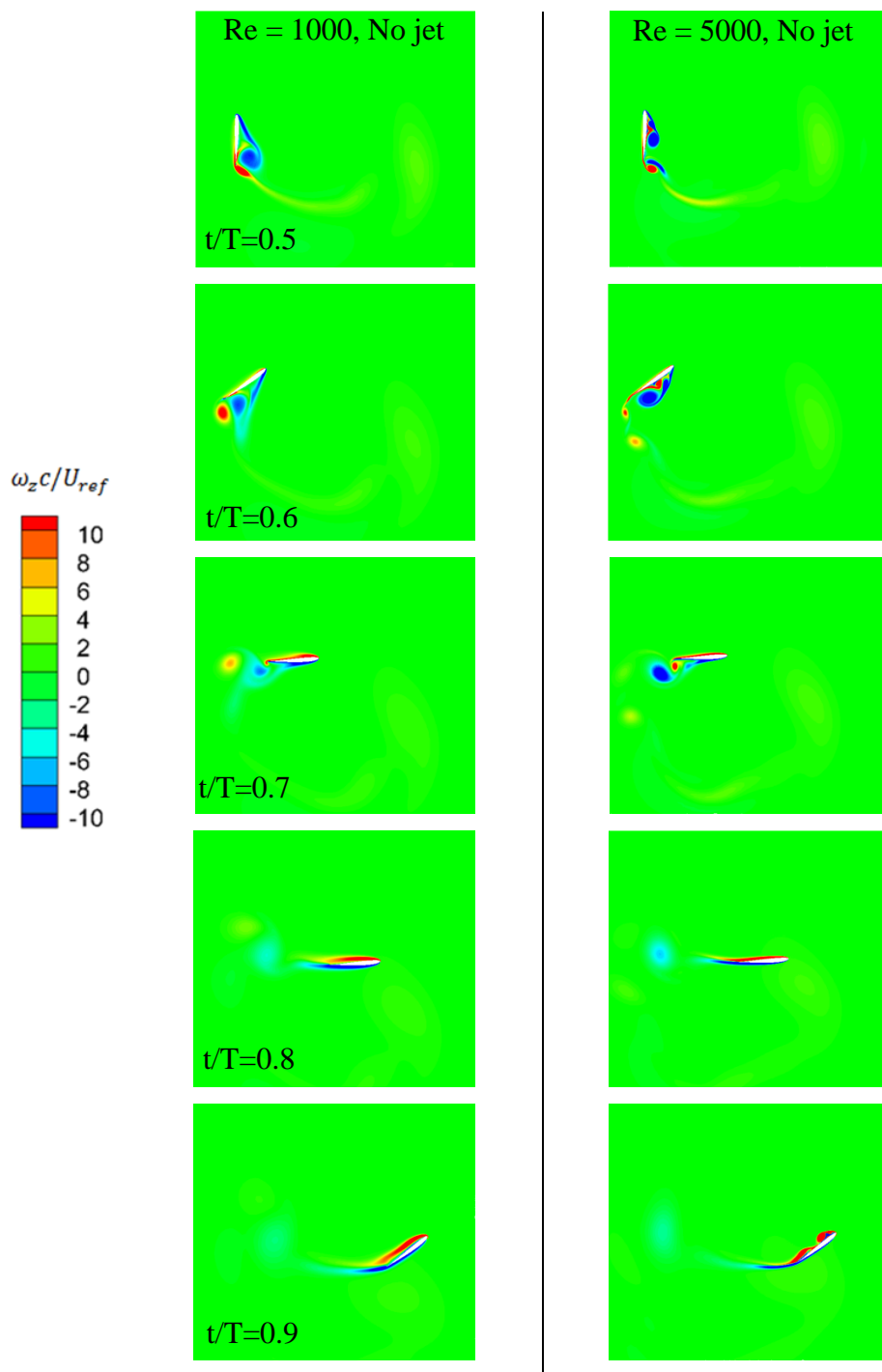
Figure 5.24 Normalized vorticity contours of hovering motion for the second half period of figure-of-eight motion at Re = 1000, Y = 0.5, $V_{jet\ max} = 0.1U_{ref}$ and $0.5 < t/T < 0.9$ with no jet (left) and synthetic jet (right) applications.
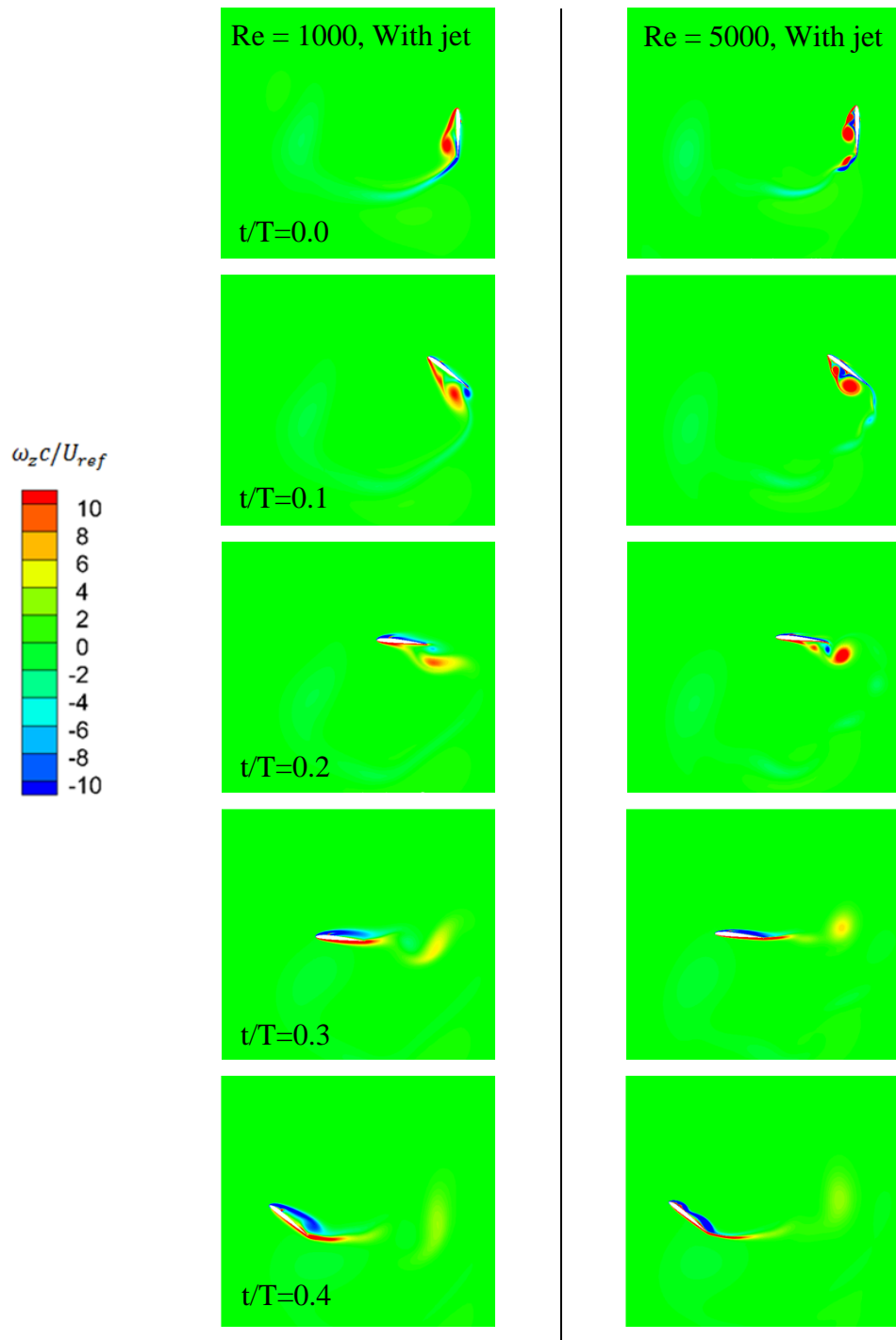
Figure 5.25 Normalized vorticity contours of hovering motion for the second half period of figure-of-eight motion at Re = 1000, Y = 0.5, $V_{jet\,max} = 0.1U_{ref}$ and $0.5 < t/T < 0.9$ with no jet (left) and synthetic jet (right) applications.
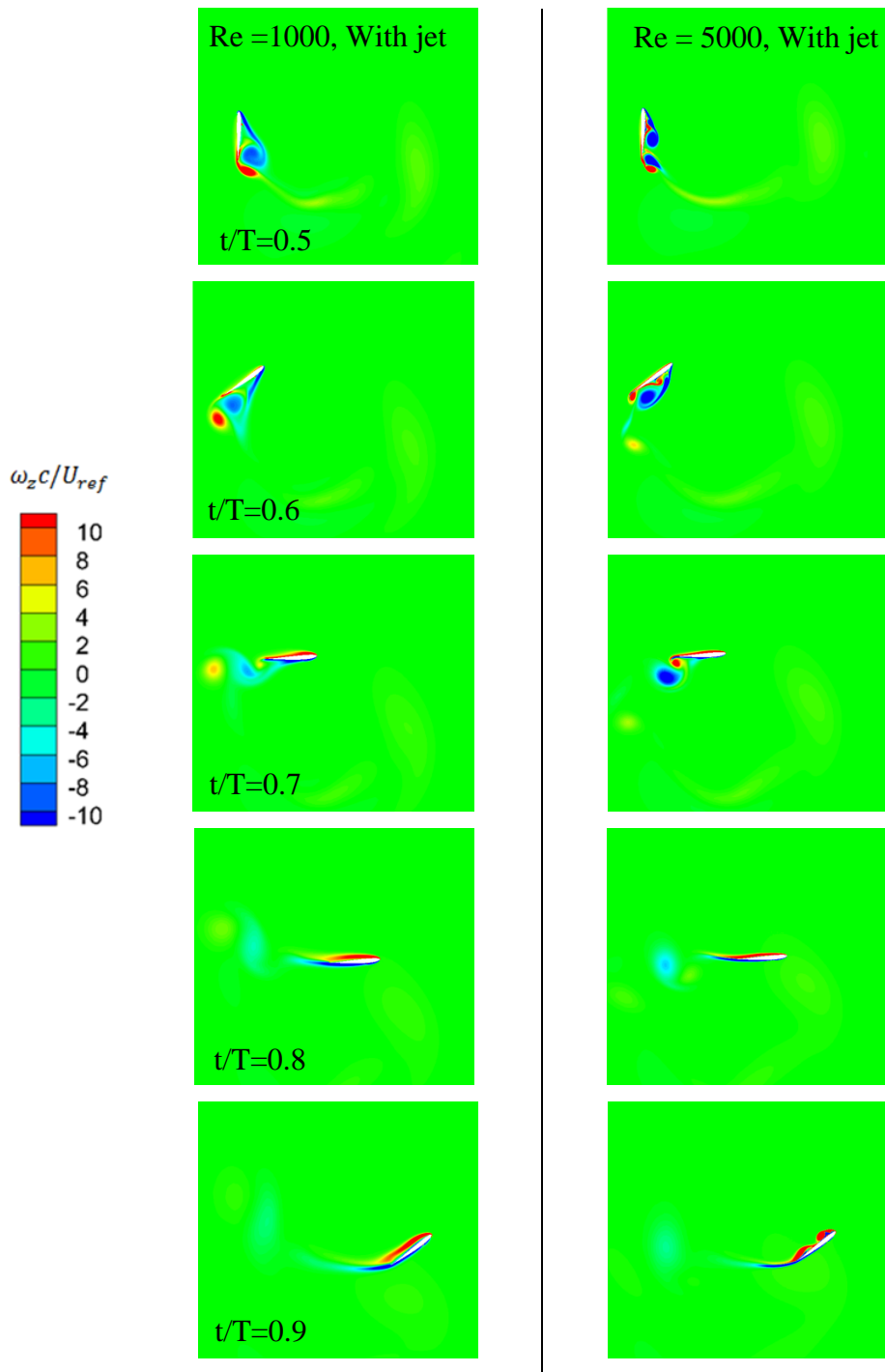
Figure 5.26 Normalized vorticity contours of hovering motion for the second half period of figure-of-eight motion at Re = 1000, Y = 0.5, $V_{jet\ max} = 0.1U_{ref}$ and $0.5 < t/T < 0.9$ with no jet (left) and synthetic jet (right) applications.

In Figure 5.27 lift and drag coefficient histories over one period are represented. It can be seen that without synthetic jet application, by increasing Reynolds number, amplitude of lift and drag coefficients are increasing. For synthetic jet application, opposite effect can be seen. For increasing Reynolds number with synthetic jet application, amplitude of drag and lift coefficient histories are decreasing.
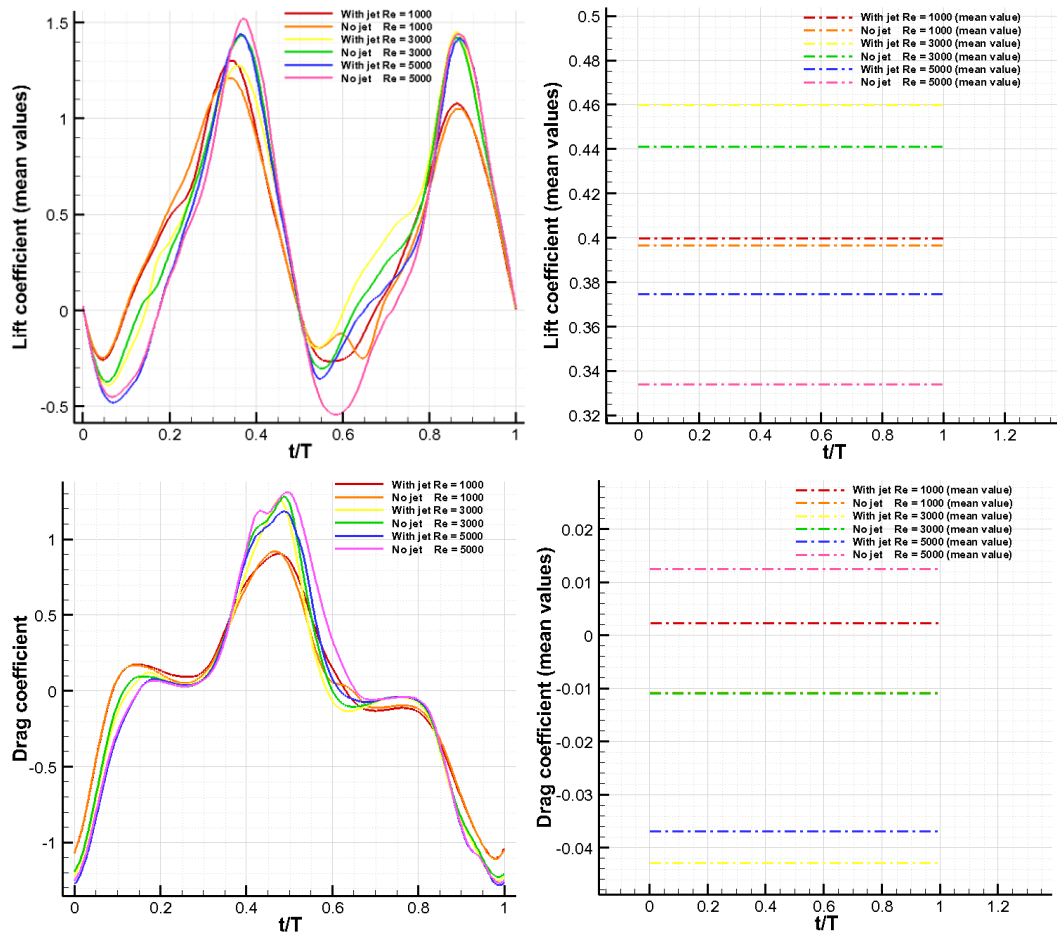
Figure 5.27 Time histories of lift and drag coefficients over one period of hover motion for varying Reynolds numbers at Y = 0.5, with and without jet applications ($V_{jet\ max} = 0.1U_{ref}$).
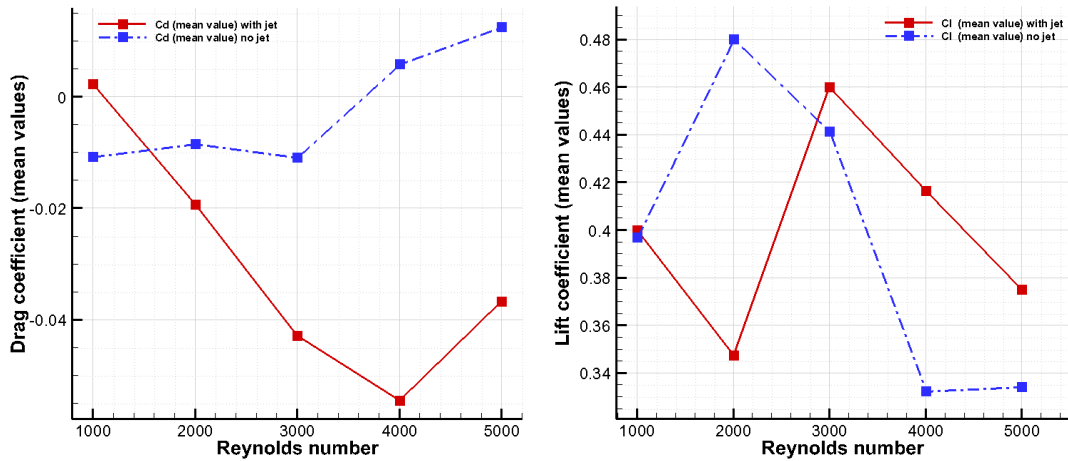
Figure 5.28 Mean drag (left) and lift (right) coefficients over one period of hover motion at Y = 0.5 for different Reynolds numbers.

Mean lift and drag coefficients for different Reynolds numbers are presented in Figure 5.28. Except Re = 1000 case, a decrease is obtained on the mean drag coefficient for increasing Reynolds numbers. However, at Re = 3000 an increase on the mean lift coefficient is obtained by the application of synthetic jet. Thus, it can be concluded that for increasing Reynolds numbers mean lift to drag ratio is improved by the application of the synthetic jet.

5.5   Effect of Jet Frequency

The last effect investigated on synthetic jet application was synthetic jet frequency. The range of the jet frequency was between 0.1Hz and 0.4Hz. Normalized vorticity contour and close-up views are shown in Figure 5.29. It is observed that the jet frequency is not a dominant parameter on the synthetic jet application. Hence, only at t/T = 0.3 and t/T = 0.7 normalized vorticity contours are presented. For increasing jet frequency the double vortex structure gets smaller on the upper surface of the airfoil close to the jet location.
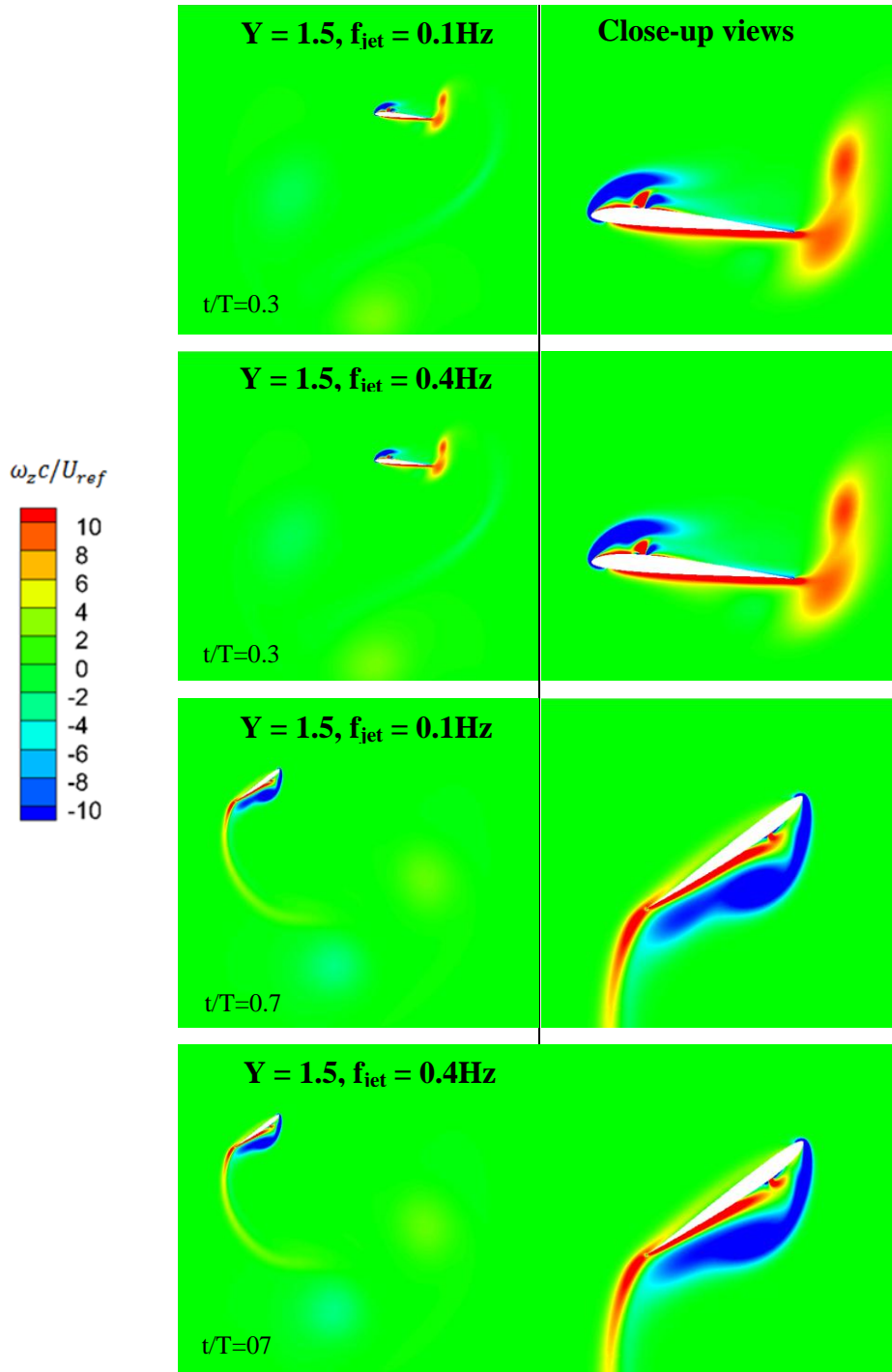
Figure 5.29 Normalized vorticity contours of hovering motion for varying vertical translation (Y), at Re = 1000, 0.0 < t/T < 0.4 and $V_{jet\ max} = 0.1U_{ref}$.
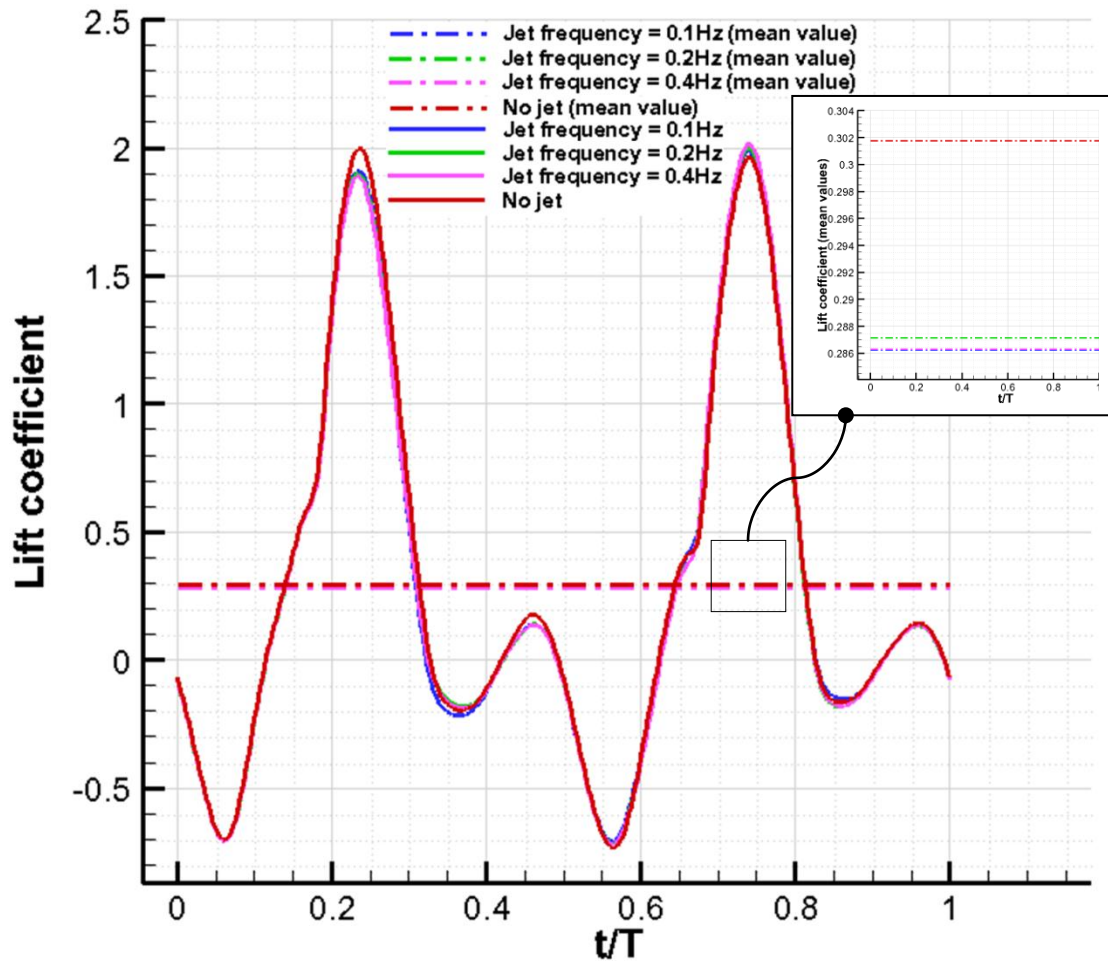
Figure 5.30 Lift coefficient histories for varying jet frequencies, at Re = 1000, 0.0 < t/T < 0.4, Y =1.5, and $V_{jet\ max} = 0.1U_{ref}$.

Figure 5.30 and Figure 5.31 present the time histories of lift and drag coefficients over one period of hover motion. By the application of the synthetic jet, general trend of the aerodynamic coefficients are not changed. Peaks and deeps of the time histories of the aerodynamic coefficients are changing for different synthetic jet frequencies. Moreover, a slight decrease observed on the lift coefficient with different jet frequencies. Decrease on the mean drag coefficient is obtained.
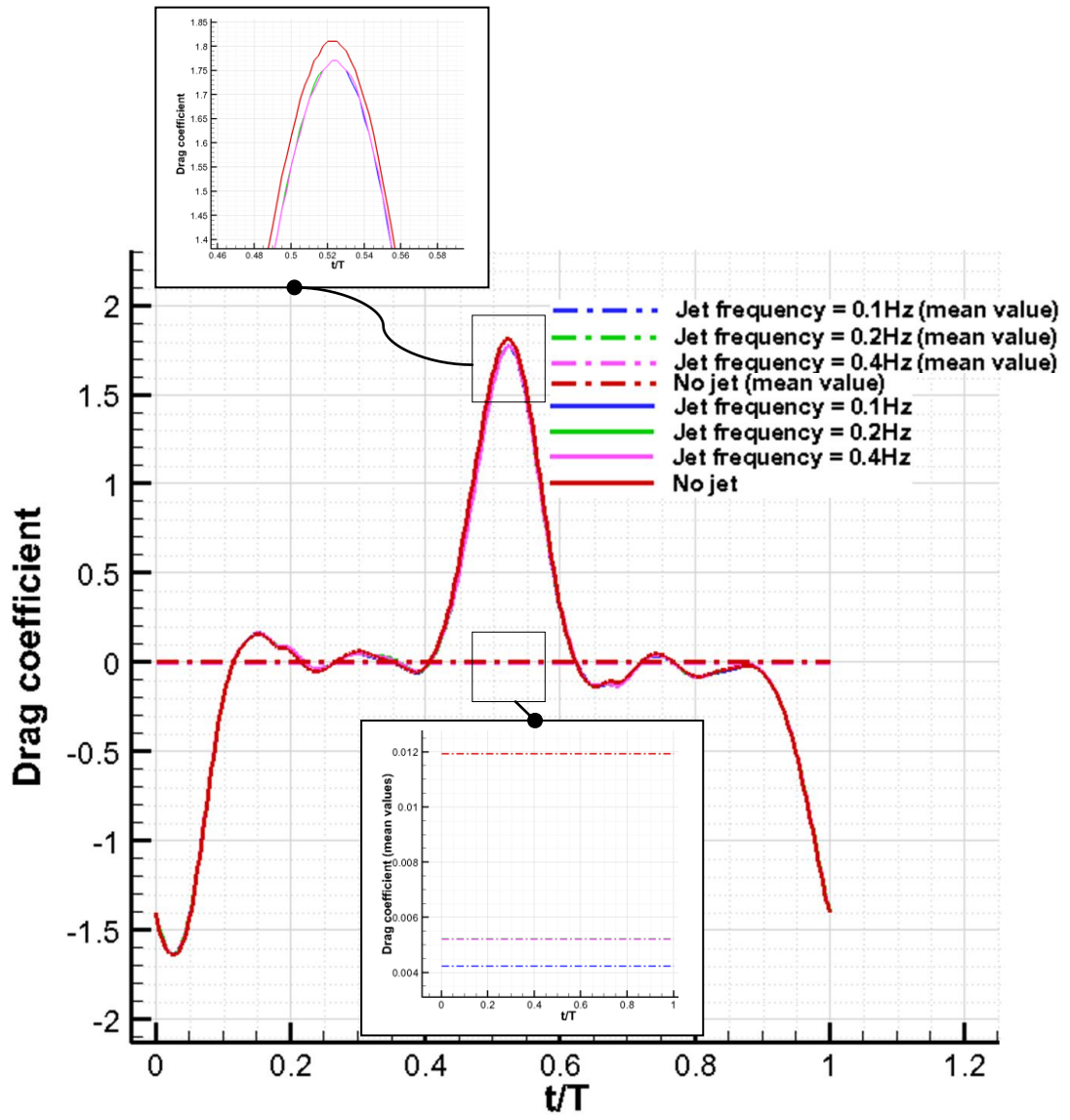
Figure 5.31 Drag coefficient histories for varying jet frequencies, at Re = 1000, 0.0 < t/T < 0.4, Y =1.5, and $V_{jet\ max} = 0.1U_{ref}$.

CHAPTER 6

CONCLUDING REMARKS

The low Reynolds number aerodynamics of steady state and figure-of-eight motion are investigated numerically. The flow fields around airfoil are visualized by solving Navier-Stokes equations with laminar and turbulent models. During steady state cases turbulent k-ω SST model is preferred for Re = 6×10^4. For low Reynolds number, laminar solver are applied for Re = 1000. Lift and drag coefficient histories in addition normalized vorticity contours are presented and discussed.

Steady state cases focused on the jet application on airfoil. In the existence of free stream flow velocity, synthetic jet velocity is also introduced to the boundary layers. With Fluent 13.0, two-dimensional, pressure based, Navier –Stokes equations are solved on O-type grid domain. Unsteady cases are performed in hover mode. The figure of eight motion is obtained by the application of User Defined Functions (UDFs). Grid independence and time-step refinement studies are performed.

As a first study, verification steady state and unsteady flow conditions are performed. Laminar and turbulent models (k- ω, and k-ω SST) models are compared with experimental results and it is concluded that the k-omega SST model supplies closer results to the experimental results.

The application of the jet on airfoil is performed and different jet velocities are computed with and without jet applications. Lift and drag coefficients are compared and improvement on L/D ratio is observed. Effect of jet angle is performed with different jet angles. It is understood that the jet angle is not a dominant jet parameter.

However the jet velocity is a dominant parameter on the active flow control application.

Angle of attack value is investigated under steady state flow conditions. Farfield flow conditions are kept constant for each case. Detachment of the flow is simulated over airfoil for high angle of attack values and the increased lift coefficient values are obtained. In addition to that, Reynolds number effect is checked between $1x10^4$ and $6x10^4$. It is understood from the results that for increased Reynolds number, detachment of the flow is delayed on the upper surface of the airfoil.

The latter studies are focused on the boundary conditions of unsteady flow conditions with the application of figure-of-eight motion. O-type grid domain is moved as rigid body and the time histories of drag and lift coefficients are obtained over one period of hover. Effect of synthetic jet is investigated by the application of constant blowing, constant suction and synthetic jet applications. According to the computations, it is concluded that by the application of synthetic jet, peak values of both lift and drag histories are shifted in time.

For hovering cases, effect of vertical translation is studied for seven different values. In both lift and drag coefficient time histories, amplitudes of the coefficient histories are decreased by the increase of vertical translation. When compared without jet applications, delay is observed on the peaks of time histories of the aerodynamic coefficients by the synthetic jet application.

Reynolds number effect on hover mode is also examined. Different Reynolds numbers are checked between 1000 and 5000. The same effect with the increase of vertical translation is observed. When the Reynolds number increased, peaks of the time histories of the aerodynamic coefficients are decreased.

The last study is performed for different synthetic jet frequencies. When different jet frequencies are employed, peak values of the drag and lift coefficient histories are slightly changed.

In this thesis study, location of the orifice is decided according to the previous studies in the literature [14]. However, for unsteady flow conditions, different locations of orifice studies can be conducted as a future work to understand the effect of suction on both sides of the airfoil. In addition, in this study jet slot size kept constant. Effect of jet slot size can be examined in further studies.

REFERENCES

[1] Fiedler, H., Gad-el-Hak, M.,Pollard, A., Bonnet, J. P., "Control of free turbulent shear flows". *In flow control:fundamentals and practices,* pp. 335-429, 1998.

[2] Buschmann, M. H., Gad-el-Hak, M., "Turbulent Boundary Layers: Reality and Myth". *International Journal of Computing Science and Mathematics*, Vol. 1, pp. 159-176, 2007.

[3] Hefner, J., Weinstein, L. Bushnell, D., "Large-eddy break-up scheme for turbulent drag reduction". *In AIAA Prog. Astro. Aero.*, volume 72, p: 447–463, 1979.

[4] Walsh, M., Weinstein, L., "Drag and heat transfer on surfaces with small longitudinal fins". *AIAA paper*, p:78-1161, 1978.

[5] Englar, R., Huson, G., "Development of advanced circulation control wing lift airfoils". *AIAA paper* 83-1847, 1983.

[6] Englar, R., Smith, M., Kelley, M., Rover, R., "Development of circulation control technology for application to advanced subsonic aircrafts". *AIAA paper* 93-0644, 1993.

[7] Joslin, R., Jones, G., "Applications of circulation control technology". Vol.214 of Progress in astronautics and aeronautics. American institute of aeronautics and astronautics, 2006.

[8] Mejia, O., "Computational Study of a NACA4415 airfoil using synthetic jet". University of Texas Ph.D. Thesis., May 2009.

[9] Smith, B. L.; Glezer, A., "Jet vectoring using synthetic jets". *Journal of. Fluid*

Mechanics, vol. 458., 2002.

[10] De Salvo, M. E., Glezer, A., "Modification of the aerodynamic performance of airfoil at low angle of attack: Trailing edge trapped vortices". *AIAA paper* 2002-3165, 2002.

[11] De Salvo, M. E., Glezer, A., "Aerodynamic performance modification at low angles of attack by trailing edge vortices". *In 2nd AIAA flow control conference*, AIAA-2004-2118, 2004.

[12] Glezer, A., Amitary, M., "Synthetic Jets". *Fluid Mechanics*, Vol.34, p:503-529, Jan 2002.

[13] You, D.; Moin, P., "Study of flow separation over an airfoil with synthetic jet control using large-eddy simulation". 2007 .

[14] Günaydınoğlu, E., "Low Reynolds number aerodynamics of flapping airfoils in hover and forward flight". M.Sc. Thesis, METU, 2010.

[15] Miranda, S.,Telionis, D., Zieger, M., "Flow control of a sharp edged airfoil". *AIAA paper* no. 2001-0119, 2001.

[16] Rullan, J., "Flow control over a circular arc airfoil by periodic blowing". Blacksburg, Virginia, Ph.D. Thesis, 2004.

[17] Roshko, A., "A review of concepts in separated flow". Proceeding of Canadian Congress Applied Mechanics, Vol. 1,3-81 to 3-115, 1967.

[18] Siefert, A., Bachar, T., Koss, D., Shepshelovich, M., Wygnanski, I. "Oscillatory blowing: a tool to delay boundary layer separation". *AIAA Journal*. Vol. 31, No 11, pp.2052-2060, 1993.

[19] Hsiao, F. B., Liang, P. F., Huang, C. Y., "High incidence airfoil aerodynamics improvement by leading edge oscillating flap". *Journal of aircraf* Vol.35, No. 3,

pp.508-510, 1998.

[20] Allen, M. G., Glezer, A., "Jet vectoring using zero mass flux control jets". *AFOSR contractor and grantee meeting on turbulence and internal flows*, 1995.

[21] Seifert, A., Darabi, A., Wygnanski, I., "Delay of Airfoil Stall by Periodic Excitation". *Journal of Aircraft*. Vol. 33, No. 4, pp. 691-699, 1996.

[22] James, R. D., Jacobs, J.W., Glezer, A., "A round turbulent jet produced by an oscilating diaphram". *Physics of Fluids*, vol. 8, no 9, pp. 2484-2495, 1996.

[23] Smith, B. L., Glezer, A., "The formation and evaluation of synthtetic jets". *Pyhsics of Fluids*, vol. 10, no. 9, pp 2281-2297, 1998 .

[24] Smith, B.L., Glezer, A., "Vectoring and small-scale motions effected in free shear flows using synthetic jet actuators". *35th AIAA Aerospace sciences meeting and exhibit* (Reno, NV) AIAA paper, Jan 1997.

[25] Rao, P., Gilarranz, J.L., Ko, J., Strgnac, T., Rediniotis, O.K., "Flow separation control via synthetic jet actuation". *AIAA paper* 2000-0407, 2000.

[26] Jacobson, S. A., Ronalds, W. C., "Active control of streamwise vortices and streaks in boundary layers". *Journal of Fluid Mechanics,* vol.*360,* pp. 179-211, 1998.

[27] Artana, G., J. D'amado, J., Leger, L., Moreau, E.,Touchard,G., "Aerodynamic flow control using synthetic jet technology". AIAA paper 98-0208, 2002.

[28] Watson, M., Jaworski, A.J., Wood, N.J., "Contribution to the understanding of flow interactions between multiple synthtetic jets". *AIAA Journal,* vol. 41, no. 4, pp. 747-749 ., 2002.

[29] Martin P., Tung C., Chadrasekhara, M., Arad E., "Active separation control: measurements and computations for a NACA 0036 airfoil". *21st AIAA Applied*

aerodynamics conference, 2003.

[30] Lee, C., Goldstein, D., "Two dimensional synthetic jet simulation". *AIAA Journal,* Vol. 40, No. 3, 2002, pp. 510-516, 2002.

[31] Mossi, K., Bryant, R., "Piezoelectric Actuators for Synthetic Jet Applications". *Materials Research Society,785*. U.S.A, 2004:.

[32] Gilarranz, J. L., Traub, L. W., Reditionis, O. K., "A new class of synthetic jet actuators -part II: application to flow seperation control". *Journal of Fluids Engineering* 127, 337 – 387, 2005.

[33] You, D.; Moin, P., "Large-eddy simulation of flow separation over an airfoil with synthetic jet control". *Center for Turbulence Research Annual Research Briefs,* 2006.

[34] Akcagoz, E., "Numerical investigation of flow control over an airfoil with synthetic jets and its optimization". M. Sc. Thesis, METU, 2008.

[35] Kang, C., Trizila, P., Rausch, J. M., Bernal, L., Ol, M. V., Shyy, W., "Modeling of pitching and plunging airfoils at reynolds number between 10000 and 60000". *27th AIAA Applied Aerodynmaics Conference*, AIAA 2009-4100, 2009.

[36] Riazi, H., "Circulation enhancement of stnthetic jet actuators via multiple orifices". M. Sc. Thesis, The University of New South Wales, 2012.

[37] ANSYS Fluent user's guide pp:93-100, 2011.

[38] Catalano, P., Tognaccini, R., "Large eddy simulation of the flow around the SD7003 airfoil". (Anonim) MEM-199-0.

[39] NATO AVT 101 "Experimental and Computational Investigations in Low Reynolds Number Aerodynamics, with Application to Micro Air Vehicles (MAVs)". Tr - Avt - 101, June 2007.

[40] ANSYS Fluent UDF Manual (2009) Pp: 8-3: 8-20.

[41] Nakhla, H., Bourlier, A., Nguyen, L., Bhatt, S., Brodnick, J., Golubev, V., "High accuracy simulations of synthetic jets for low-Re flow control". AIAA 2011-469, 2011.

[42] Siefert, A., Pack, L., "Oscillatory Excitation of Unsteady Compressible Flows Over Airfoils at Flight Reynolds Number". *AIAA paper* 99-0925, 1999.

[43] Mc Cormick, D., "Boundary Layer Separation Control with Directed Synthetic Jets". *AIAA Paper* 2000-0519, 2000.

[44] Menter, F. R., "Two-Equation Eddy-Viscosity Turbulence Models for Engineering Applications". *AIAA Journal*, Vol. 32, No. 8, pp. 1598-1605, August 1994.

[45] *Ekaterinaris, J. A., Menter, F. R., "Computation of Oscillating Airfoil Flows with One-and Two- equation Turbulence Models". AIAA Journal, Vol. 32, No. 12, pp. 2359-2365, December 1994.*

[46] Patankar, S. V., "Numerical Heat Transfer and Fluid Flow". *Hemisphere Publishing Corporation,* Washington New York London, 1980.

[47] Çiftci, M., Kurtuluş, D. F., "Kanat kesiti üzerinde düşük Reynolds sayıları için yapay jet uygulaması". UHAT-2013-058. İzmir, Gaziemir, Ulusal Havacılık ve Uzay Kongresi, 2013.